Norwegian University
of Life Sciences

Master's Thesis 2017 30 ECTS
Department of Mathematical Sciences and Technology

Parametric Study of Reinforced Concrete Columns under Axial Loading Retrofitted with Fibre-Reinforced Polymer Composites.

David Treffen
Civil Engineering and Architecture

Preface

This master thesis has been written at the Norwegian University of Life Science (NMBU), in the spring of 2017 at the Faculty of Science and Technology.

The topic of this thesis was proposed by Professor Themistoklis Tsalkatidis, who also was my thesis supervisor. This thesis is an important contribution to current state-of-the-art knowledge related to strengthening or retrofitting of reinforced concrete members. Already constructed reinforced concrete (RC) members such as columns are usually designed after older codes and standards that are often insufficient in comparison to the current codes and standards, norms and regulations. The main reason is that previous standards do not offer adequate transverse reinforcement, which makes members more vulnerable to brittle shear failure under dynamic loads. A governing principle when designing reinforced concrete columns after current codes and standards is the shift of the failure mode of the column from a brittle failure mode, which was the case in older codes and standards, towards a more ductile failure mode. A key feature to understand more about the ductility of columns is to understand more about its shear behaviour and the parameters affecting it. Therefore, the main focus of the presented thesis is placed there.

Working on this master thesis has been a time consuming experience were the teaching curve has been relatively steep. This thesis has been my first encounter with ANSYS, and I had only limited experience using the finite element software from before. Much time has been spent on learning the FEM philosophy, but the benefits of mastering a FEM program like ANSYS are not trivial.

Acknowledgments

I would like to thank my advisor Professor Themistoklis Tsalkatidis for his guidance and motivation during the writing of this master thesis. Finally, I would like to thank my family and friends for their vote of confidence, encouragement and support through this time.

Abstract

Retrofitting of reinforced concrete (RC) columns with FRP (fibre-reinforced polymers) is an effective way to increase their capacity. Externally wrapped FRP is a retrofitting method that has been used especially during the last two decades. This technique offers highly improved mechanical properties of the column and has a variety of application fields. Much research has been conducted on short concrete columns with different configurations of FRP and different stirrup ratios however, significantly less research has been conducted on taller RC columns typically used in structural engineering applications, where the critical height of the column with respect to shear has been studied in detail. Even though the interface between the concrete and the FRP has been studied quite extensively, there exist several different approaches on how to model the FRP composite and the interaction conditions between each layer of laminate. Therefore, the latter is still open to research. The objective is herein to investigate the shear behaviour within the critical height of the column with respect to shear forces under different configurations of FRP, different configurations of the shear reinforcement and different numerical modelling approaches of the FRP composites. Moreover, three dimensional finite element models have been generated using ANSYS 17.2 software in order to evaluate the influence of different parameters on a concentrically loaded RC column under a load of 80% of its concentric capacity. In specific the influence from varying stirrup cross section, stirrup centre distance, FRP configurations, different base materials, namely CFRP and GFRP and different modelling approaches for the FRP is evaluated. The results show almost insignificant stress differences for the critical height between the different stirrup arrangements, the different FRP configurations and the different base materials used. However, significant differences in the confinement action of the FRP occur due to different modelling approaches of the FRP composite. The results from the FE modelling compared to hand calculations are in close agreement.

Sammendrag

Forsterkning av armerte betongsøyler med fibervev er en effektiv måte å øke søylens kapasitet på. Metoden med bruk av utvendig pålimt fibervev er en forsterkningsmetode som har blitt mer og mer bruk gjennom de siste tiårene, grunnet dets gode mekaniske egenskaper samt dets mangfoldige bruksområder. Forholdsvis mye forskning har blitt utført på relativt korte søyler, med forskjellige konfigurasjoner av fibervev samt forskjellige mengder skjærarmering. Mindre forskning har derimot blitt utført på lengere betongsøyler som er vanlig å benytte innenfor byggenæringen, hvor den kritiske søylehøyden med henblikk på skjær krefter har blitt studert i detalj. Selv om interaksjonen mellom betong og fibervev har undergått mye forskning, er det ulike måter å modellere fiberveven og interaksjonen mellom hvert lag med laminat som fortsatt er åpent for mer forskning. Hovedformålet med denne oppgaven er derfor å utforske en armert betongsøyles oppførsel i skjær innenfor søylens kritiske skjærhøyde med henblikk på ulik konfigurasjoner av fiberforsterkning, forskjellig mengde med skjærarmering og forskjellige modelleringsmetoder av fiberveven. Flere 3D modeller basert på elementmetoden ble laget ved hjelp av ANSYS 17.2, hvor de ulike parameternes påvirkning på en konsentrisk lastet betongsøyle med en last tilsvarende 80% av dens aksiale kapasitet ble studert. Mer eksakt har ulike tverrsnitt med skjærarmering og innvirkningen fra ulike senteravstander, ulike fibervevkonfigurasjoner, forskjellige grunnmaterialer for fiberveven (karbonfiber samt glassfiber), samt forskjellige modelleringsmetoder for fiberveven blitt studert. Resultatene viser nesten ikke-signifikante spenningsforskjeller for den kritiske skjærhøyden med henblikk på forskjellige konfigurasjoner av skjærarmering, forskjellige konfigurasjoner av fibervev og de forskjellige grunnmaterialene benyttet i fiberveven. Derimot vil signifikante forskjeller i omsnøringstrykket fra fiberveven oppstå som følge av forskjellige modelleringsmetoder av fiberveven. Resultatene fra de numeriske modellene dannet ved hjelp av elementmetoden stemmer godt overens med utførte håndberegninger.

Table of contents

List of figures

Figures in Appendix

List of tables

List of symbols

FRP-Fibre-reinforced polymers

CFRP- **carbon** fibre reinforced polymer

GFRP-**glass** fibre reinforced polymer

f_{ck}- the characteristic concrete strength for a cylinder after 28 days

f_{ctm} - the average axial tensile strength for concrete

f_{yk} - the characteristic yield strength for the reinforcement

A_c - gross area of the concrete column

α_{cc} - coefficient for load duration and inconvenient application of the load

γ_c - partial safety factor for the concrete

γ_s - partial safety factor for the steel

c_{nom} - nominal concrete cover

$c_{min,b}$ - cover due to bonding

$c_{min,dur}$ - cover due to environmental effects

$\Delta c_{dur,\gamma}$ - parameter for safety

$\Delta c_{dur,\mathrm{st}}$ - reduction of cover due to the use of stainless steel

$\Delta c_{dur,add}$ - reduction of cover due to extra protection measures

λ - slenderness factor

ε - strain

Equations

1 Introduction

1.1Background

Over the last decade the use of fibre reinforced polymers (FRP) has experienced a continuous surge in structural engineering applications all around the world. The main reason is that many civil engineering structures are becoming structurally or functionally deficient after many years in service (Yu 2011). Many of the structures are designed with older design codes, which also make them more vulnerable if extreme events would occur. Retrofitting of exciting structures are in many cases needed in order to meet with the current codes and standards (Parvin & Brighton 2014). Other reasons for retrofitting of such structures can also be the deterioration, attributed to aging of the structure, steady increase in loading or deterioration due to environmental attacks (Yu 2011). FRP characteristics such as high strength, high tensile modulus, light-weight, installation facilities and corrosion resistance have all contributed in creating greater interest for the use of FRP in structural repair and strengthening applications (Yu 2011). Strengthening with externally wrapped FRP can be applicable within different types of reinforced concrete structures such as columns, beams, slabs, walls, chimneys, tunnels and silos (Khalifa et al. 1998). The use of FRP for structural strengthening can generally be classified into flexural strengthening, improving the confinement and ductility of compression members, as well as shear strengthening (Khalifa et al. 1998).

It has been proved that confinement of a compressively loaded column increases its ductile behaviour and provides a considerable plastic hardening behaviour. This behaviour is very different from the one of unconfined concrete columns that behave in a quasi-brittle or strain-softening manner (Dandapat et al. 2011). This improved property when using confining action, has governed the design and explains the use of FRP composites in reinforced concrete columns. FRP confined concrete columns are said to be under passive confinement (Dandapat et al. 2011), implying that under a moderate load the column remains within its linear-elastic range, so the confinement has little effect on the overall force-deflection behaviour of the column. This is because the column achieves only a small amount of lateral displacement within the elastic range, since the loads are relatively small. However, when more load is applied to the column and the post-elastic state is reached, even small stress changes within the column will lead to comparatively larger lateral displacements of the column (Dandapat et al. 2011). This results in having higher internal pressures on the FRP and mobilizing higher confining stresses in the composite material. It is these confining stresses that according to Dandapat et

al. (2011) limit the growth of tensile cracks in the concrete, resulting in achieving significant higher failure loads of the concrete members .

When modelling the interaction between concrete and FRP as well as between the FRP layers, a perfect bond is often assumed for the contact surfaces interface. However, in reality this is not always the case, since relative tangential slip or normal gaps at the interface may occur. According to Dandapat et al. (2011), tangential slip and normal gaps can typically occur when the interfacial bond undergoes degradation or damage during the loading process.

The main Fibre-Reinforced Polymer types used for retrofitting purposes are CFRP and GRFP, with carbon (C) and glass fibres (G) respectively. Each of these composites has different properties and different areas of use. CFRP composite has more tensile strength than GFRP whereas GFRP achieves greater strain capacity than the CFRP. The retrofitting technique of RC concrete columns with FRP can both be used as a component that increases the load carrying capacity, or as a component that that increases the safety of structures. In this way, the environmental effects on the concrete such as carbonation and chloride-induced corrosion (Dhakal 2014; Yu 2011) are also reduced. Retrofitting with FRP has been seen as a great economical alternative to conventional methods as RC jacketing and steel jacketing or even replacement of existing structures in order to achieve satisfying capacities (Yu 2011). The application of FRP laminates is also a fully reversible retrofitting technique (Hollaway & Teng 2008), which means that any material used for strengthening as well as the layers of adhesive, may be completely removed from the structure and be recycled if more advanced techniques will be developed in the future.

1.2 Objectives

The objectives of this thesis is to create an accurate and realistic model of a typical circular reinforced concrete column that is commonly used in structural engineering applications, using a highly recommended finite element software, ANSYS, and to investigate the shear stress behaviour within the critical height of the column. Research has been conducted (Belouar et al. 2013; Karim et al. 2016; Moshiri et al. 2015) on the behaviour of short RC columns with different configurations of FRP and different stirrup ratios. However, significantly less research has been conducted on taller RC columns typically used in structural engineering applications, where the critical height of the column with respect to shear has been studied in detail. In specific is the influence from varying stirrup cross section, stirrup centre distance, FRP

configurations, different base materials, namely CFRP and GFRP, and different modelling approaches for the FRP, evaluated when the column still is within the linear-elastic range.

1.3 Scope of the thesis

The retrofitted column is only loaded with a static concentric axial load. The reason for this is that the static load on the column in most cases is the dominating one under normal conditions. This is also valid for Norwegian constructions where seismic loads are not significant. The eccentricity of the column is omitted in this thesis. The critical height with respect to shear is the region where extra reinforcement must be added in order to enhance the shear behaviour of the column. For the column studied in this thesis is the critical height of 350mm from each end of the column. The aggregates are expected to be evenly distributed giving an even stress distribution. The FRP has been added to the column with the dominating fibre direction in the hoop direction. The parametric study is conducted within the linear-elastic range of the concrete with a load of 80% of the concentric capacity of the RC column.

2 Theory

2.1 The finite element procedure

The finite element analysis determines the overall behavior of a structure by dividing it into a number of simple elements (Kachlakev et al. 2001), where each of these simple elements will have well-defined mechanical and physical properties. The initial physical problem will typically involve a structural component that is subjected to a certain load. In order to idealize physical problems to a mathematical model, certain assumptions are needed to be made such as boundary conditions and geometry, that together lead to differential equations that governs the mathematical model (Bath 2014). It is the finite element analysis that solves this mathematical model. The finite element solution technique is a numerical procedure, it is therefore necessary to assess the accuracy of the solution. If the accuracy is not acceptable, the numerical solution (finite element solution) has to be repeated with refined solution parameters until a sufficient accuracy is reached (Bath 2014). Such a refined solution parameter can be a mesh refinement.

2.2 Element types and interface definitions used in ANSYS

2.2.1 Reinforced concrete

SOLID65 elements can be used for the 3D modelling of reinforced concrete. This element is able to crack under tension in three orthogonal direction, crush under compression, deform plastically and creep (ANSYS 2016). In SOLID65 is crushing defined as the complete deterioration of the structural integrity of the material (e.g. material spalling). When crushing have already occurred, the material strength is assumed to be degraded to an extend that the stiffness contribution from a certain integration point of an element can be ignored (ANSYS 2016). The SOLID65 element is defined by eight nodes with three degrees of freedom (DOF) in each node, -translations in x, y and z direction. The treatment of nonlinear material properties is the most important aspect of this element and the node location and geometry of the element is given in the Figure 2.1 (ANSYS 2016).

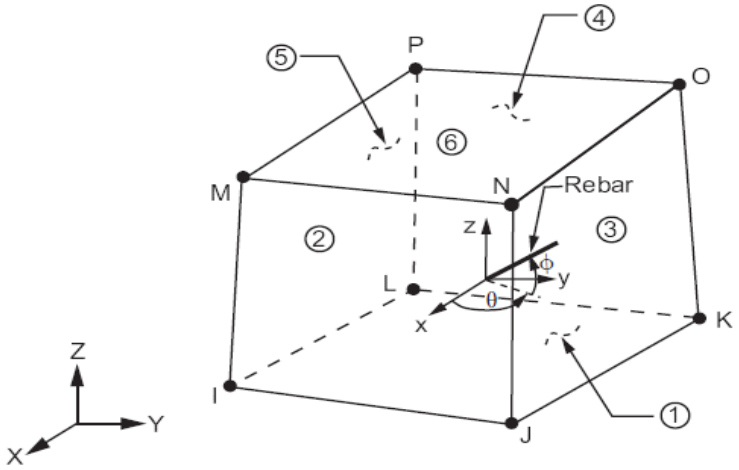

Figure 2.1. SOLID65, the 3D element used to model the reinforced concrete.

In ANSYS 17.2 are two methods supported for modelling of reinforced concrete, namely the discrete and smeared method. Discrete method allows reinforcement bars to be accounted for individually. The smeared reinforcing method is applicable for modelling clusters of reinforcement fibres appearing in layer or sheet form (ANSYS 2016). Each layer of the fibres is simplified as a homogenous membrane having unidirectional stiffness. The SOLID65 element has one solid material and up to three rebar materials. The rebar specifications in ANSYS are set as real constants for the material type, volume ratio and the orientation angle. The volume ratio is defined as the rebar volume divided by the total element volume, and the orientation is defined by two angles given in degrees, relative to the element coordinate system (ANSYS 2016).

2.2.2 FRP

SOLID186 elements can be used to model the fibre-reinforced polymers. The 3D elements consists of 20 nodes, which exhibits a quadratic displacement behaviour. Each node have three degrees of freedom in each node, -translation in x, y and z direction (ANSYS 2016). The element supports plasticity, creep, stress stiffening, large deflection and large strain capabilities. SOLID186 elements are available in two forms, i) Homogenous Structural Solid shape which is well suited for modelling irregular meshes (those produced by CAD/CAM systems) and ii) Layered Structural Solid shapes, which are well suited to model layered thick shells or solids

(ANSYS 2016). The geometry and node location for Homogenous Structural Solid and Layered Structural Solid are shown in Figure 2.2 a. and 2.2 b., respectively (ANSYS 2016).

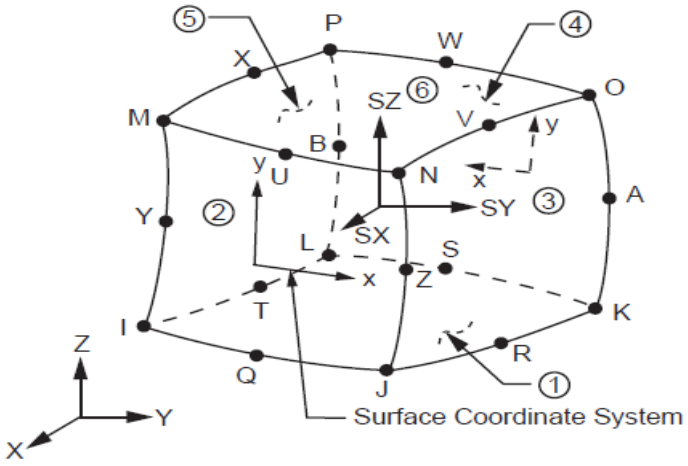

Figure 2.2a. Homogenous Structural Solid.

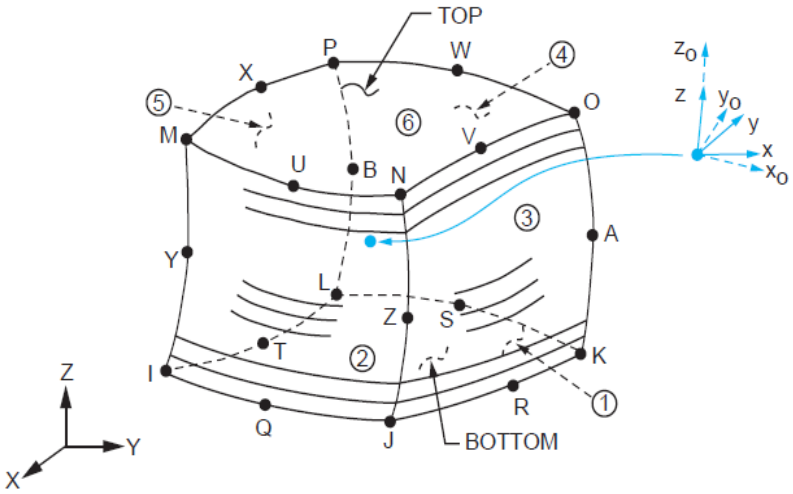

Figure 2.2 b. Layered Structural Solid.

2.2.3 Epoxy

There are different approaches that can be used in order to model the interface between concrete and FRP and between each FRP laminate layer. ANSYS provides the user with three different approaches to model these contact interaction i.e. using contact elements, create constraint equations or by using coupled degrees of freedom (ANSYS 2016). The approaches of

constrained equations and coupled degrees of freedom are often being used when some distinctive features of a connection cannot be adequate modelled with the use of elements only. Such distinct features are e.g. rigid regions, pinned structural joints, sliding symmetry boundaries, periodic conditions and other special inter-nodal conditions (ANSYS 2016).

2.2.3.1 Contact definition

Contact problems are according to ANSYS (2016) divided into two general classes: rigid-to-flexible or flexible-to-flexible. When dealing with rigid-to-flexible contact problems, one or more of the contacting surfaces is treated as rigid, meaning that it has much higher stiffness relative to the deformable body it contacts. Any time a soft material will be in contact with a hard material the contact problem is generally assume as a rigid-to-flexible one. Flexible-to flexible is a more common type of contact problems (ANSYS 2016). In these cases both or all contacting surfaces are regarded as deformable, meaning they have similar stiffness. Two main problems when defining the contact are: i) it is generally difficult to know which regions that will come in contact a priori, before running the simulation and ii) the fact that most contact problems have to account for friction. The frictional forces that are developed are very complex to describe since there are several contact friction laws and friction models, which are all nonlinear, often leading to nonconvergence of the numerical analysis (2016). In cases where there is no friction and the interaction between the bodies is always bonded, the use of internal multipoint constraints (MPC) is considered as a good alternative. Other ways to model these kind of contact problems are according to ANSYS (2016), by using constraint equations or coupled degrees of freedom. The external constrain equation or the coupled degrees of freedom are only suitable in small strain applications.

In ANSYS Mechanical APDL, there are three approaches to define the contact interactions using elements: pair- based contact definition, general contact definition and node-to-node elements. Both the pair based contact definition and the general contact definition uses surfaces to define the contact. These contact definitions are suitable for solving either small-displacement or large -displacement contact problems. If the location of the contact is known beforehand and the contact problem involve relative small sliding between the contacting surfaces, the node-to-node contact elements are often used. Each of these contact formulation have some unique advantages and limitations, but in general according to ANSYS (2016), it is recommended to use either pair based contact definition or the general contact definition. By specifying the following can both pair based contact and general contact be defined:

- Surface definition for the bodies/parts that potentially could be in contact (flexible/rigid)
- Interaction for the surfaces that interact with one another
- Contact interface behaviours
- Contact properties and control parameters
- Contact formulations and settings

When using a general contact definition, general contact surfaces need to be defined. The contact elements (CONTA171-CONTA174) are overlaid on the exterior surface of deformable bodies, whereas the target elements (TARGE169 and TARGE170) are used to cover standalone rigid bodies. Some advantages of the general contact definition over the pair-based contact definition are listed below (ANSYS 2016):

- The general contact surfaces are formed automatically based on physical parts and the geometric shapes in the model.
- The contact searching is executed among all general contact surfaces, so that contact between multiple thin layers are accounted for.
- The general contact formulation is by default settings automatically designating contact and target pairing for contact interactions.
- In a 3D general contact definition, the surface-to-surface contact formulation may be combined with the 3D edge-to-surface formulation.
- The general contact formulation is mainly useful when it is difficult if not impossible to determine the contact pairs between many parts.

According to ANSYS (2016), the pair-based contact approach gives a more robust solution and is usually more efficient than the general contact definition. The general contact formulation is on the other hand mainly useful when it is difficult or even impossible to determine the contact pairs between many parts (ANSYS 2016). The main differences between these two types of contact definition is the input syntax used. For the pair-based contact formulation, the "Augmented Lagrange method" is used as default by the program, but for the general contact formulation, the "Penalty method" is used as default. For the pair-based contact formulation in ANSYS, five contact models are available: node-to-node, node-to-surface, surface-to-surface, line-to-line and line to surface. Each of these models use a different set of contact elements and are applicable for different types of problems (ANSYS 2016). However, this thesis will only emphasize on the use of surface-to-surface contact elements, and not the use of node-to-node contact elements.

Surface-to-surface contact elements

This approach can be used in both rigid-to-flexible and flexible-to-flexible surface-to-surface contact problems. In order to create a contact pair using contact elements, it is necessary to define a “contact surface” and a “target surface”. The same real constant number have to be assigned to both the contact and target elements (ANSYS 2016). A target surface is modelled using TARGE169 and TARGE170, for 2D and 3D problems respectively, while the contact surface is modelled using CONTA171, CONTA172, CONTA173 and CONTA174. The first two contact elements are used to model 2D problems and the last two are used to model 3D problems. Following are some advantages of the use of surface-to-surface elements over the node-to-node elements (ANSYS 2016):

- The surface-to-surface elements support lower and higher order elements on the contact and target surface, e.g. by the use of corner-noded or midside-noded elements.
- There is no restriction on the shape of the target surface when using surface-to-surface elements.
- Surface-to-surface elements provide better contact results in typical engineering applications such as normal pressure and contour plots for frictional stresses.

The contact elements are constrained against penetrating the target surface however, the target elements are able to penetrate through the contact surface. For a rigid-to-flexible problem, the designation of the target surface is relatively easy. The surface that is the most rigid should be assigned the target surface and the most deformable surface should be assigned the contact surface (ANSYS 2016) Choosing wrong surfaces for the target and contact elements can lead to a different amount of penetration and thus affect the solution accuracy. Some guidelines from ANSYS Help Viewer are given below:

- If one surface has a finer mesh than the other, the surface with the finer mesh should be the contact surface, and the surface with the coarser mesh should be the target surface.
- If one surface is stiffer than the other, the softer surface should be the contact surface and the stiffer surface should be the target surface.
- If one surface is larger than the other, i.e. if one surface surrounds the other surface, the outer surface should be the target surface and the inner surface should be the contact surface.
- If a convex surface is expected to come into contact with a concave or flat surface, the flat/concave surface should be the target surface.

- If higher-order elements underlay one of the external surfaces, where the external surfaces consists of lower-order elements, the surface with the higher order elements should be assigned the contact surface and the surface with the lower-order elements should be the target surface.

Symmetric and asymmetric contact.

Asymmetric contact is defined as having all target elements on one surface and all contact elements on the other surface (ANSYS 2016). This is sometimes called “one-pas contact”. Usually, this contact modelling is the most efficient way to model surface-to-surface contact. Asymmetric contact will however, under some circumstances not perform satisfactorily. In such cases, each surface can be designated to both a target and a contact surface, where two sets of contact pairs on each surface will be created using symmetric contact. The symmetric contact is less efficient compared to the asymmetric one. However, many analyses requires its use in cases where it is desire to reduce the penetration. Some situations where symmetric contact is required are shown below (ANSYS 2016):

- No clear distinction between the contact and the target surface.
- If both surfaces have very coarse meshes, the symmetric contact algorithm will enforce contact constrain conditions at more locations at the surface, than the asymmetric contact algorithm would do.

Contact algorithms

For surface-to-surface problems, it is necessary to choose a mathematical formulation that should be used in the contact region in order for the ANSYS code to enforce the contact conditions. ANSYS offers following contact algorithms when dealing with surface-to-surface contact problems:

- Penalty method
- Augmented Lagrange method
- Lagrange multiplier on contact normal and penalty on the tangent plane
- Pure Lagrange multiplier on contact normal and the tangent plane
- Internal multipoint constraint

By the penalty method, a contact “spring” is used to establish a relationship between the two contacting surfaces. The spring stiffness is called the contact stiffness FKN and is updated between each iteration (ANSYS 2016). Other real constants that also need to be defined for this

method are: target penalty stiffness factor FKT, penetration tolerance factor FTOLN, and allowable elastic slip SLTO. This formulation is useful when the contact occurs on an edge or a vertex. The contact detection for this method is conducted on the integration points.

The augmented Lagrange method is in fact an iterative series of penalty methods (ANSYS 2016). If one compare the penalty method with the augmented Lagrange method, the augmented Lagrange method usually lead to better conditioning and is less sensitive to the magnitude of the contact stiffness. The drawback with the augmented Lagrange method is that it leads to more iterations, especially if the deformed mesh becomes too distorted. The contact detection is as with the penalty method, taking place on the integration points.

The Lagrange multiplier on contact normal and the penalty method on the frictional plane is an alternative contact algorithm. It enforces zero penetration and allows a small amount of slip during sticking contact conditions (ANSYS 2016). This method requires chattering control parameters, penetration tolerance factor FTOLN and maximum allowable tensile contact pressure TNOP as well as the allowable elastic slip SLTO. This method enables contact by both material nonlinearities and large sliding. The contact detection for this method is however, only conducted at the nodes.

With pure Lagrange multiplier on both the contact normal and the tangent plane, a zero penetration is enforced when the contact is closed and a “zero slip” enforced when sticking contact occurs (ANSYS 2016). This method does not require normal penalty stiffness factor (contact stiffness) or the tangent penalty stiffness. However, it requires penetration tolerance factor and allowable tensile contact pressure. The method often requires additional iterations in order to stabilize the contact conditions. With this method, the contact detection is conducted at the nodes.

The internal multipoint constraint (MPC) is used in conjunction with bonded contact and no separation contact in order to model several types of contact assemblies and kinematic constraints (ANSYS 2016). This contact formulation creates a linear way to connect contacting bodies without the needed of defining any stiffness parameters. When the program uses this method, internal multipoint constraint equations are built based on the contact kinematics. The contact detection is conducted at the nodes.

Setting the real constants

ANSYS uses real constants and KEYOPTs to control contact behaviour when using surface-to-surface contact elements. For some of the real constants it is possible to specify both positive values and negative values, where a positive value is interpreted by the program as a scaling factor and a negative value as an absolute value.

Contact stiffness and allowable penetration

The normal stiffness is governing the amount of penetration that will occur between the target and contact surfaces and the tangential stiffness is governing the amount of slip in sticking contact (ANSYS 2016). A higher stiffness value can lead to decreased amounts of penetration/slip, but also ill conditioning of the global stiffness matrix and difficulties with the convergence. Smaller stiffness values can on the other hand lead to increased amounts of penetration/slip and to an inaccurate solution. The desired combination is therefore a stiffness that is high enough to give a penetration/slip that is acceptably small and a well-behaved contact problem with respect to the convergence of the model. ANSYS has default values for the following stiffness and penetration parameters: normal penalty stiffness factor FKN, tangent penalty stiffness factor FKT, penetration tolerance factor FTOLN and allowable elastic slip SLTO.

A normal range for the normal penalty stiffness factor is from 0.1 up to 10, where the default value is 1.0. Penetration tolerance is often used in conjunction with the augmented Lagrange method. The penetration tolerance factor is based on the depth of the underlying solid, shell or beam element and is less than 1.0, with a default value of 0.1 (ANSYS 2016). This factor will determine if the penetration compatibility is satisfied. In a case of very small penetration tolerance, a large normal contact stiffness is often needed. ANSYS is automatically updating the tangential contact stiffness based on current contact normal pressure and the maximum allowable elastic slip. The default tangential contact stiffness is by the program put to 1.0. Allowable elastic slip is used to control the maximum sliding distance when the tangential contact stiffness is updated at each iteration.

Contact detection

The surface-to-surface contact elements use Gauss integration points as default for the contact detection (ANSYS 2016). This generally produce more accurate results than the nodal contact detection, which uses the nodes themselves as integration points. Figure 2.4 (ANSYS 2016)

show on the left, contact detection on Gauss integration points (between the red nodes) and on the right, contact detection on the nodes (the red circles).

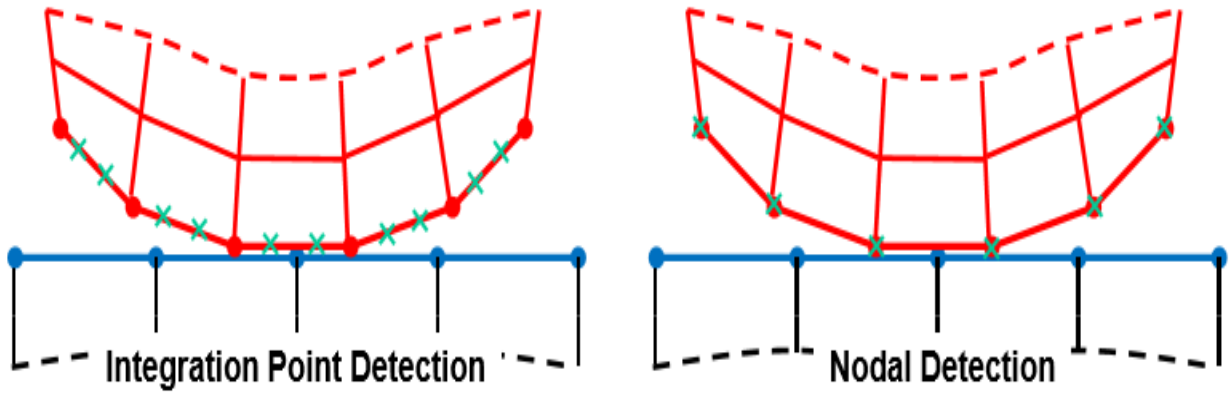

Figure 2.3. Contact detection for a typical surface-to-surface contact problem.

Pinball region

The pinball region is according to ANSYS Help Viewer, the distance between the integration points of the contact elements and the code-calculated or user defined distance to the corresponding target surface. The integration points can be either Gauss points or nodal points. In 2D problems is the pinball region a circle, while in 3D problems it is a sphere centred about the Gauss point.

Different contact surface behaviours

The surface-to-surface contact elements in ANSYS support different mechanical contact models as well as the normal unilateral contact models. The different contact surface behaviours that can be defined in ANSYS are shown below:

- Standard
- Rough
- No separation
- Bonded
- No separation always
- Bonded always

- Bonded initial

For standard unilateral contact, the normal pressure is equal to zero if contact occur. No sliding will occur for a perfectly rough behaviour of the contact surface. This case correspond to an infinite friction coefficient and ignores the material properties. In no separation contact, the contact and target surfaces are tied (although sliding is permitted) for the remaining time of the analysis, once the contact between the two surfaces is established. Bonded contact imply that the contact and target will act as bonded in all direction once contact is established. In non-separation contact, where contact detection points are initially inside the pinball region, these detection points are always attached to the target surface (sliding is permitted). The "Bonded always" contact is almost the same as the non-separation contact, only that no sliding is permitted and the contact and target surfaces are fully bonded. In a "Bonded initially" contact, the contact detection points that are initially closed will remain attached to the target surface and the contact detection points that are initially open remain open through the analysis.

Contact Wizard

The *contact wizard* for pair-based contact problems is shown in Figure 2.4 (ANSYS 2016) and leads the user through the process of manually creating contact pairs. The wizard supports both rigid-to-flexible and flexible-to-flexible contact and surface-to-surface and node-to-surface configurations (ANSYS 2016). In the *contact wizard* are also surface-based constraint contact pairs supported. In order to define contact it is necessary to mesh a part of the model first. If a rigid-to-flexible contact is desired, only the model part that will be used for the flexible contact surface need to be meshed, before the *contact wizard* is launched. For a flexible-flexible contact, all the contact surfaces can be meshed before the c*ontact wizard* is launched. Within the *contact wizard* can different parameters be adjusted in order to e.g. eliminate small gaps or penetrations caused by numerical round-off due to mesh generation (ANSYS 2016). However, the changing of the parameters in the *contact wizard* is not intended to correct gross error in either the mesh or the geometrical data (ANSYS 2016). The figure below shows the user face of the *contact wizard* (ANSYS 2016)

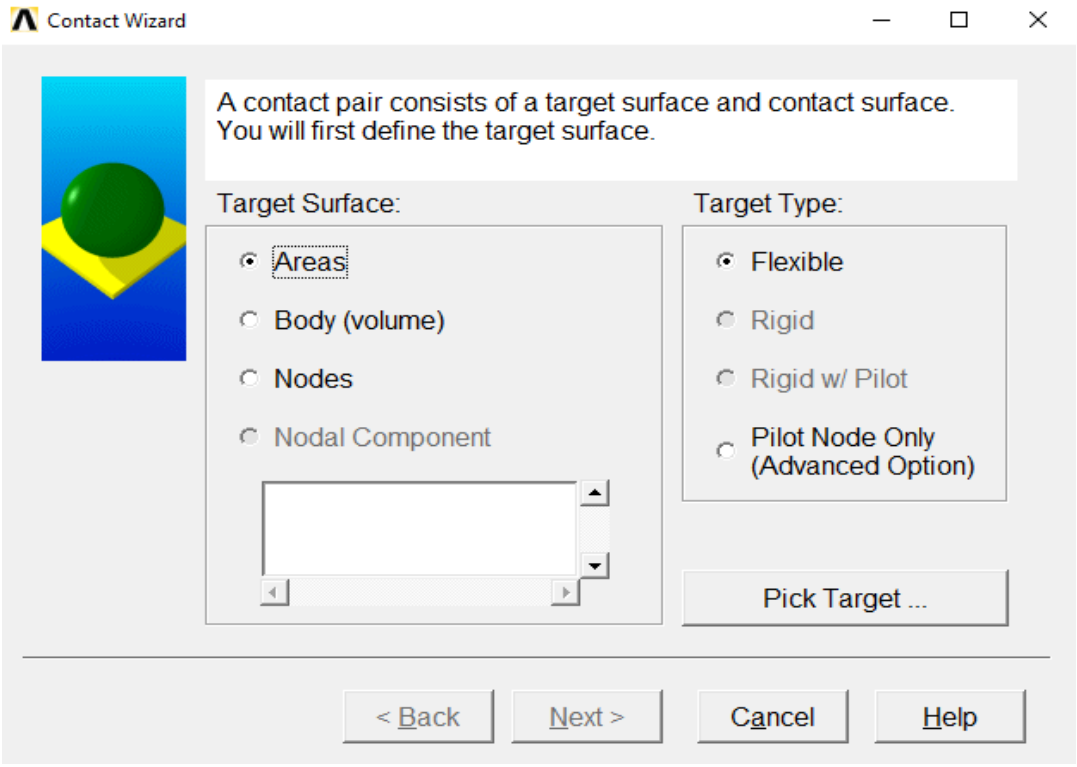

Figure 2.4. The Contact Wizard for pair-based contact problems.

Theoretical contact formulation consider a close to perfect geometry however, when a physical problem is discretized into a finite element model, some nodes will penetrate the opposite element, leading to ill-conditioning of the model (ANSYS 2016). In most of the cases, this is unwanted and the key option for excluding the initial penetration may be used in order to avoid this problem. The idea behind excluding initial penetration (overclosure) is shown in Figure 2.5 (ANSYS 2016).

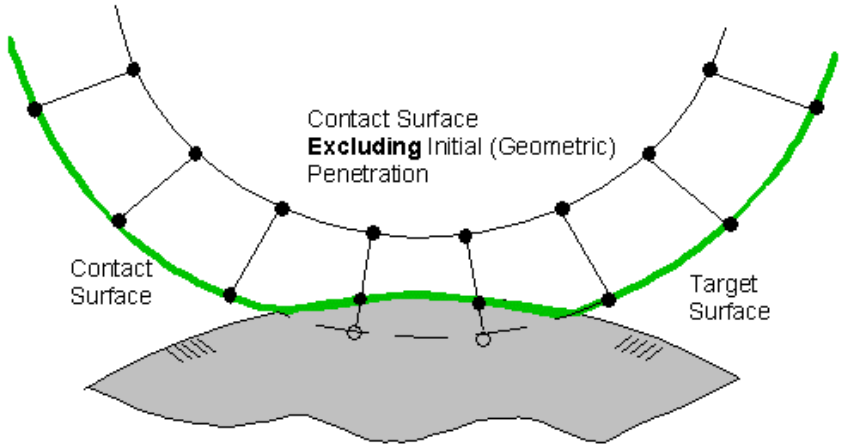

Figure 2.5. Principle behind the exclusion of the initial penetrations (overclosure).

The different equation solvers used by ANSYS

In the solution phase of an analysis is the computer solving the simultaneous set of equations that are generated by the finite element method (ANSYS 2016). ANSYS have following methods available for solving the simultaneous equation: sparse direct solution, Preconditioned Conjugate Gradient (PCG) solution, Jacoby Conjugate Gradient (JCG) solution, Incomplete Cholesky Conjugate Gradient (ICCG) solution and Quasi- Minimal Residual (QMR) solution. The sparse direct solution is the only solver that uses direct elimination and is in many cases more robust than the iterative solvers. The other mentioned solvers are iterative solvers, which in many cases uses less computation time and are more scalable for parallel performance (ANSYS 2016). The direct elimination uses primarily a Gauss elimination, involving solving for an unknown vector of variable [u] as shown in Equation 2-1. By iterative solvers is the solution obtained through an iterative process, which successively refines an initial guess to a solution that is within an acceptable tolerance of the exact solution (ANSYS 2016).

Equation 2-1. System used to solve a FE problem with an iterative approach.

$$[K][u] = [F] \tag{2-1}$$

Where:

- [K] is the global stiffness matrix
- [u] is the global vector of nodal unknowns
- [F] is the global applied load

The process of direct elimination involves decomposing (factorization) of the matrix [K] into a lower and an upper triangular matrix [K] = [L][U]. The triangular system [L] and [U] are used for forwards and backwards substitutions until the solution vector [u] is computed (ANSYS 2016). The system shown in Equation 2-2 is solved iteratively (ANSYS 2016).

Equation 2-2. System used to solve a FE problem with direct elimination.

$$[K][u] = [F] \tag{2-2}$$

Where:

- [K] is the global coefficient matrix
- [u] is the unknown vector
- [F] is the global load vector

Sparse direct solution

This method is based on a direct elimination of equations, as opposed to iterative solvers. The sparse direct solver has large disk or in-core memory requirements. The reason is that direct elimination requires as mentioned above, the factorization of an initially very sparse linear system of equations into a lower and upper triangular matrix. Sparse direct solution is a solver method often used in e.g. nonlinear or transient analyses. This direct elimination solver has an ideal model size of 100 000+ DOF (ANSYS 2016).

Preconditioned Conjugate Gradient solution [PCG]

This iterative solver starts with an element matrix formulation. The PCG solver is not factoring the global matrix, but instead assembles the full global stiffness matrix calculating the DOF solutions by iterating until convergence is achieved. The Preconditioned Conjugate Gradient uses a certain preconditioner that is depending on the material properties and the elements (ANSYS 2016). The PCG solver show good performance for most static and certain nonlinear analysis and the ideal model size is 500 000 to 20 000 000+ DOF (ANSYS 2016).

Jacoby Conjugate Gradient solution [JCG]

The JCG solution is an iterative solver, which also starts with an element matrix formulation. The JCG is not factoring the global matrix, but instead assembles the full global stiffness matrix calculating the DOF solution. This calculation is done by iterating until convergence is achieved (ANSYS 2016). By this solver, the diagonal of the stiffness matrix is used as a preconditioner.

The Jacoby Conjugate Gradient, often used in thermal analysis, is best suited for the scalar field analyses that involve large, sparse matrices. An ideal model size for this solver is according to ANSYS Help Viewer, 500 000 to 20 000 000+ DOF.

Incomplete Cholesky Conjugate Gradient solution [ICCG]

The Incomplete Cholesky Conjugate Gradient is an iterative solver that operates quite similar to the Jacoby Conjugate Gradient with some exceptions as following (ANSYS 2016):

- For matrices that are not well- conditioned, the ICCG solver is more robust than JCG.
- The ICCG solver uses a more sophisticated preconditioner than the JCG solver, which is the reason why the ICCG solver requires approximately two times more memory than the JCG solver.

Some fields of application for the ICCG solver are unsymmetrical thermal analyses and electromagnetic analyses. It is available only for static analyses, full harmonic analyses and full transient analyses. Some other useful application fields are structural and multiphysics, symmetric, unsymmetric, complex and definite or indefinite matrices. The ideal model size for this solver is 50 000 to 1 000 000+ DOF (ANSYS 2016).

Quasi-Minimal Residual [QMR] solution

QMR solution is an iterative solver with a main application field of electromagnetic analyses. The solver is only available for full harmonic analyses and it can be used for symmetric, complex, definite and indefinite matrices. This solver is more robust than the ICCG solver and its ideal model size is 50 000 to 1 000 000+ DOF (ANSYS 2016)

2.2.3.2 Alternative approaches to define contact

Coupled DOF's and constrain equation

When a model is generated, elements are typically used in order to define a relationship between different degrees of freedom and the nodes (ANSYS 2016). It is however, in some cases necessary to model distinctive features such as rigid regions, pinned structural joints, sliding symmetry boundaries, periodic conditions and other special intermodal connections, which cannot be adequately described using elements. In order to establish such associations among the nodal degrees of freedom, coupling and constraint equations can be used. These methods enables the user to link degrees of freedom in ways that are impossible for elements. External

constrain equations and coupled degrees of freedom are only suitable in small strain applications (ANSYS 2016).

Coupled degrees of freedom

If it is desired to force two or more degrees of freedom to take on the same, but unknown value, coupling of these DOFs is a good method to achieve this. A coupled set of DOFs contain a prime DOF and one or more other DOFs. When coupling occur, only the prime DOF will be retained in the matrix equation of the analysis, causing all the other DOFs in a coupled set to be eliminated. That value calculated for the prime DOF will be assigned to all the other DOFs in a coupled set. Some typical application fields for this method are as following (ANSYS 2016):

- Maintaining symmetry on partial models
- Forming pin, hinge, universal and slider joints between two coincident nodes
- Forcing parts of the model to behave as a rigid body

Constraint equations

Constraint equations combine the motion of one node to another node by creating a linear relationship between the nodal degrees of freedom (ANSYS 2016). This is a more general way to relate the degrees of freedom than using simple coupling. Some of the ways to create constrain equations are as following: direct method, by the creation of a rigid region or by tying dissimilarly meshed regions together (ANSYS 2016). In either way, the constraint equation must have the form shown below (ANSYS 2016):

Equation 2-3. The form of the constraint equation.

$$Constant = \sum_{I=1}^{N}(Coefficient\ (I) * U(I))) \tag{2-3}$$

Where:

- U (I) is the degrees of freedom of term (I)
- N is the number of terms in the equation

2.2.4 Modelling of the reinforcement

It is assumed by ANSYS that the cross section area of the fibre is small compared to the length of the fibre. In the program, only the axial stiffness is considered and the bending, torsion and transverse shear stiffness are all ignored (ANSYS 2016). The program adopts the same nodes and connectivity for the reinforcing elements and the base element, leading to the programs assumption of a secure bond between these two components. ANSYS has two different approaches to model the reinforcement: i) one can use the discrete approach or ii) the smeared approach. The discrete approach is used in order to model reinforcing fibres with nonuniform material, cross section or orientation. Each fibre is modelled separately as a spar having uniaxial stiffness (ANSYS 2016). Figure 2.6 from the ANSYS Help Viewer show the modelling of the reinforcement, with the discrete modelling approach on the left and the smeared modelling approach on the right. The smeared approach is used to model reinforcement fibres that appear in form of layers. Each fibre in a layer is treated with the same material properties, cross section and orientation as with a homogenous membrane having that same unidirectional stiffness (ANSYS 2016).

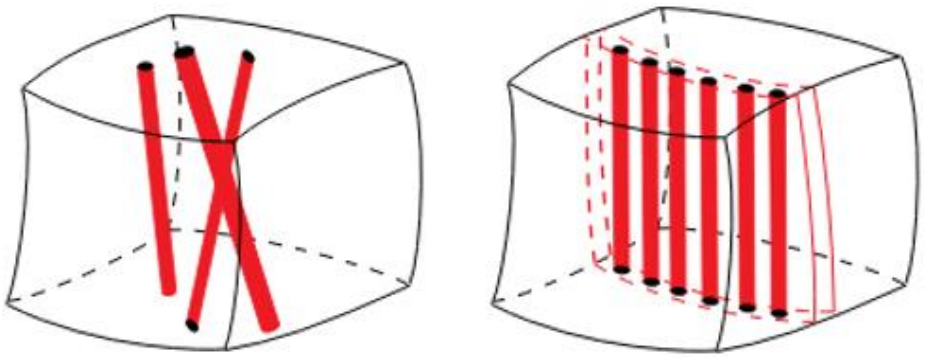

Figure 2.6. The different approaches to model the reinforcing fibres.

When the discrete modelling of the reinforcement fibres is used, it is possible to calculate the discrete rebar stresses and the yield of individual fibres. For the smeared approach, a much coarser mesh can be defined since this approach do not require the explicit modelling of the reinforcement fibres. A paper written by Barbosa and Ribeiro (1998) studies different approaches to model the reinforcement in a RC structure and compare the results obtained from the numerical analyses in ANSYS with experimental data. Both the smeared and discrete

approaches for the modelling of the reinforcement were compared against experimental data. The conclusion drawn from the research show that that despite employing relatively simple models for the reinforced concrete, a satisfactory prediction of the structural response of the RC member could be obtained. The orientation of the reinforcement fibres is shown in Figure 2.7 (ANSYS 2016) where θ is the angle in the xy-plane and φ is the angle from the xy-plane and towards the x-axis.

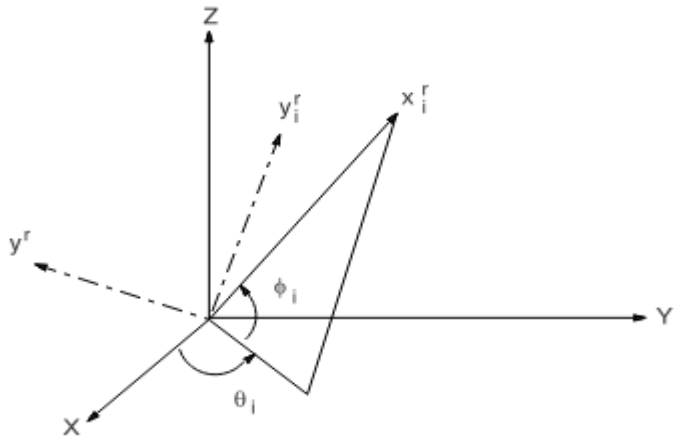

Figure 2.7. Orientation of the reinforcement fibres in a global 3D coordinate system.

2.3 Material properties

2.3.1 Concrete

The development of a model for concrete can be a challenging task. Reasons for this are mainly the different behaviour of concrete in compression and tension and the fact that concrete can be characterized as a quasi- brittle material (Bajer et al. 2007). The concrete will have a linear stress strain relation up to approximately 30-40% (Bajer et al. 2007; Shah et al. 1995) of the maximum compressive strength and a nonlinear behaviour until failure. The tensile strength of the concrete is approximately 8-15% of the compressive strength (Pawar & Pawar 2016). Due to low tensile strength is concrete very susceptible to cracks, which greatly can reduce the service life of a specimen in a certain environment (Audenaert et al. 2009). Figure 2.8 from Bangash 1989, shows the stress – strain relationship of normal weight concrete, with the behaviour in both the compressive range and the tensile range. As mentioned above, the concrete in compression will experience a linear elastic behaviour until approximately 30% of the maximum compressive strength. After passing this level, the stress and strains will increase gradually in a nonlinear behaviour approaching maximum compressive strength, ε_0. When ε_0 is reached, the concrete will start the softening and reach its ultimate strain capacity ε_{cu} . When ε_{cu} is reached, crushing failure of the concrete will occur. The concrete will in the tensile mode perform linear elastic approximately until the maximum tensile strength, σ_{tu} , is reached. When this point is reached, the concrete will crack and the strength will gradually go to zero (Bangash 1989; Kachlakev et al. 2001)

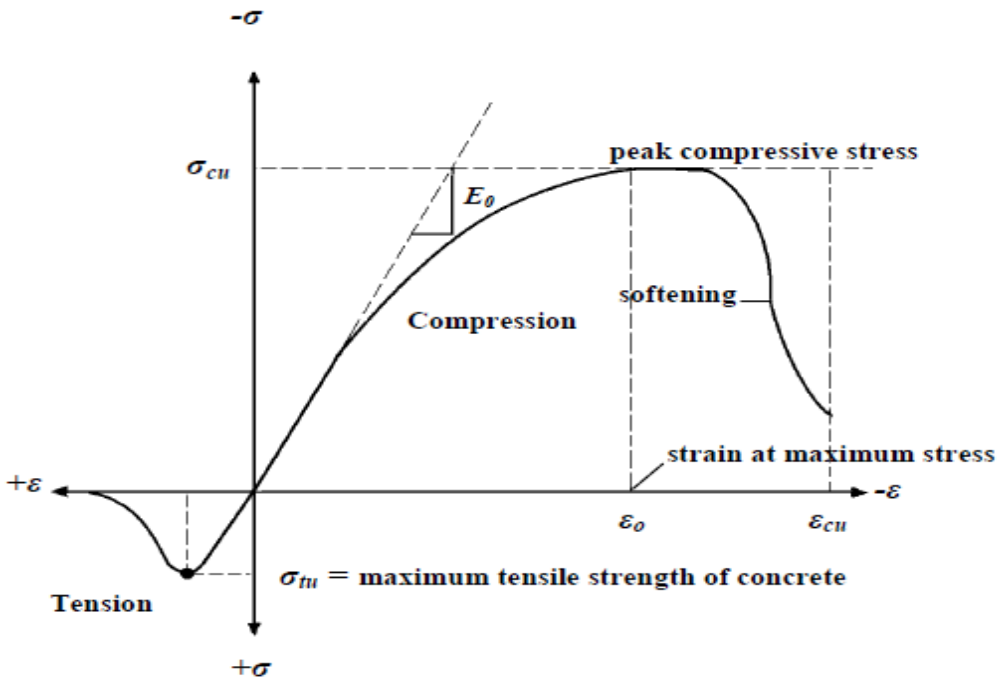

Figure 2.8. A typical stress - strain relationship for normal weight concrete.

Failure criteria for concrete.

Concrete has a certain failure criteria to fulfil in order to either crush or crack (William & Warnke 1975). The figure below shows a model that has the capability of predicting the failure of concrete. In order to define a failure surface of the concrete, it is necessary to determine the two strength parameters, ultimate tensile strength and ultimate compressive strength. According to the model proposed by William and Warnke (1975), the failure criteria for the concrete due to a multi axial stress state can be calculated as shown in Figure 2.9 (ANSYS 2016)

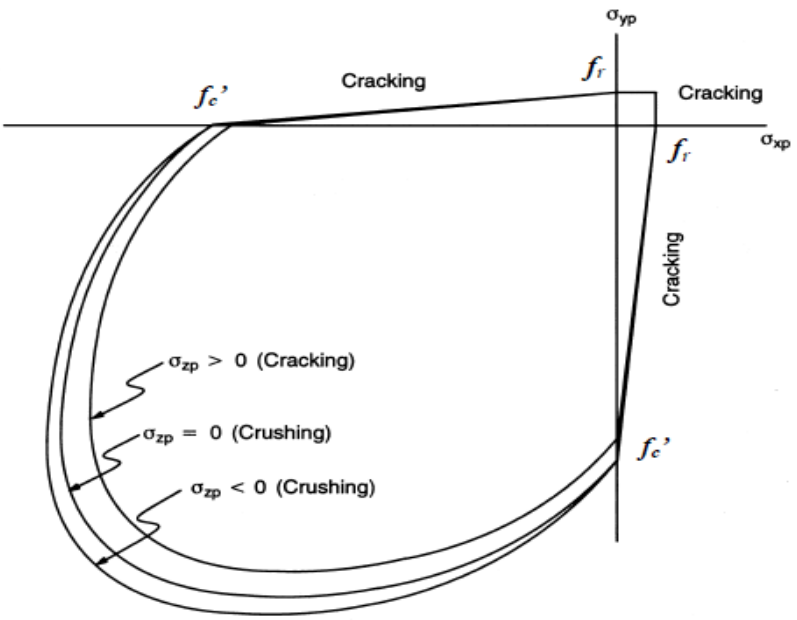

Figure 2.9. The 3D Failure surface for concrete.

The most significant nonzero principal stresses in the x and y direction are represented by σ_{xp} and σ_{yp}, respectively, as seen in Figure 2.9. There are three different failure surfaces shown as projections on the σ_{xp}- σ_{yp} plane. The mode of failure is a function of the sign of σ_{xp}, which is the principal stress in the z-direction. If $\sigma_{xp}$and σ_{yp} are both negative, meaning compression and $\sigma_{zp}$is slightly positive, cracking will be predicted in a direction perpendicular to σ_{zp}. If σ_{zp} is zero or negative, crushing will be predicted in a direction perpendicular to σ_{zp} (ANSYS 2016)

In order to implement in ANSYS the material model proposed by William and Warnke (1975), the following values need to be determined:

1. The shear transfer coefficient for an open crack
2. The shear transfer coefficient for a closed crack
3. Uniaxial tensile cracking stress
4. Uniaxial crushing stress (positive)
5. Biaxial crushing stress (positive)
6. Ambient hydrostatic stress state for use with constant 7 and 8
7. Biaxial crushing stress (positive) under the ambient hydrostatic stress state

8. Uniaxial crushing stress (positive) under the ambient hydrostatic stress state
9. Stiffness multiplier for cracked tensile condition

Typical shear transfer coefficient range from 0 to 1.0 where 0 represent a smooth crack (total loss of shear transfer) and 1.0 represent rough crack (no loss of shear transfer). Classification after these values can be used for both open and closed cracks (ANSYS 2016).

2.3.2 Steel reinforcement

Steel is an elasto-plastic material that by loading exhibits a linear elastic behaviour followed by a yield plateau, strain hardening, and stress drops until fracture occurs (Pawar & Pawar 2016). For the steel reinforcement, the behaviour is the same under both compressive and tensile loading, as shown in Figure 2.10 proposed by Pawar & Pawar (2016). The post-linear behaviour is described with the tangent modulus E_t.

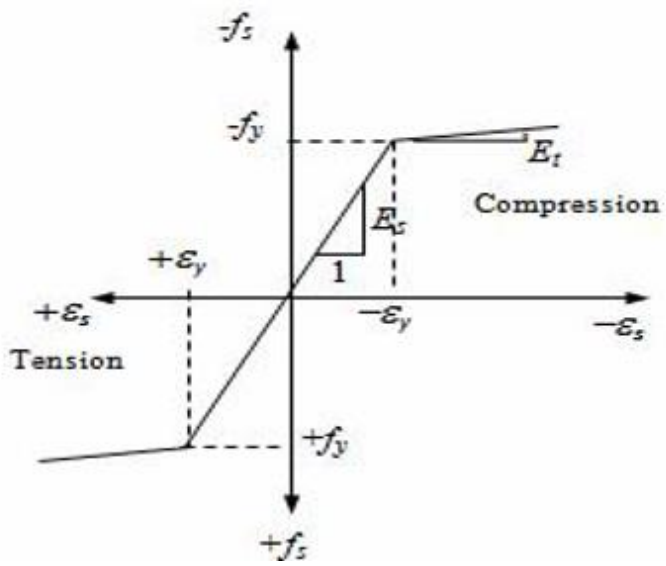

Figure 2.10. Stress-strain curve for the reinforcement.

Steel is the product of choice for reinforced concrete due to a combination of some unique factors listed below from the Concrete Reinforcing Steel Institute (2017):

- The elastic properties are similar under both tensile and compressive loads.

- Significant elongation under loading provides well-defined cracks in the concrete structure during overload conditions.
- Mainly uniform properties in all directions, where the shear strength will be similar to the longitudinal yield strength.
- The thermal expansion properties for concrete and steel are relatively similar, which will not lead to extra stresses and deflections of significance introduced from heating of the concrete structure.

2.3.3 FRP and epoxy

FRP is a composite material, which primarily is composed of reinforcement fibres and polymer matrix. The polymer matrix consists mainly of thermosetting raisins such as polyester, urethane methacrylate, vinylester, epoxy and phenolic (Yu 2011). They are isotropic materials that primarily are responsible for the load transfer. However, they can also perform several other duties. The matrix protects the notch sensitive fibres from abrasion as well as forming a protective barrier between the fibres and the environment, thus preventing attacks from moisture, chemicals and oxidation. The properties of the composites are determined by the following parameters: the properties of each fibre, the properties of the resin, the ratio of fibre to resin in the composite (Fibre Volume Fraction) and the geometry and orientation of the fibres in the composite (Yu 2011).

Classification of FRP

Depending on the base material of reinforcement fibres, FRP can be divided into three main categorises of glass, carbon and aramid (Cogswell 1992).

Glass fibres are widely used and one of the cheapest reinforcements available. Glass fibres are available in three main types. E-glass is the standard form and known as electrical grade. Its main features are the very low alkali content and good electrical, mechanical and chemical properties. C-glass has a high chemical resistance and often used where protection from corrosive environment is required. S-glass or also referred to as R-glass, has enhanced mechanical properties and is often used for aerospace applications (Yu 2011).

Carbon fibres are produced by a controlled oxidation and carbonisation of cellulose, pitch or polyacrylonitrile materials, also known as precursors (Yu 2011). The Aerospace industry has mainly been the driving force behind the development of carbon fibres. This was due to the

industry's need for a material that had both high strength, high stiffness and low weight (Chung 2012). Carbon fibres can as glass fibres come in various forms such as woven materials, chopper strand or continuous filaments. Carbon fibres however, have a slightly negative thermal expansion coefficient along the fibre axis. This mean that the fibres contract upon heating (Takenaka 2012). Carbon fibres can therefore be used to create forming composites with a longitudinal coefficient of thermal expansion of zero, since the polymer matrix will have a positive thermal expansion coefficient. A negative aspect with the carbon fibres is the limitation in the low impact resistance.

Aramid fibres belong to a class of materials known as liquid crystalline polymers. The fibres exhibit both a superior strength to weight ratio when compared to glass fibres and provide an excellent abrasion resistance in a composite. They are however poor in compression, offering typically 1/3 of their tensile performance (Yu 2011). A comparison of the mechanical properties for the different materials is presented in Table 2.1, based on Yu (2011) and a comparison of the tensile properties of CFRP and GFRP with mild steel is shown in the Figure 2.11 (Benzaid & Mesbah 2013). It is generally stated in Bulletin 14 from the International Federation of Structural Concrete (2001), that the carbon fibres are preferred for if strength increase is desire and glass (or aramid) fibres if ductility increase of a RC member is sought instead.

Table 2.1. Comparison of the mechanical properties for different fibre materials.

Fibre	Unit	Carbon	Glass	Aramid
Density	[x 10^3kg/m^3]	1.5-1.6	1.9-2.0	1.3
Tensile Modulus	[N/mm^2]	80 000-400 000+	38 000-45 000	70 000-75 000
Tensile strength	[N/mm^2]	1500-3000+	800-1200	800-1500

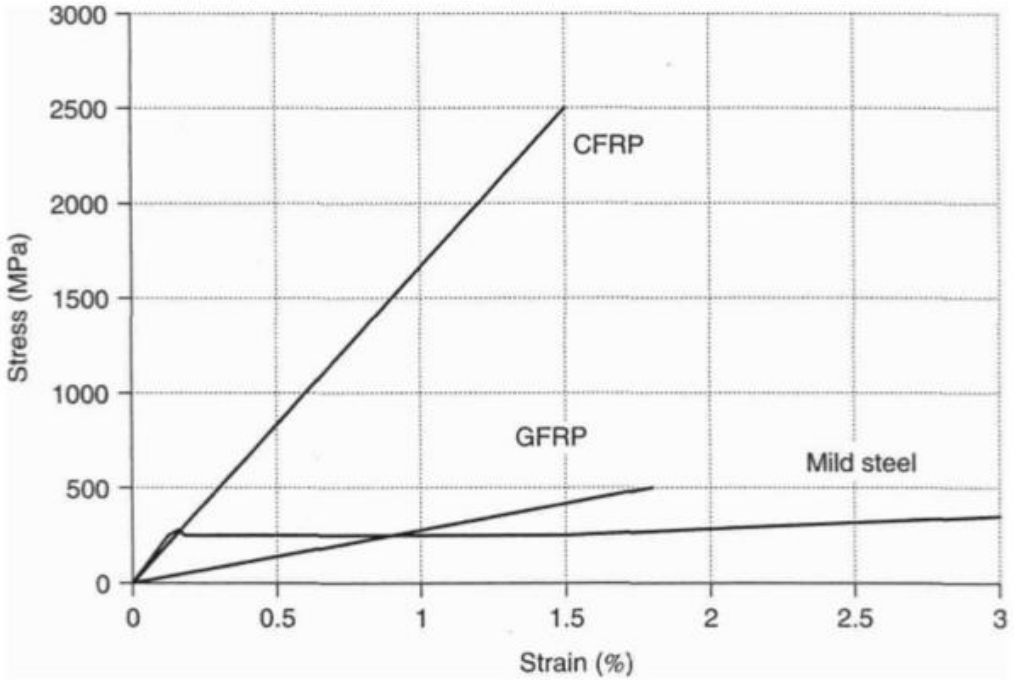

Figure 2.11. The tensile properties of CFRP and GFRP in comparison with mild steel.

Design consideration and environmental effects

If the FRP strengthening system is applied properly, it can offer the same or improved life cycle costs compared to other strengthening systems according to *fib*, the International Federation of Structural Concrete (2001). The durability of concrete and FRP is well documented, but according to Bulletin 40 in *fib* , the combined system has raised some warranted concerns regarding the overall long term behaviour. The interface between the concrete and the FRP is the critical component to the effectiveness of most FRP structural strengthening applications, as this location is where the transfer of stresses occur. Based on field experiences collected by the International Federation of Structural Concrete (2001), in Bulletin 40, it has been found difficult to assure proper bond between the concrete and FRP. According to Bulletin 40, the quality of the bond is influenced by the conditions of the existing concrete, surface preparation of the concrete substrate, quality of the FRP application, quality of the FRP it selves and durability of the resin. Following aspects have according to Bulletin 40 (2001) great influence on the durability of the FRP and the whole strengthening system:

- *Glass transition temperature*. This is the temperature above which the performance of FRP is expected to drop dramatically. Thermal energy supplied above this temperature allows the resin to move and become more flexible.
- *Fire design and protection*. If no special measures are taken such as protective linings, the externally bonded FRP may be lost during fire due to weakening of the adhesive. A temperature limit for the adhesive will depend on the type of adhesive, but usually the temperature limit will be in the range of 50^0 C to 100^0 C.
- *Effect on water absorption on FRP*. Damage of fiberglass/epoxy composites may occur due to intrusion of moisture on the resin-fibre interface. An intrusion may break the bonds between the silane coupling agent and the glass or the bonds between the coupling agent and the resin.
- *Freeze- Thaw effects*. Expansion of freezing water in cracks or voids on an uneven concrete surface may cause delamination between each laminate layer of FRP, or at the concrete-FRP interface.
- *UV light exposure*. When polymeric materials are exposed to UV-A and UV-B they undergo degradation that can lead to dissociation of chemical bonds. A subsequent exposure and reaction with oxygen can lead to oxidation as well as chain-cutting, chain-linking, hydrolysis or loss of other small molecules. Carbon and glass fibres are however, largely unaffected by the UV light exposure. The amount of deterioration will mainly depend on the type of resin, fibre stacking and the fibre orientation.

2.4 Confined concrete columns

Wrapping of FRP is acting on the columns as a passive confinement. When a concentrically axial load P is applied to a column and P is increasing from 0 to P_n , where P_n is the nominal axial capacity of the column, the column starts to crack and expand laterally until failure. The FRP is partially resisting the lateral expansion, gradually placing the concrete in a state of triaxial confining stress. This condition leads to a significant increase in both compressive strength and ductility of the brittle concrete (Ghanem 2016). Concrete confined with unidirectional FRP is exhibiting a specific failure behaviour due to the nature of the FRP. The stress strain relationship of the composite material is linear up to failure and has no significant yielding compared to steel. The confining pressure provided by the FRP will consequently increase with the lateral strain until rapture of the FRP (Lam & Teng 2003). FRP usually begins

to confine the concrete shortly after the unconfined concrete reaches stresses of f_{cu}. For circular FRP confined columns, the failure is governed by the FRP rapture in the hoop direction of the column (Karbhari & Gao 1997; Xiao & Wu 2000).

The confinement of columns is according to Bulletin 40 from *fib* (2001) achieved by means of internal lateral reinforcement (hoop or closed stirrups) or by external reinforcement (steel or FRP jackets). In the latter case, the confining reinforcement can be provided either through external strengthening of existing columns, or as formwork that acts as structural reinforcement after construction of the columns (International Federation of Structural Concrete 2001) Depending on the column shape and strengthening layout, a non-uniform confining stress distribution is obtained (International Federation of Structural Concrete 2001). The following cases are of interest when applying externally bonded FRP to RC columns:

Fully wrapped column with fibres perpendicular to the axis. If the total column surface is covered, a uniform tension in the FRP can be assumed leading to a uniform lateral confining pressure in the concrete core. Figure 2.12 from the International Federation of Structural Concrete (2007), shows the relation between the lateral confining pressure on the concrete denoted as σ_l and the confining stresses from the FRP denoted as σ_f.

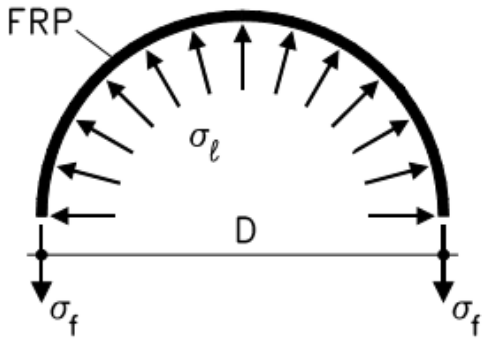

Figure 2.12. Confining action from a FRP wrap in a circular column.

Influence of partial wrapping. Both confined and unconfined zones will exist in concrete columns that are partially wrapped with FRP. In these cases, the effective lateral confining pressure is calculated by using a confinement effectiveness factor (International Federation of Structural Concrete 2001). The transverse pressure from the confining device is only effective where the confining pressure has fully developed due to the arcing action. This arcing effect is

described by a parabola with an initial slope of 45^0, as seen in Figure 2.13 (International Federation of Structural Concrete 2001).

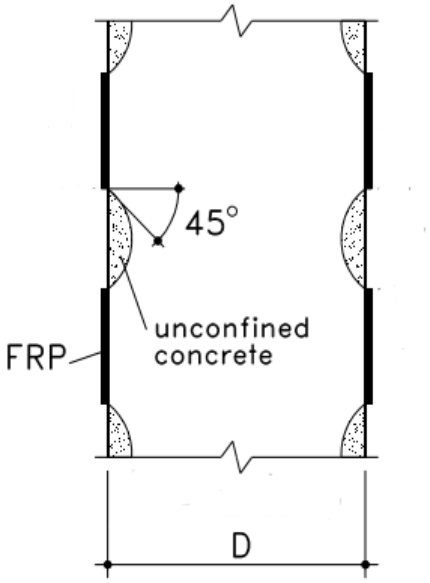

Figure 2.13. Confined and unconfined zones of a concrete column.

Influence from fibre orientation. If externally bonded FRP is helically applied (in a spiral around the outer surface), the fibre alignment is less effective to retain the lateral expansion of the column. With the use of the confinement effectiveness factor, this effect can be accounted for also in cases with helically applied FRP (International Federation of Structural Concrete 2001).

Influence from the column shape. For both square and rectangular columns wrapped with FRP and with corners rounded to a radius r_c, the arching action is assumed for the concrete core where the confining pressure is fully developed (International Federation of Structural Concrete 2001). The arching effect is described with a parabola with an initial slope of 45^0. This effect implies that large parts of the cross section for square and rectangular columns remain unconfined, as shown in Figure 2.14 (International Federation of Structural Concrete 2001). The opposite will be the case for a circular cross section where the concrete core is fully confined.

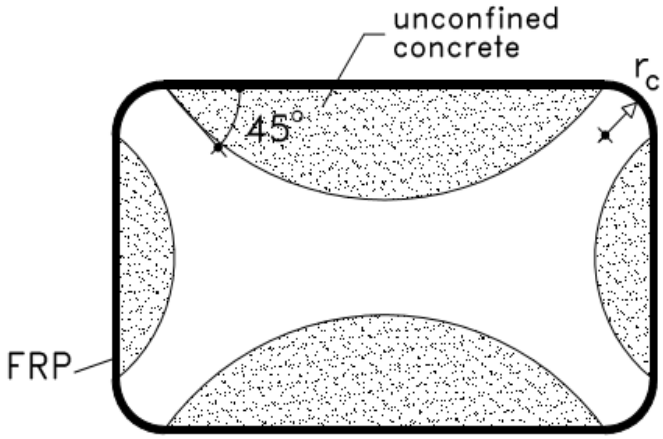

Figure 2.14. The effective confined area for a rectangular section.

Confinement pressure for different configurations of externally bonded FRP

The confinement pressure for different configurations of FRP can be calculated based on the formulas proposed by Ghanem (2016) that are shown below. Figure 2.15 (Ghanem 2016) shows the confinement action of externally bonded FRP for a circular column, where the FRP will provide a uniform pressure around the circumference of the column f_{fu} is the ultimate strength of the FRP material and $f_{l,f,max}$ is the maximum lateral confining pressure from the FRP on the column.

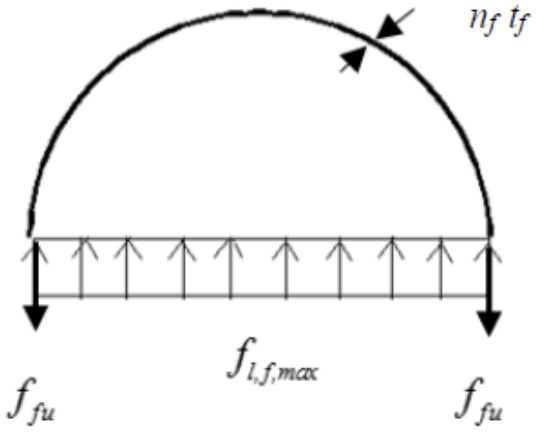

Figure 2.15. Confinement action from externally bonded FRP.

The symbols from Figure 2.15 are shown in Equation 2-4 (Ghanem 2016).

Equation 2-4. Calculation of the maximum lateral confining pressure.

$$f_{l,f,max} = \frac{\rho_f E_f \varepsilon_{fu}}{2} \tag{2-4}$$

Where ρ_f is the reinforcement ratio, E_f is the tensile modulus of elasticity for the FRP and ε_{fu} is the design rapture strain of the FRP. f_{fu} is the ultimate strength of the FRP material, $f_{l,f,max}$ is the maximum lateral confining pressure from the FRP, n_f is the number of FRP sheets and t_f is the thickness of each FRP layer. In order to achieve confinement of the concrete using FRP, a fully wrap all over the column can be applied, or a partial wrapping, covering parts of the columns with FRP strips can be applied. The reinforcement ratio of both a fully and a partially confined column can be found using Equation 2-5 proposed by Ghanem (2016).

Equation 2-5. Calculation of the reinforcement ratio for FRP confined columns.

$$\rho_f = \frac{4 t_f w_f n_f N_f}{D l_u} \tag{2-5}$$

Where t_f is the thickness of the FRP, w_f is the FRP width, n_f is the number of FRP sheets per strip, N_f is the number of strips along the column, D is the diameter of the column and l_u is the unsupported length of the column.

Thin walled cylindrical pressure vessels

A general relation for thin walled cylindrical pressure vessels is shown in Equation 2-6 (Hibbeler 2008). This relation can also be used for confined concrete columns in order to calculate the confining pressure from the FRP on the concrete if when the hoop stresses σ_1 from the FRP are known. Figure 2.16 (Hibbeler 2008) show a free-body diagram for a segment of a cylindrical vessel, with a pressure of p from the inside and hoop stresses σ_1, which are expected to be constant throughout the thickness of the segment.

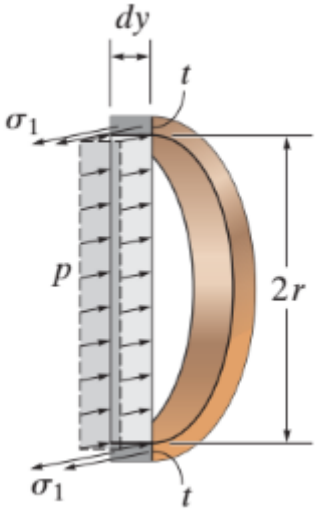

Figure 2.16. Free-body diagram for a segment of a cylindrical vessel.

Equation 2-6. A general relation for a thin walled cylindrical pressure vessel.

$$\sigma_1 = \frac{pr}{t} \tag{2-6}$$

Where:

- p is the pressure from the inside
- r is the radius of the segment
- t is the thickness of the segment

2.5 Shear behaviour of RC columns

For a RC column under axial compression (P), shear force (V) and a bending moment (M), as shown in Figure 2.17 (Sasani 2004), the shear forces should be resisted by forces generated at the compressive zone V_{cz}. In detail, the transverse component of the shear force due to interfacial aggregate by interlock on the crack surface V_{aT}, the dowel action from the flexural tensile reinforcement V_d, and the transverse reinforcement V_s are the three components that consist of the shear forces (Sasani 2004). The arc (strut) action is another mechanism to transfer the shear forces, where arc (strut) action according to Sasani (2004) can participate in transferring some parts of the lateral loads to the supports. As a result, some portions of shear

forces in the compressive zone V_{cz} may be caused by the arc (strut) action. The transverse reinforcement of the RC column will restrict the width of the diagonal tension cracks and in turn improve the shear transfer mechanism due to the aggregate interlock (Sasani 2004). The confining effects from the transverse reinforcement will according to Sasani (2004), also improve the behaviour of compressive struts, particularly during cyclic loading and after formation of intersecting diagonal cracks.

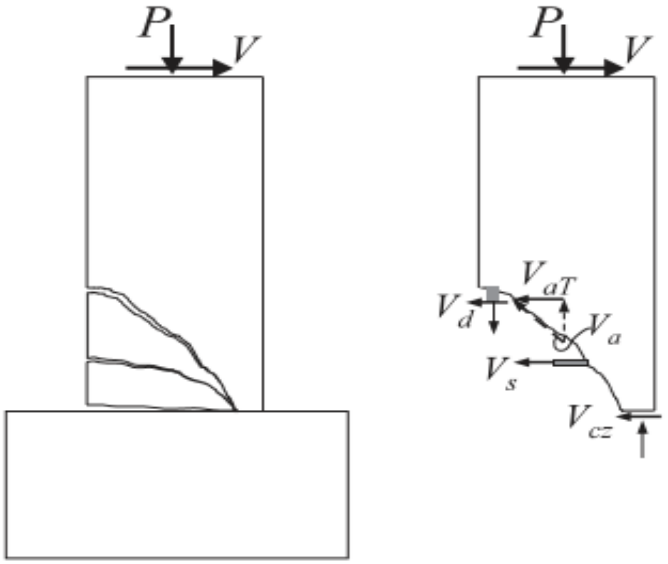

Figure 2.17. The shear transfer mechanisms in a RC column.

2.6 Design codes, standards and guidelines for FRP retrofitting of RC members

A general design code for the seismic retrofitting of structures with FRP is given in the European Standard EN 1998-3: Design of structures for earthquake resistance: Assessment and Retrofitting of Buildings. The design code has been prepared by the technical committee CEN/TC 250 "Structural Eurocodes" (2005). The Standard covers both the strengthening of undamaged structures and the repair of earthquake damaged structures. The scope of the Standard is as following:

- Provide evaluation criteria for the seismic performance of existing individual building structures.
- Describe the approach in selecting the necessary corrective measures.

- Set forth criteria for the design of retrofitting measures (i.e. conception, structural analysis including intervention measures, final dimensioning of structural parts and their connections to existing structural elements.)

Beside the EN 1998-3, which is a standard that most of the European countries have committed themselves to follow, the International Federation for Structural Concrete *fib*, which is a not-for-profit organization, has put working parties of experts together in order to work on different topics and publish technical reports related to concrete. Bulletin 40 is a technical report about FRP reinforcement in RC structures. The main objective of the task groups put together in the field of non-metallic reinforcement was to elaborate design guidelines for the use of FRP in concrete structures, in accordance with the design format of the CEB-FIP Model Code (2007). CEB-FIP was the precursor of *fib* (merged in 1998). Bulletin 14 is a technical report about externally bonded FRP reinforcement for RC structures. This bulletin is published by *fib* as well. Bulletin 14 (2001) gives detailed design guidelines on the use of externally bonded fibre-reinforced polymers (FRP), the practical execution and the quality control. The bulletin is based on current expertise and state-of-the-art knowledge of the members in the task groups. Bulletin 14 (2001) is however, only regarded as a progress report, mainly due to ongoing research and the fact that this report focuses on aspects that form the majority of the design problems (not all aspects with FRP strengthening with composites are covered). Some countries have also made publications within the field of FRP retrofitting of RC structures, such as ACI Committee 440 in USA, DAfSt in Germany and CUR Building and Infrastructure in the Netherlands (2007).

2.7 Application of FRP in concrete structures

The combination of properties from the fibres and the matrix, potentially gives a designer a wide range of material choices to fit the specific requirements of the structure. It also shows a great potential to expand the current palette of materials being used in civil engineering structures (Yu 2011). Some of the important advantages of FRP in civil engineering structures are according to Yu (2011): high specific strength and stiffness, enhanced fatigue life, corrosion resistance, controllable thermal properties, tailored properties and non-magnetic properties. The application of FRP laminates have also been proven reversible (Hollaway & Teng 2008), meaning that the material used for strengthening and the layers of adhesive may be completely removed from the structure. Therefore, the structure can be returned to the same condition as

before the application of FRP. In order to remove the FRP and the adhesive is the temperature of the FRP raised above the glass transition temperature of the resin (Hollaway & Teng 2008). In recent times have also transparent FRP laminates for application on historic masonry structures been developed, with the result that the intervention on a macroscopic level is almost invisible (Hollaway & Teng 2008). These features have made the FRP a competing and attractive alternative to the conventional strengthening and repair materials and methods. In recent years, the FRP materials have experienced a continuous increase in usage, especially for strengthening and repair applications around the world. Through experimental and theoretical studies, it have been shown that externally bonded FRP composites can be used to improve the desired performance of a concrete structural member. Examples on such improved performances can be: increased load carrying capacity and stiffness, increased ductility, better performance under cyclic and fatigue loading and enhanced environmental durability (Bakis et al. 2002; Einde et al. 2003; Oehlers & Seracino 2004; Teng et al. 2004).

Depending on the member type can the objective be one or a combination of the following (Yu 2011):

- Increase the axial, flexural or shear load capacity
- Increase the ductility for improved seismic performance
- Increase the remaining fatigue life
- Increase the durability against environmental effects

Especially the desirability of increasing the ductility of the structure in order to improve the seismic performance is an important application field for externally bonded FRP. Columns or bridge piers built in the past are design after the design criteria of former codes. These codes focus on the strength aspect of the structural members, while less concern is placed on the ductility and the stability of structures in the post-elastic phase. Because these existing structural elements were designed according to previously used codes, they are inadequate to meet the higher requirements imposed by the new generation of codes (2001)

2.7.1 Failure modes for RC columns under static loads and under dynamic loads

Enhanced ductility and strength of FRP-confined columns comes from the confinement provided by the FRP to the lateral expansion of the concrete. The concrete core will therefore be in a triaxial stress state (Teng 2001) and the FRP will be subjected to tension in the hoop direction. The governing failure mode for a *statically axially loaded* column will in general be tensile failure of the FRP. However, failure of the column may also occur at positions of vertical

overlapping of the longitudinal rebars, because of insufficient lap length (Teng 2001). For column cross sections with corners, the FRP will rapture prematurely and the starting point of the rapture is one of the corners of the column, whereas for a circular column the rapture can start at a random point within the cross section (Teng 2001).

For a column subjected to *dynamic loads*, it is the energy absorption capacity rather than the load capacity that is the main concern (Teng 2001). In case of seismic retrofit, the main purpose is not to increase the specific strength of the column rather to increase its energy absorbing capacity. This goal can effectively be achieved using externally bonded FRP. Under seismic loads, the main failure modes are according to Teng (2001): shear failure, flexural plastic hinge failure, debonding of lap-spliced longitudinal reinforcement or flexural-shear failure of columns with cut-off of the longitudinal reinforcement. Even after FRP confinement of columns, these are still potential failure modes. A key aspect by the design of the FRP jacket is to enhance the shear capacity of columns so that a ductile failure will occur rather than a brittle shear failure. Ductile failure is preferred over brittle failure, while it generates a predictable form of failure so that the structure do not collapse without prior warning. The FRP jacket should also provide sufficient lateral confinement to the plastic hinge regions in order to prevent buckling of the longitudinal reinforcement, prevent the overlapping of the longitudinal reinforcement (lap-splices) from debonding and achieve greater ultimate strength for the concrete (Teng 2001).

2.7.2 Failure modes of FRP

Debonding and bond failure modes

Bond is necessary to transfer the forces from the concrete and into the FRP or from one laminate layer of FRP layer to the next and bond failure between these components must be accounted for. A bond failure when using externally bonded reinforcing leads to a complete loss of composite action between the different components and occurs at the interface between the FRP and the concrete substrate. The bond failure may occur on different interfaces between the concrete and the FRP as listed below (International Federation of Structural Concrete 2001):

- Debonding in the concrete near the surface.
- Debonding in the adhesive (cohesion failure), typically occurring in the concrete that has lower tensile and shear strength than the adhesive (epoxy resin)

- Debonding on the interface between the concrete and the adhesive (epoxy) or between the FRP and the adhesive (epoxy), called adhesive failure. This failure mode will only occur in case of insufficient surface preparation.
- Debonding inside the FRP laminar (interlaminar shear failure) between the fibres and the resin.

Rapture of FRP due to its confining action

Numerous experimental results show that circumferential failure of the FRP in most cases will occur for lower strain values than the ultimate tensile strain obtained by standard tensile testing of FRP sheets. There are several reasons for this phenomenon (International Federation of Structural Concrete 2001):

- *Triaxial state of stress for the FRP wrapping*
- *Quality of the execution*, if the fibres of FRP are locally ineffective aligned due to voids or inadequate surface preparation, then a part of the circumferential strain is used to stretch the fibres, reducing the ultimate strain of the FRP.
- *Curved shape of wrapping reinforcement*, especially at corners with low radius.
- *Size effect* when multiple layers are applied.

In *fib* are mainly the *triaxial state of stress for the FRP wrapping* emphasized as a reason for the strain reduction. This phenomenon is shown in Figure 2.18. In this figure is the composite action introduced, which denoted the ability of the FRP jacketing to provide lateral confinement and at the same time load carrying capacity (International Federation of Structural Concrete 2001). The fibre confining action depends on the arrangements of the fibres and the characteristics of the bonding. Stiffness of the adhesive and the surface preparation conditions are also parameters that according to Bulletin 14 in *fib* (2001) have an effect on the composite action. In cases where there is no composite action, the FRP jacketing will only undergo transverse strain and fail in extension mode. This failure will occur due to fibre collapse or delamination between the concrete and FRP, or between the FRP laminate layers at a strain level lower than ε_{fu}. This is due to the stress gradient in the FRP jacket that in some extent will influence the FRP jackets ultimate strength. On the other hand, in cases with full composite action, the FRP jacket will undergo both longitudinal and transversal strain. According to Bulletin 14 in *fib* (2001), the ultimate stresses and strains are then reduced, with the potential of micro buckling and delamination to develop. Failure of a specimen with composite action

will therefore occur at even lower circumferential strains that would have be the case if there were no composite action (Bulletin 14 2001).

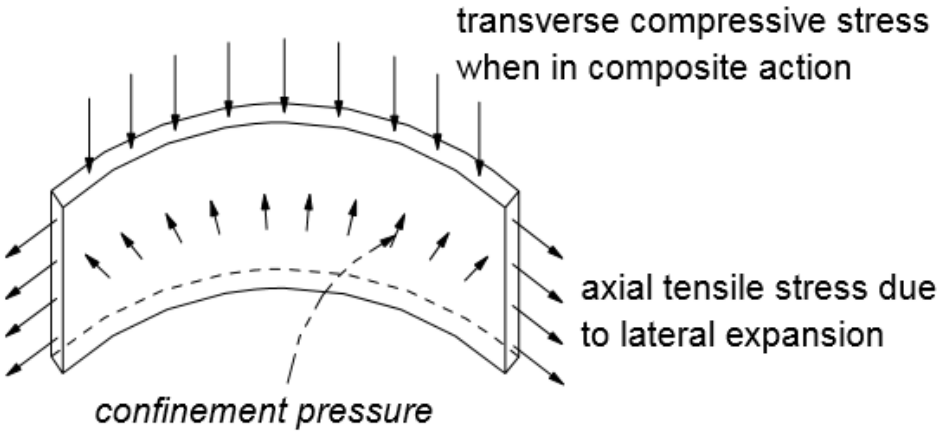

Figure 2.18. A state of triaxial stress in a FRP jacket.

2.8 Alternative retrofitting techniques

The FRP retrofitting technique has a few drawbacks mainly associated with the use of epoxy, the high costs, poor performance in high temperatures and inability to apply on wet surfaces (Tetta et al. 2015). However, various jacketing techniques exist that can be applied to reinforced concrete columns as an alternative to the FRP solution. The techniques most commonly used are shown below (Dubey & Kumar 2016):

- Conventionally vibrated concrete (CVC)
- Steel jackets.
- Ferrocement.
- Textile composites and textile reinforced mortars (TRM)
- Reinforced concrete Jackets
- Shotcrete
- Self-compacting concrete (SCC)

In the retrofitting technique of steel jackets are steel angles/ plates used to confine the concrete in different configurations. This can be in the form of steel wrapping (for circular columns) or steel plates and steel caging (Islam & Hoque 2015). Ferrocement is a thin walled concrete with

wiremesh reinforcement. The reinforcement can be single or multiple layers of continuous and relatively small diameter mesh. Textile reinforced mortars (TRM) is a retrofitting technique that combines advances fibres in form of textile with an open mesh configuration and inorganic matrices such as cement-based mortars (Tetta et al. 2015). According to Tetta et al. (2015), experiments have been conducted showing that the TRM is a promising alternative to FRP retrofitting. The application of a layer of reinforced concrete around a RC column is referred to as RC jacketing (Islam & Hoque 2015). In order to ensure proper bond between the surface of new and old concrete, anchored bars/shear crosses and adhesive materials are used. Shotcrete is a retrofitting method that in some cases will be most cost efficient, particularly where forms can be eliminated and normal casting techniques cannot be applied (Tsonos 2010). In many cases, the performance characteristics for shotcrete with respect to strength, stiffness and bond are according to Tsonos (2010), comparable to those of cast-in concrete (CVC and SCC). It is worth to mention that all of the listed retrofitting methods in a significant way lead to a section enlargement, which in many cases can be ignored when a FRP retrofitting solution is applied. Some key aspect for the application of different retrofitting techniques for RC columns, are the enhancement of the load carrying capacity along with the possibility to change the failure mechanism from brittle to ductile.

2.9 Discretization of the finite element model

A finite element analysis requires as an initial step, meshing of the model. That means that the model is divided into a certain number of small elements. After loading and application of boundary conditions, stresses and strains can be calculated at integration points of these small elements (Ghanem 2016). The mesh density is an important aspect in finite element modelling, while a convergence of the results only is obtained when an adequate numbers of elements are used in the model. In practice, this is achieved when an increase in mesh density has a negligible effect on the results. A convergence study can then be carried out to determine an appropriate mesh density (Adams & Askenazi 1999; Ghanem 2016).

2.10 Loading and boundary conditions

Monotonic compressive loading

For a nonlinear analysis of a finite element model due to monotonic compressive loading, the total load that is applied to the model is being divided into a number of load increments called load steps. At the completion of each incremental solution, the stiffness of the model is adjusted

in order to reflect the nonlinear changes in structural stiffness before proceeding to the next load increment. ANSYS uses the Newton-Raphson equilibrium iteration for the update of the model stiffness and Figure 2.19 shows this iteration approach for a single degree of freedom system (ANSYS 2016).

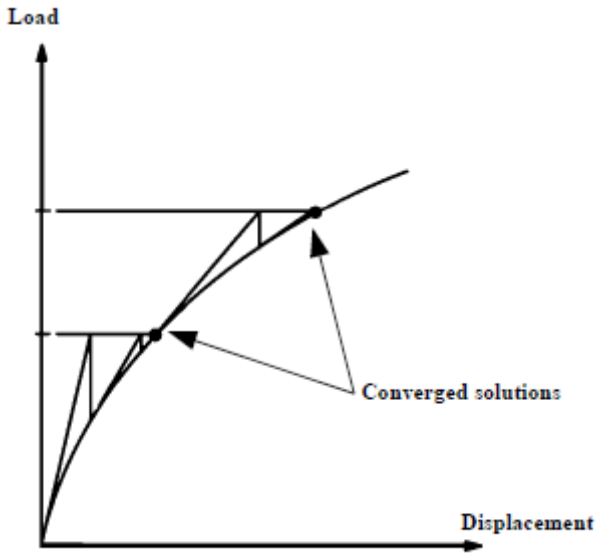

Figure 2.19. Newton-Raphson approach for a single degree of freedom nonlinear analysis.

At each substep and the end of each load increment, as shown in the figure above, the program performs a number of equilibrium iterations within a tolerance limit in order to obtain a converged solution (ANSYS 2016; Bajer et al. 2007; Kachlakev et al. 2001). Prior to each solution, the Newton-Raphson approach assesses the out of balance load vector, which is the difference between the restoring force (the load corresponding to the element stresses) and the applied load (ANSYS 2016). Subsequently, the program carries out a linear solution, using the out of balance loads and checks for convergence. If convergence is not satisfied, the out of balance vector is re- evaluated, the stiffness matrix is updated and a new solution is attained. This iterative procedure continues until the problem converges (ANSYS 2016; Bajer et al. 2007; Kachlakev et al. 2001). In some nonlinear static analyses, when the Newton-Raphson method is used alone, there is a possibility for the tangent stiffness matrix to become singular (non-unique), causing problems with convergence (ANSYS 2016). The boundary conditions are crucial to ensure that the model acts in the same way as the structure in real life, and these need to be applied on points of symmetry and where the loadings and supports exist. Moreover, the

boundary conditions are necessary to constrain the model so that a unique solution can be found (Izzet & Zahra 2016).

2.11 The geometry of the model

The dimension of the column is Ø350 with a height of 2400mm. It is fixed in both ends and has a stirrup cross section of 8mm with a centre distance from the end of the column towards the middle of 140mm, 240mm and 200mm, respectively. The arrangement of the stirrups can also be seen in Figure 3.3. The design of the reinforcement and the concrete cover was performed with respect to the Eurocode, NS-EN 1992 - 1 - 1:2004+NA:2008. The dimensions of the column before the externally bonded FRP was applied is shown in Figure 2.20 and Figure 2.21.

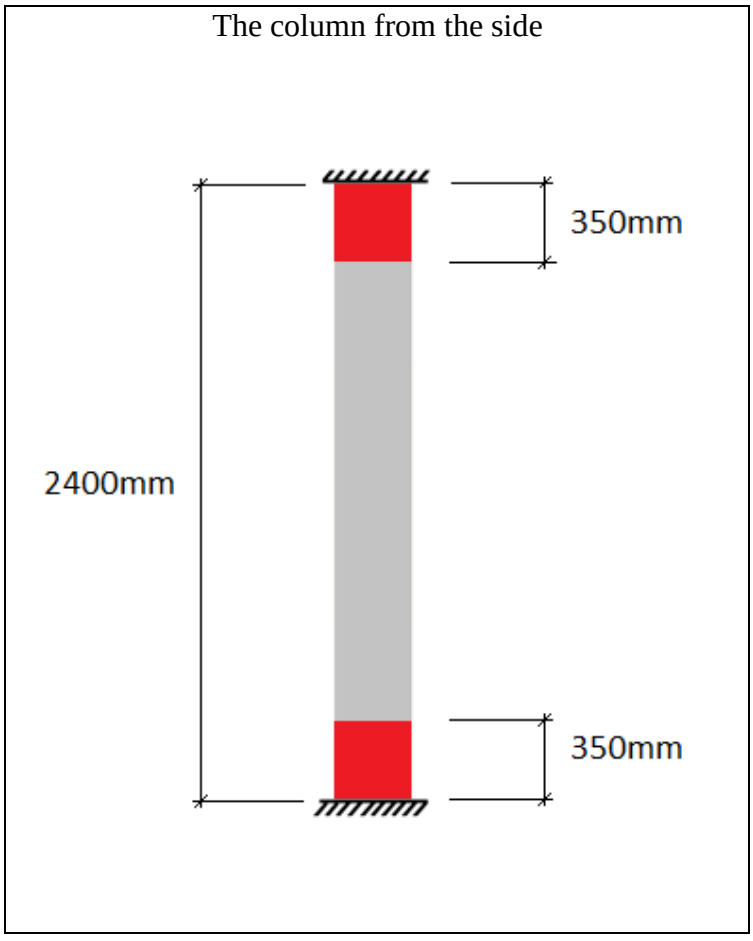

Figure 2.20. The column with the critical height in red.

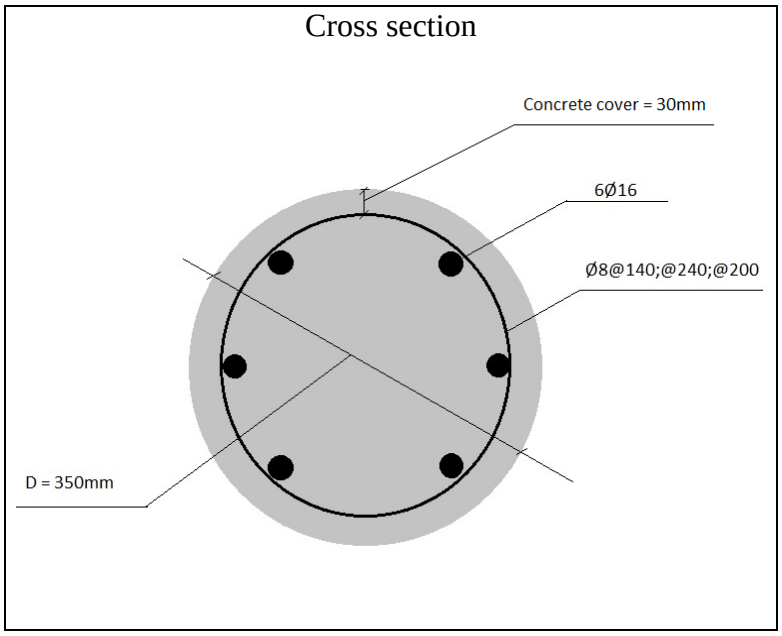

Figure 2.21. The cross section of the column.

3 Methodology

3.1 Preface

In order to get a deeper insight on how the program works and gain some confidence and experience before it was decided which cases to test in the thesis, numerous simple models were built, tested and compared to hand calculations. Then the final study cases were determined and the first challenge was the modelling of the reinforcement in the RC column. Both the discrete and the smeared approach in the modelling of longitudinal reinforcement were tested and it was realized that the discrete modelling of the rebars works well for relatively simple geometries, but later the models experienced problems with the convergence as the level of complexity increased. Therefore, all the study cases were modelled using the smeared approach for the reinforcement. Defining a realistic contact interaction using contact elements has been proven a time consuming process because many parameters that in smaller or larger extent influence the results, need to be investigated.

3.2 Case studies under investigation

Table 3.1. Different case studies.

Cases	Stirrup cross section	Number of layers	Centre distance for stirrups	FRP material
Case1	Ø8	None	@140;@240;@200	None
Case2A	Ø8	None	@240;@480	None
Case2B	Ø6	None	@240;@480	None
Case3A	Ø8	One, two and three	@240;@480	CFRP
Case3B	Ø6	One, two and three	@240;@480	CFRP
Case4	Ø6	One, two and three	@240;@480	GFRP
Case5	Ø6	One, two and three	@240;@480	CFRP
Case6	Ø6	One, two and three	@240;@480	CFRP
Case7	Ø6	One, two and three	@240;@480	CFRP
Case8	Ø6	One, two and three	@240;@480	CFRP
Case9	Ø6	Only one layer	@240;@480	CFRP

Each laminate layer of CFRP and GFRP has a thickness of 1mm and were applied to the column with the dominating fibre direction in the hoop direction. Case3A to Case8 were modelled with both one, two and three layers on laminate. Case9 was modelled with only one layer of laminate with a thickness of 3mm.

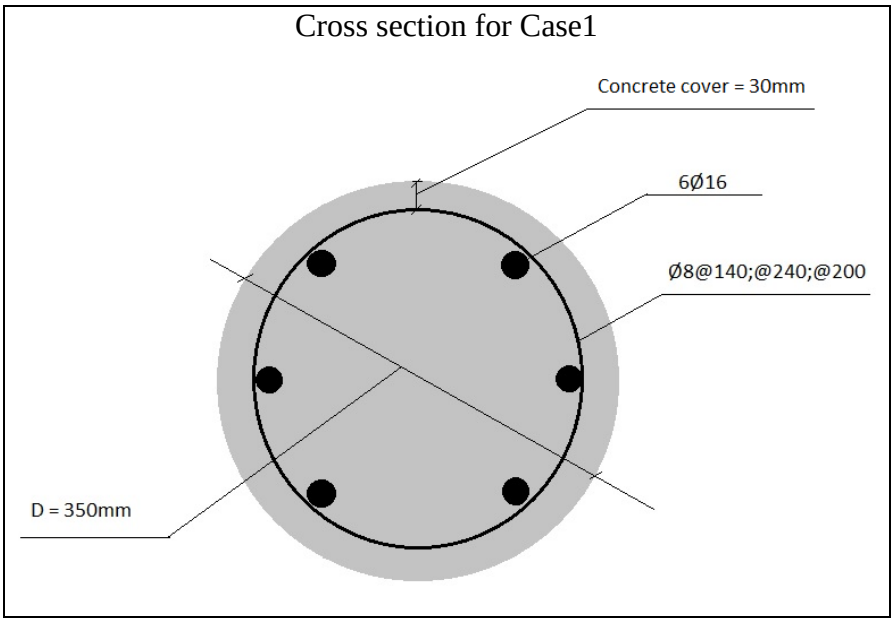

Figure 3.1. The cross section for Case1.

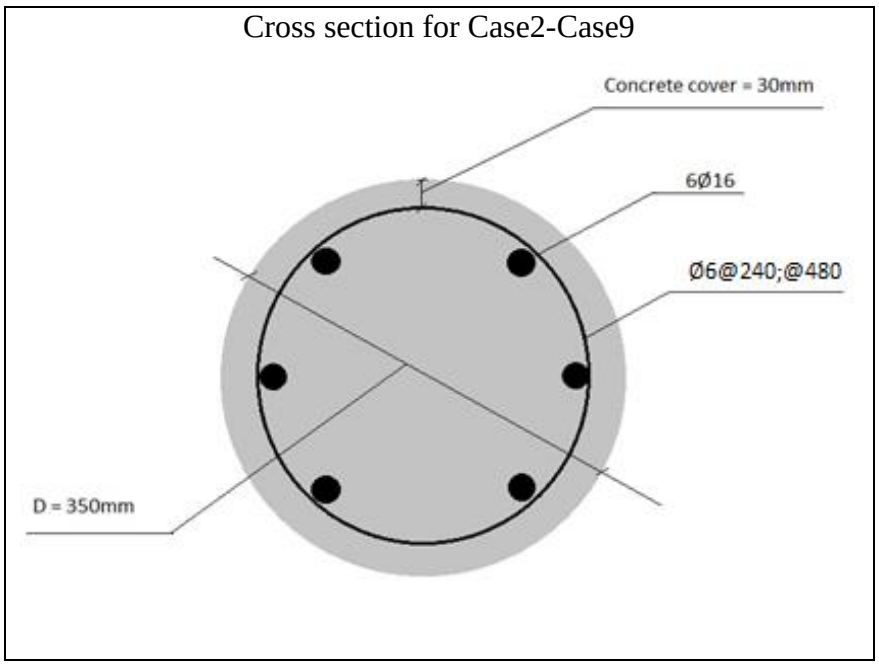

Figure 3.2. The cross section for Case2-Case9.

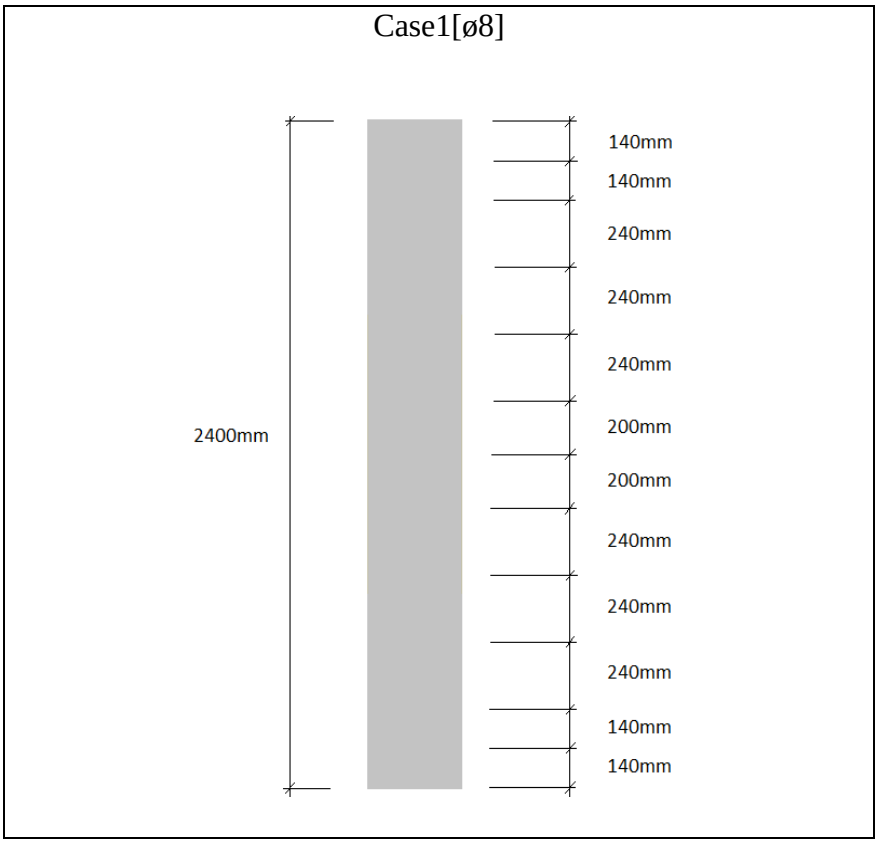

Figure 3.3. Case1 with a stirrup cross section of 8mm.

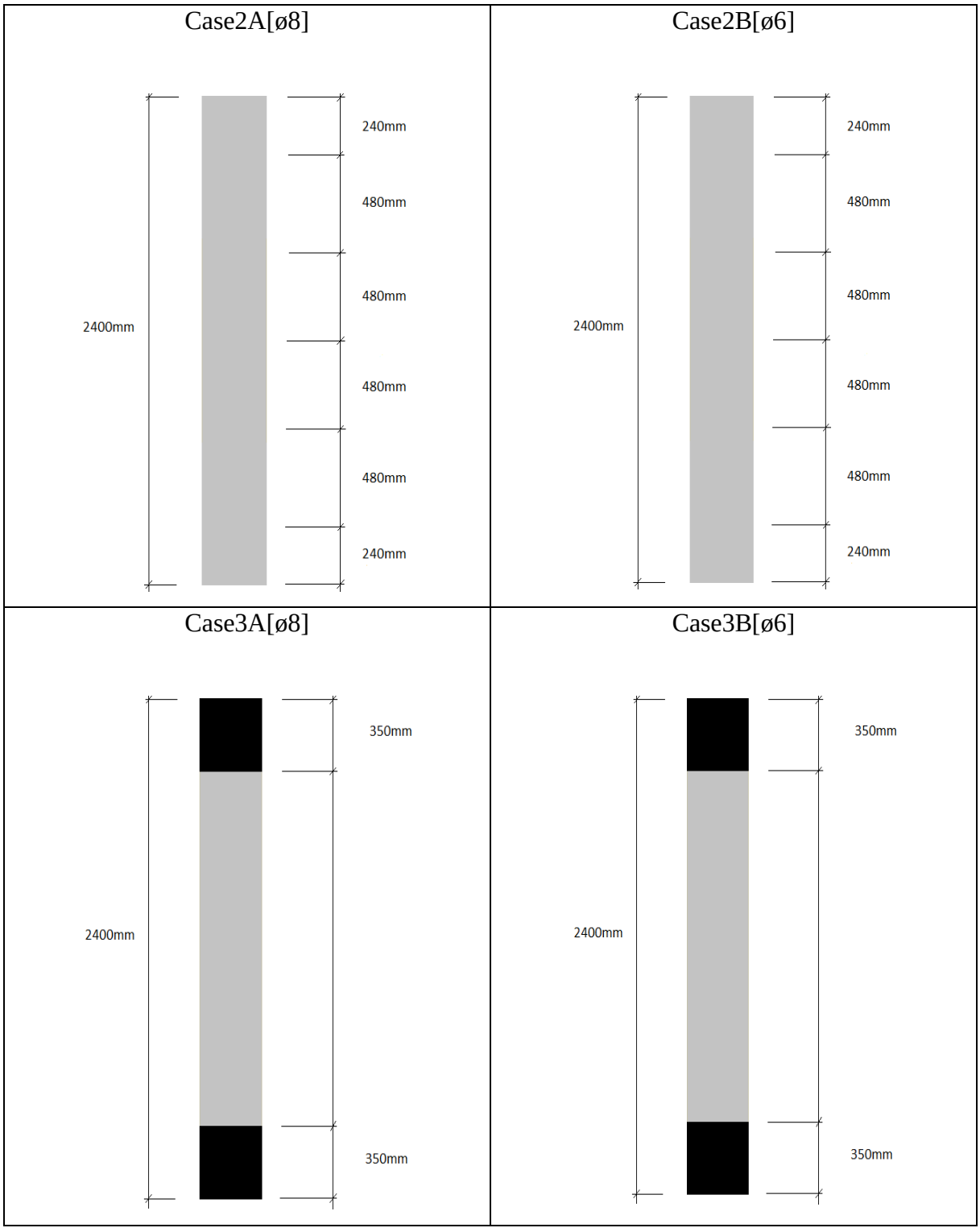

Figure 3.4. Different cases with and without FRP.

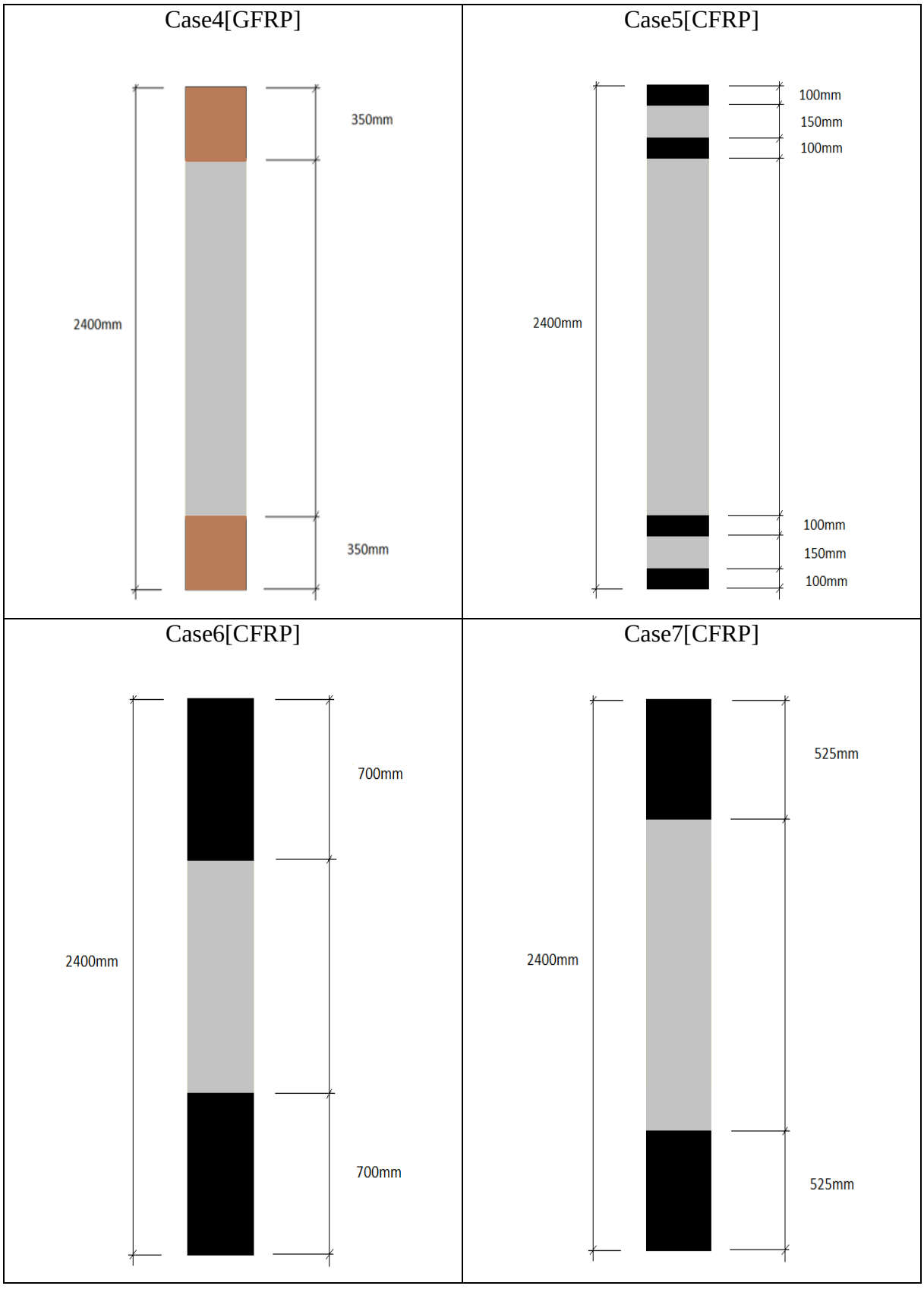

Figure 3.5. Case4 with GFRP, the rest with CFRP.

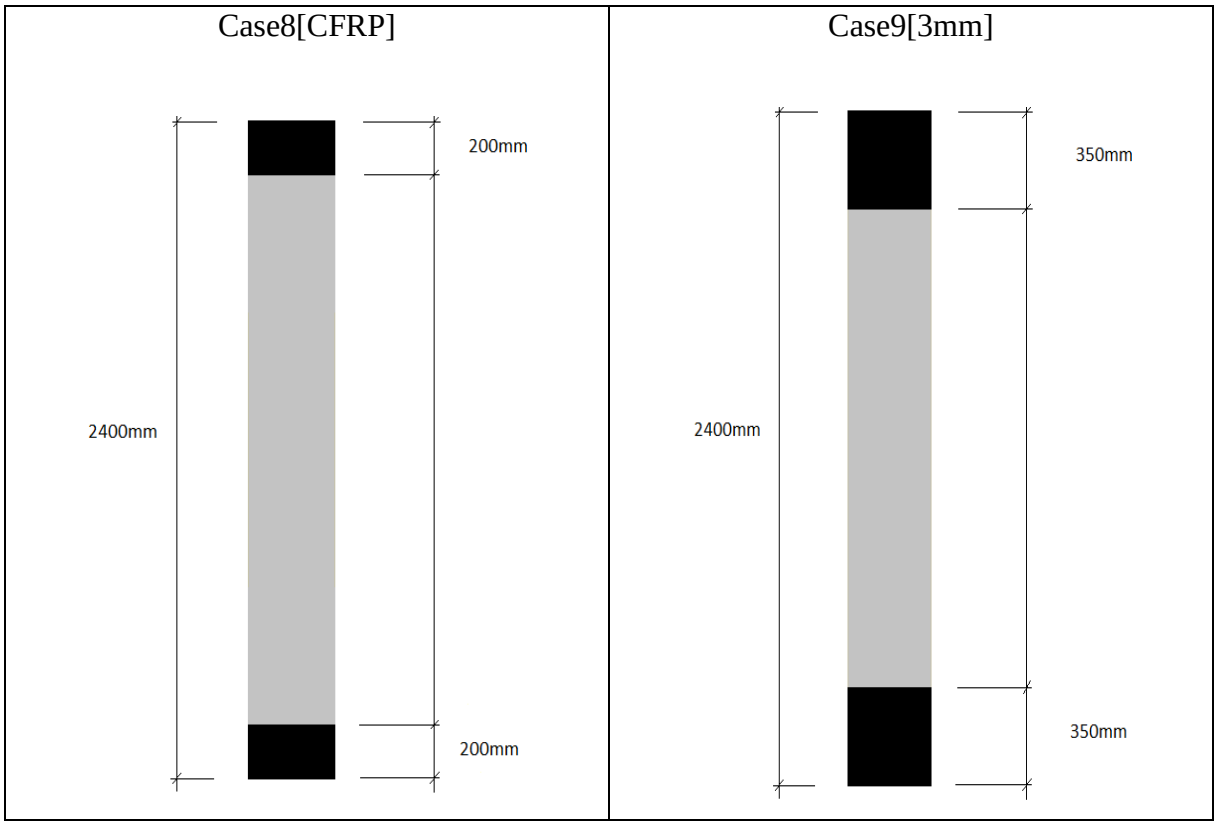

Figure 3.6. Case9 with one thick laminate layer of 3mm and Case8 as the previous cases with CFRP.

3.3 Input data to ANSYS

Concrete and steel

B25 was chosen for the concrete, with material properties from NS-EN 1992 - 1 - 1:2004 of E_s= 31000N/mm^2,f_{ck}= 25N/mm^2 ,f_{ctm}= 2.6N/mm^2 , a density of 0,0025g/mm^{3}and Poisson's ratio of 0.2. The specific values used in order to define the failure criteria of concrete (William and Warnke 1975) were chosen based on values proposed by Rudeng (2008): 0.37 for the shear transfer coefficient for an open crack and 0.97 for the shear transfer coefficient for a closed crack. 0.6 was used for the tensile crack factor. The default ANSYS values were used for the remaining parameters defining the failure criteria for concrete. For the reinforcement steel grade B500C was chosen with an elastic perfectly plastic behaviour E_s = 200 000N/mm^2, f_{yk}= 500N/mm^2 , ε_s= 0,2%, tangent modulus E_t for the nonlinear properties of 20 000 N/mm^2 (1/10 of the modulus of elasticity), a density of 0,00785g/mm^{3}and a Poisson's ratio of 0.3 (NS- EN 1992 - 1 - 1:2004).

FRP

FRP was modelled as a linear elastic orthotropic material. The input data used for the FRP composites in the finite element model are as following:

- Thickness of each layer
- Orientation of the fibre direction for each layer
- Elastic modulus for the FRP composites in three direction (E_x, E_y, E_z)
- Shear modulus for the FRP for the three planes (G_{xy}, G_{yz}, G_{xz})
- Major Poisson's ration in the three planes ($\nu_{xy}, \nu_{yz}, \nu_{xz}$)

Because of the orthotropic properties, the subscripts are needed in order to define the properties of the FRP composites in the various directions. The Major Poisson's ratio used in ANSYS is calculated using Equation 3-1 (Kaw 2006). The equation shows the relationship between the minor Poisson's ratio and the elastic modulus, $E_x$and $E_y$where x is the fibre direction and the y is the direction perpendicular to the fibres. Minor Poisson's ratio ν_{yx} is smaller than ν_{xy} whereas E_x is larger than E_y (Kaw 2006).

Equation 3-1. The relation between the major and minor Poisson's ratio.

$$\nu_{yx} = \frac{E_y}{E_x}\nu_{xy} \quad (3\text{-}1)$$

Where:

- ν_{yx} is minor Poisson's ratio
- E_x is the elastic modulus in x direction
- E_y is the elastic modulus in y direction
- ν_{xy} is major Poisson's ratio

The material properties for the FRP composites used in the modelling are displayed in Table 3.2 below based on Kachlakev and McCurry (2000). However, for modelling purposes 1,0mm laminate thickness of the GFRP was used instead of 1,3mm as initially proposed by Kachlakev and McCurry (2000).

Table 3.2. Orthotropic material properties used in ANSYS.

FRP composites	Elastic modulus [N/mm^2]	Poisson's ratio	Shear modulus [N/mm^2]	Thickness of laminate [mm]	Tensile strength[MPa]
CFRP	E_x= 62 000 E_y= 4800* E_z= 4800*	ν_{xy}= 0,22 ν_{xz}= 0,22 ν_{yz}= 0,3*	G_{xy}= 3270* G_{xz}= 3270* G_{yz}= 1860**	1,0	958
GFRP	E_x= 21 000 E_y= 7000* E_z= 7000*	ν_{xy}= 0,26 ν_{xz}= 0,26 ν_{yz}= 0,3*	G_{xy}= 1520 G_{xz}= 1520 G_{yz}= 2650**	1,0	600

*(Kachlakev 1998)

Equation 3-2. Relation for the calculation of the shear modulus in the yz-plane.

$$**G_{yz} = \frac{E_z \text{ or } E_y}{2(1+\nu_{yz})} \quad (3\text{-}2)$$

3.4 Creation of the finite element model in ANSYS

Case1

By taking advantage of the symmetry of the column only one quarter of the column was modelled. The concrete part was modelled using SOLID65 elements, and in the option menu for this element extra displacement during cracking was excluded and the Newton -Raphson approach was chosen. In order to improve the accuracy of the solution the "searching on integration points'' option was employed. Relaxation of the concrete was set on and included in the analysis, provided there were cracks in the concrete elements. The model was meshed using the mapped mesh option with an element size of maximum 10mm. Figure 3.7 shows the cross section of the modelled column, with the mapped mesh and the smeared elements for the longitudinal reinforcement.

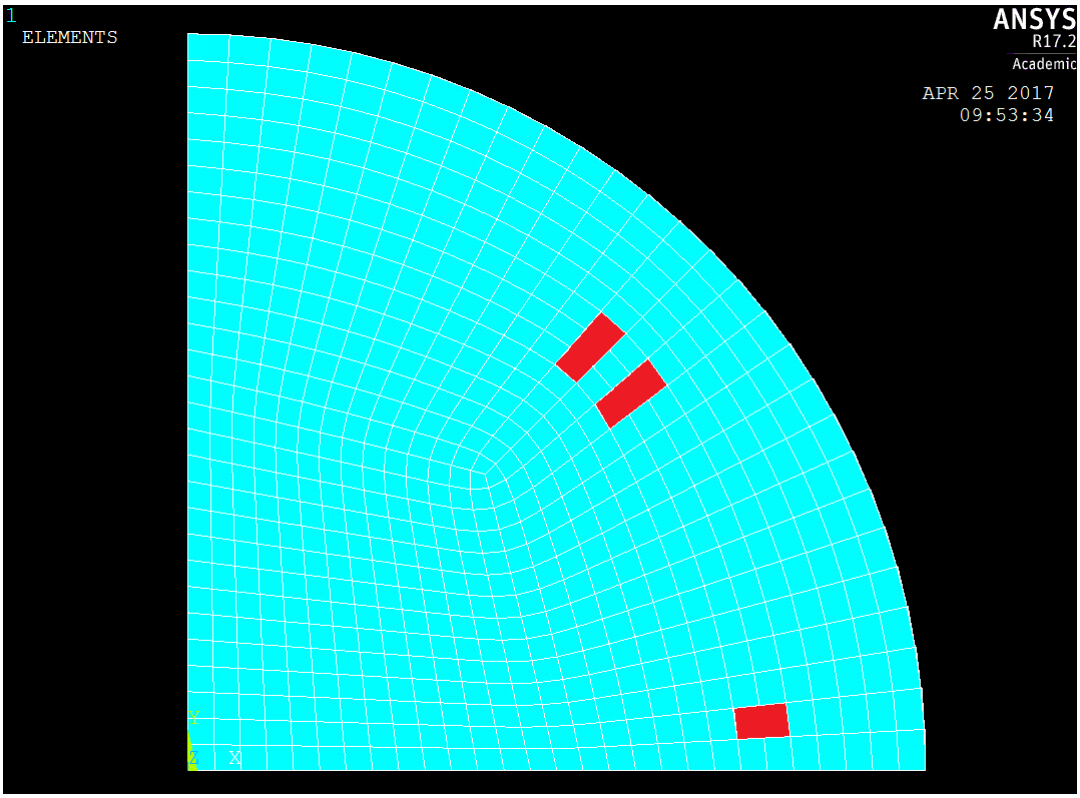

Figure 3.7. The modelled quarter of the column with the smeared reinforcement in red.

The longitudinal rebars and the stirrups were modelled using a smeared approach, namely by specifying that a certain percentage of each concrete element should be steel. The detailed calculations of the number of elements needed for the longitudinal reinforcement and the steel volume ratio for the stirrup elements are presented in Appendix A.6. A summary of the key results from the detailed hand calculations can be found in chapter 3.5.1. For the solid elements

acting as longitudinal reinforcement, the volume ratio of steel was put to 0.999999. When looking at the cross section were in total 8 elements times 240 elements in the depth of the column selected. The longitudinal rebars were therefore focused into a total of 1920 elements. The orientation of the rebars were set to $\theta = 0^{0}$ and $\phi = 90^{0}$. For the stirrups a volume ratio of $7{,}871*10^{-5}$ per selected element was used for the ø8 stirrups with an orientation of $\theta = 90^{0}$ and $\phi = 0^{0}$.

Case 2 to 9

In Cases 2 to 9 the stirrup distance was increased and the cross section of the stirrups was changed from ø8 to ø6, as shown in Table 3.1. The nonlinear concrete model and the other parameters remained unchanged from Case1. When using ø6 for the stirrups, the model was created using a steel volume ratio of $4{,}459*10^{-5}$ per selected finite element.

FRP composites

The FRP composites were modelled using SOLID186 elements as a homogenous solid. First, the inner surface was created as an area and then extruded in the desired thickness of the FRP composite. The volumes were then meshed using a mapped mesh with a maximum element length of 10mm. The dominating direction for FRP is the x-direction and according to the element's coordinate system, this is the hoop direction of the column.

3.4.1 Interaction between the concrete and FRP and between laminate layers of FRP.

For Cases3 to Case8, contact pairs were created between the concrete and the FRP and between the different FRP laminate layers, while for Case9 contact pairs were only created between the concrete and the FRP.

The contact between concrete and FRP was modelled using contact and target elements, CONTA174 and TARGE169, respectively. TARGE169 was used for the concrete surface and CONTA174 was used for the surface of the FRP. These elements were automatically chosen by the program. Between each FRP laminate layer, the outer surface of the inner layer was defined with TARGE169 and the inner surface of the outer layer was assigned as the contact surface with CONTA174. The Epoxy layer between the composites was modelled as a 0,5mm gap giving a contact surface offset of 0.5mm. For the contact surface were all initial penetrations excluded. Augmented Lagrange was chosen as the contact algorithm and bonded (always) was the contact formulation used between the two adjacent surfaces. The Sparse matrix solver was

used to calculate the contact problem, chosen automatically by the program. The contact stiffness was set to a factor of 10 and for all the other parameters the default value of the program was used.

3.5 Loads and boundary condition

The application of the load was done incrementally as required by the Newton- Raphson procedure. Therefore, the total applied load was divided into a series of load increments (load steps). Within each loadstep a maximum of 30 iterations was permitted. Within 20 seconds it was expected that the pressure load should be applied in 50 steps, with a maximum number of 60 step and a minimum of 40 steps. The convergence criteria for the concrete elements were based on force and displacement and the default tolerance limit of 0.01 was used both for the force and the displacement. A load of 1496,58kN was distributed over the cross section of the column and applied as a pressure load of 15,56N/mm^2 . This load magnitude is equal to 80% of the theoretical capacity of the concrete column with respect to axial compression only. Since only a quarter of the column was modelled, planes of symmetry were required on the internal faces of the column and the planes from the FRP.

3.5.1 Hand calculations for the modelled column.

Hand calculations of the axial capacity, rebar and stirrup amount, control of the slenderness criterion and the minimum concrete cover are based on NS-EN 1992 - 1 - 1:2004+NA:2008. The hand calculations of the confining pressure from the FRP are based on the dissertation from Ghanem (2016).

The concrete reinforcement was initially design based on an assumption that the column was regarded as a short column, implying that the 2. order effects were excluded. The slenderness criterion for the RC column was afterwards calculated to control if the assumption of a short column was valid. The calculation of the slenderness criterion is found in the Appendix A-5.

Some key results from the hand calculations are shown below, and a full presentation of the hand calculation can be found in the Appendix.

Longitudinal reinforcement bars

A_s= 1206,37mm^2 with 6xØ16 NA. 9.5.2(2) and NA. 9.5.2(3)

Stirrups

$S_{cl,max}$= min {15*16mm; 350mm; 400mm} = 240mm NA. 9.5.3(3)

Concrete cover

c_{nom} = 16mm + 10mm = 26mm choosing a concrete cover of c_{nom}= 30mm. 4.4.1.1(4.1)

Axial capacity

N_{Ed}= f_{cd}*(A_c– A_s) + f_{yd}*A_s= 1870,7kN (A-1)

The slenderness criterion for the column

$\lambda_n \leq \lambda_{n,lim}$ leading to 10,77 ≤ 11,206 => O.K NA. 5.8.3.1

The 2. order effects do not have to be taken into account since the assumption of a short column is valid.

Smeared modelling of the longitudinal reinforcement

With a cross section areas for the rebars of 24052,82mm^2 , an element length of 10mm, where each element consist of approximately 409,06mm^3 and a cross section consisting of 588 elements, a total of 7,37 concrete elements are smeared with steel. For simplicity are 8 elements

filled with steel when looking at the cross section of the column. This can also be seen in Figure 3.7.

Smeared modelling of the stirrups

A stirrup cross section of **ø8** give a stirrup ratio of 4,628%. When this amount is distributed into 588 elements, the volume ratio of each concrete element with smeared stirrups will be equal to $7{,}871*10^{-5}$.

A stirrup cross section of **ø6** give a stirrup ratio of 2,622% and a volume ratio for the smeared reinforcement of $4{,}459*10^{-5}$.

Hand calculations of the confining pressure for Case3B with one layer of FRP

According to Equation (2-4) and Equation (2-5), the reinforcement ratio of FRP ρ_f will be equal to $3{,}333*10^{-3}$ and the maximum lateral confining pressure $f_{l,f,max}$ will be equal to $1{,}5965 N/mm^2$.

4 Results

4.1 Axial shortening of the column

Table 4.1. Axial shortening of the columns for some chosen cases.

Some reference cases	Number of layers	Axial shortening
Case1	None	1,12093mm
Case2A	None	1,12093mm
Case2B	None	1,12093mm
Case3A_1layer	One layer CFRP	1,12047mm
Case3B_1layer	One layer CFRP	1,12047mm
Case3B_2layers	Two layers CFRP	1,12002mm
Case3B_3layers	Three layers CFRP	1,11959mm

When Case1, Case2A and Case2B are compared, where both the cross section area of the stirrups and the centre distance of the stirrups are modified, no significant change in the axial shortening of the column was observed. Also for Case3A and Case3B with one layer of CFRP and with the cross section area as the only changed parameter, no changes in the axial shortening of the column was observed. The only parameter that significantly reduced the axial shortening of the column was the adding of numerous layers of externally bonded CFRP.

4.2 Load-deflection curve for the column

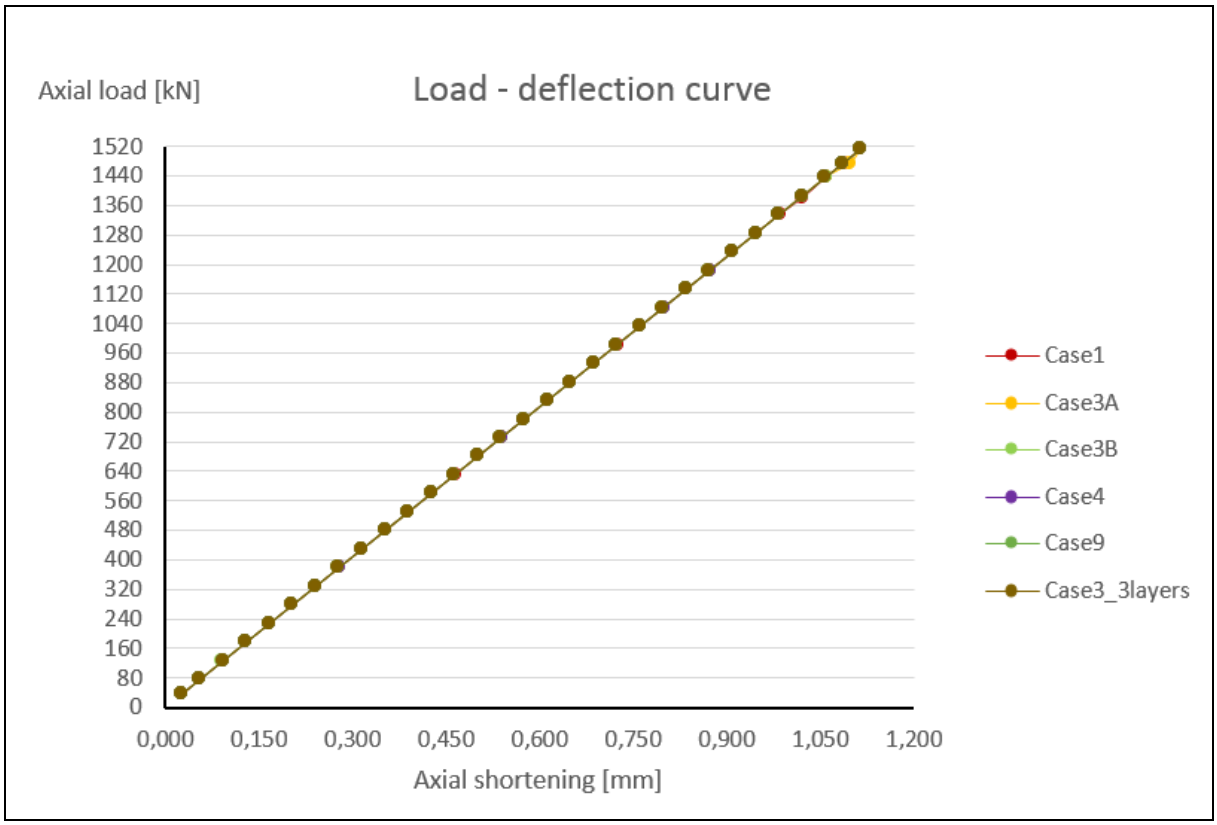

Figure 4.1. Load-deflection curve for the different cases.

The load-deflection curves for the finite element models under a concentric load equal to 80% of the theoretical axial capacity of the RC column, are presented in Figure 4.1. Under this load condition, there are no significant differences between the load-deflection curves for the different cases. The straight lines with the constant slope is an indicator that the column during the loading regime will remain within the linear-elastic range.

4.3 Crack and crush distributions

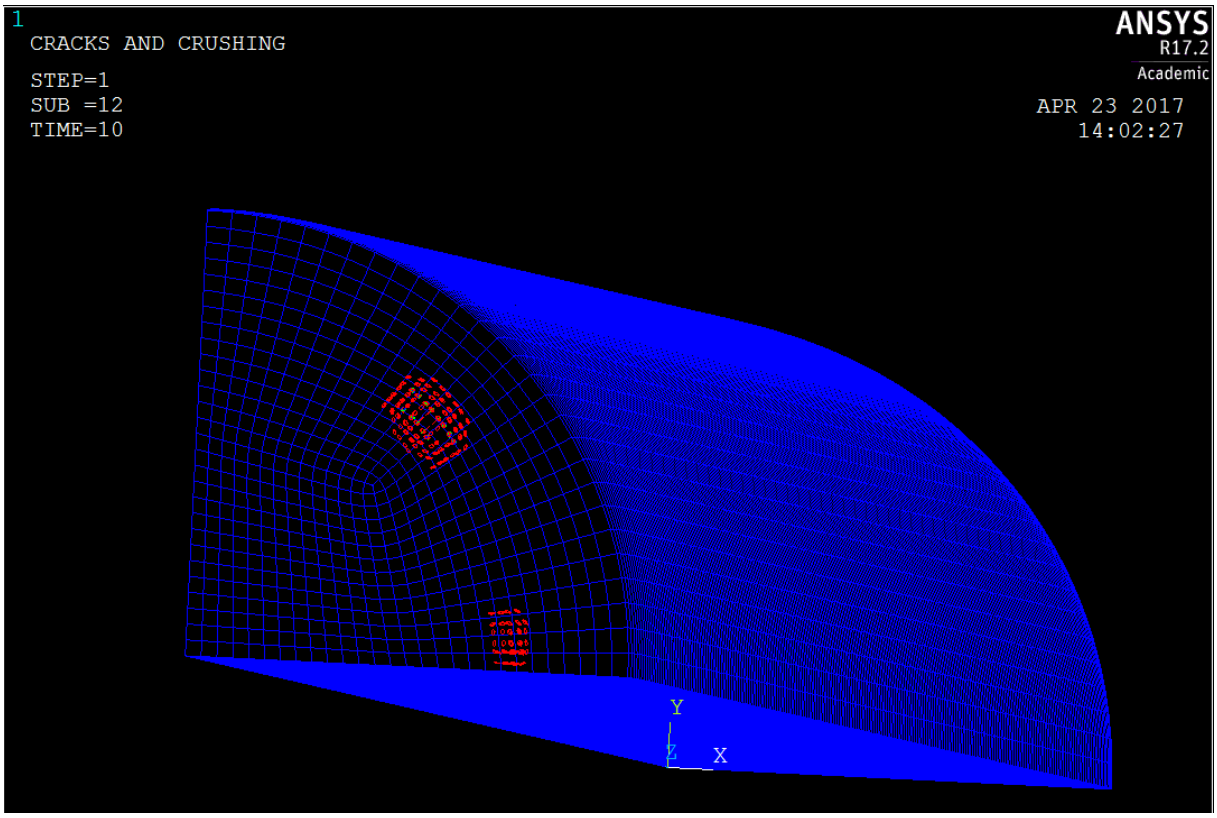

Figure 4.2. Cracking and crushing of the concrete elements.

A presentation of the quarter of the column that was modelled is shown in Figure 4.2, with red circles showing where cracks will occur in the concrete. The cracks will occur in the elements where the smeared reinforcement is added and in some of the elements closest to the reinforcement.

4.4 Different stirrup ratios and FRP configurations

All the following shear stress and strain results are extracted from the bottom end of the column, the 350mm that is expected to be the critical height with respect to shear forces.

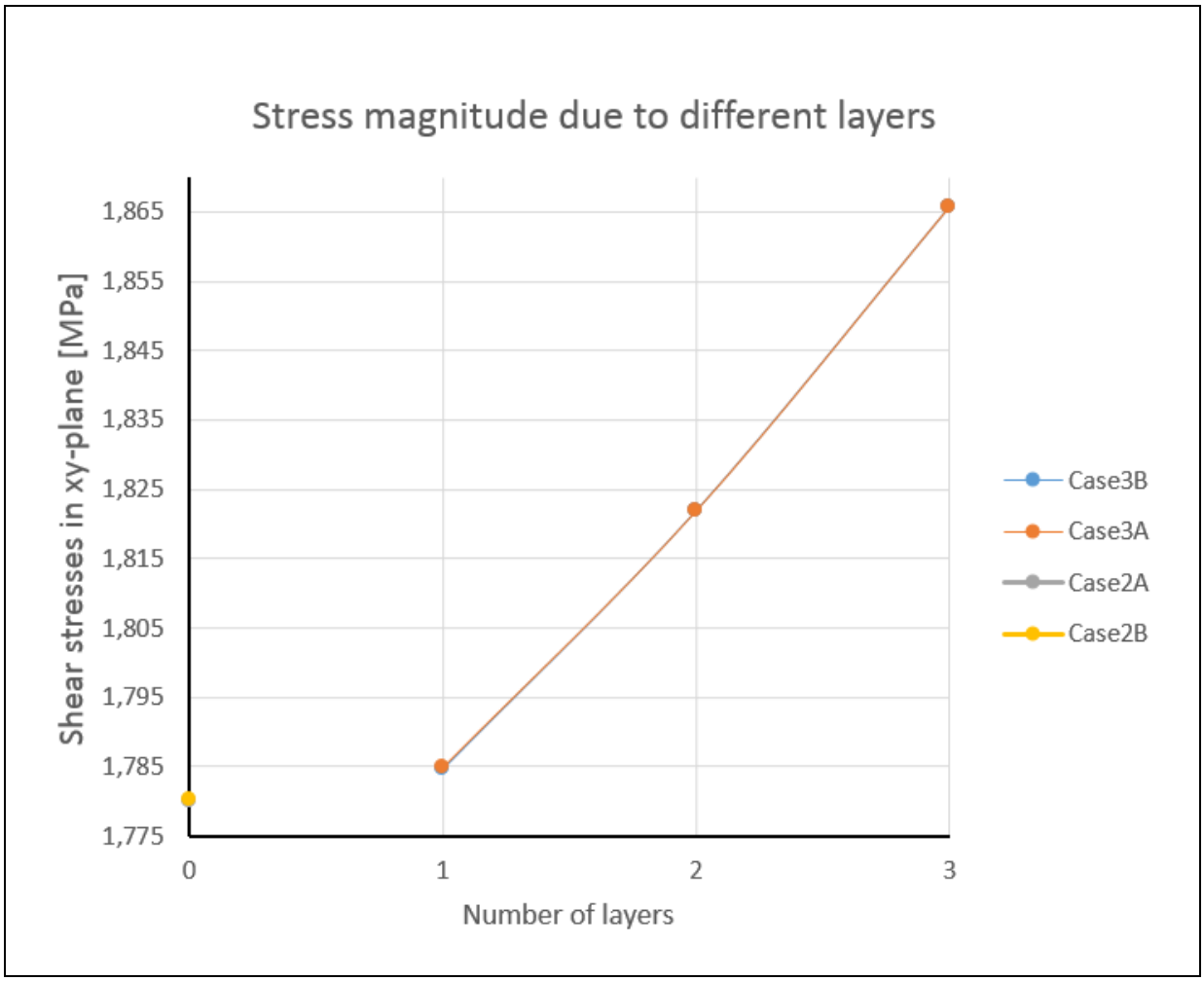

Figure 4.3. Shear stresses due to different stirrup cross section and number of CFRP layers.

As shown in Figure 4.3, the stress reference points for Case2A and Case2B with varying cross section for the stirrups are located in the same point. This implies that there are no differences in the shear stress in the xy-plane when a stirrup cross section of ø8 and ø6 are compared. The number of CFRP layers seems to be the only factor influencing the shear stresses in the bottom part of the column.

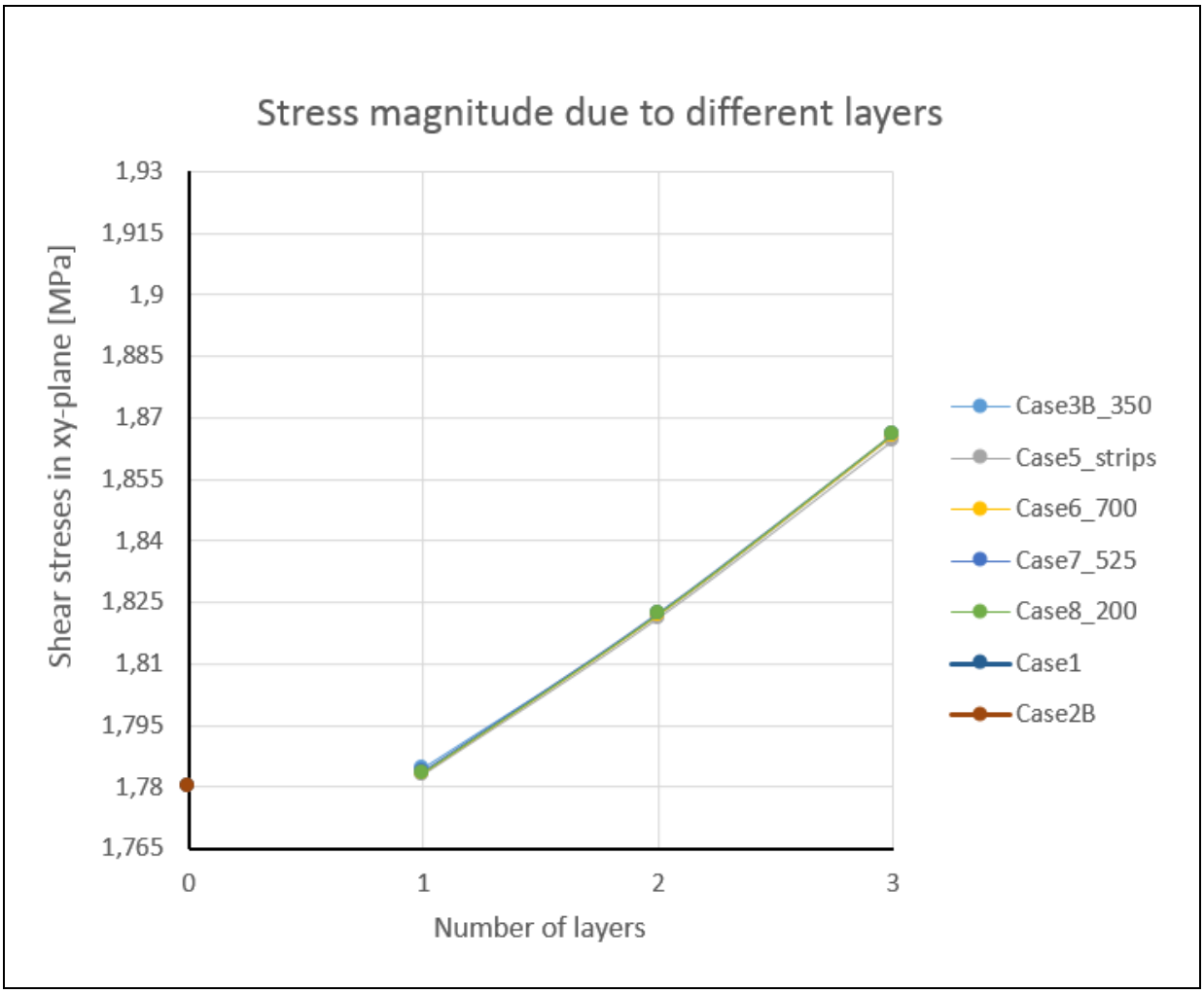

Figure 4.4. Shear stresses in the xy-plane due to different configurations of CFRP.

As shown in Figure 4.4, there are no significant stress differences between the different cases of the strengthened column for a specific number of layers. For each layer of CFRP added, the shear stresses in the xy-plane of the column increase, as a result of increased confining pressure from the CFRP.

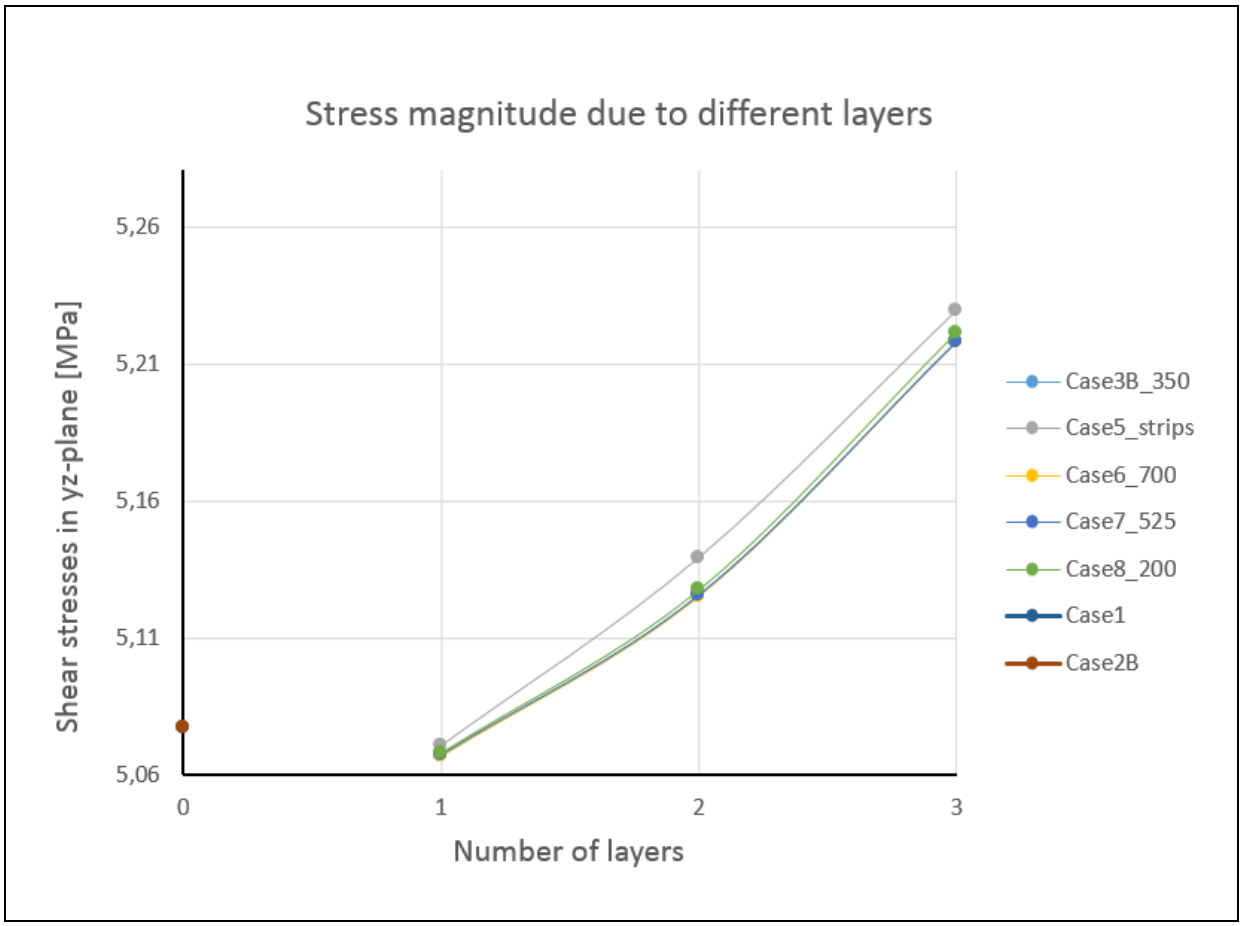

Figure 4.5. Shear stresses in the yz-plane due to different configurations of CFRP.

As observed in Figure 4.5, Case5 will lead to slightly higher shear stresses because of the discontinuity of the wrapping, resulting in stress concentrations in this area. The stresses resulting from Case5 will be slightly higher, but the confinement pressure on the column will not be as large as from the other configurations, Case3B and Case6 to Case8. Case8 show however, a similar behaviour as Case5, even though the behaviour is not as extreme as Case5, where a relatively low width of the CFRP lead to stress concentrations near the edges of the wrapping. The reference values for Case1 and Case2B will lay slightly above the stresses when the first layer of FRP is added. This is not an expected result but it can be related to the unsymmetric placement of the reinforcement within the quarter column, since the modelling of the column have been performed using symmetric boundary condition.

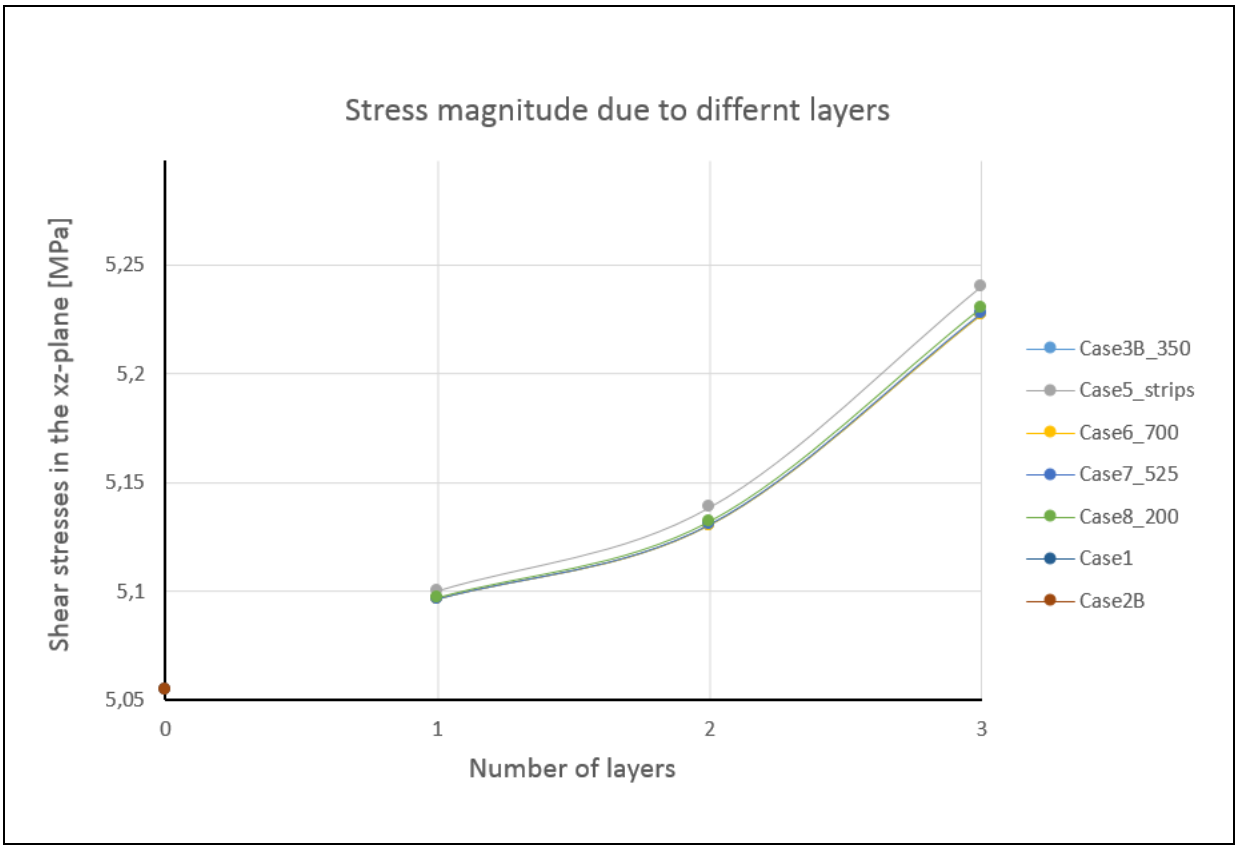

Figure 4.6. Shear stresses in the xz-plane due to different configurations of CFRP.

In Figure 4.6 it can be observed that Case5 will lead to slightly higher shear stresses because of the discontinuity of the wrapping, which causes stress concentrations on the edges of the sheets. The stresses resulting from Case5 will be slightly higher, but the confinement effect on the column is not be as beneficial as from the other configurations, Case3B and Case6 to Case8. Each layer of laminate causes larger shear stresses as a result from the increased confinement from the CFRP.

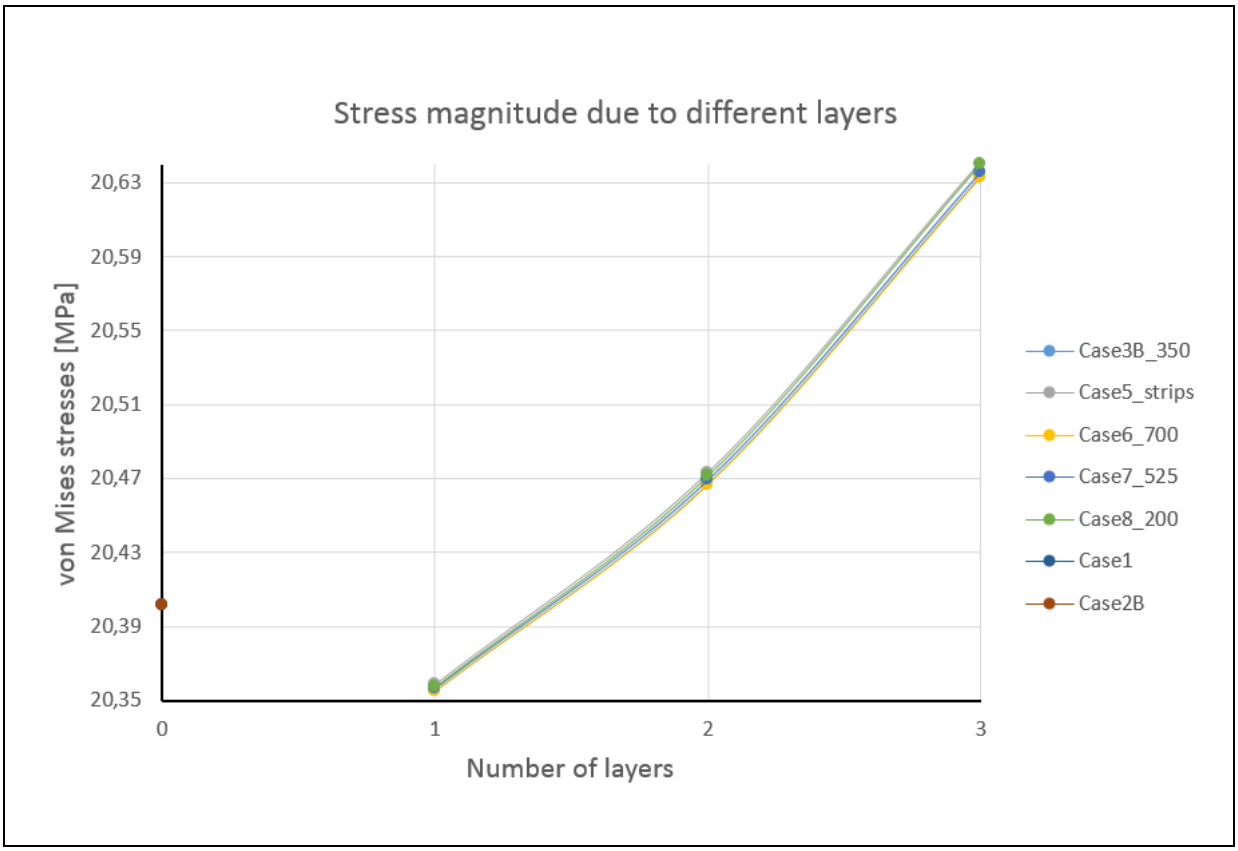

Figure 4.7. von Mises stresses due to different configurations of CFRP.

According to Figure 4.7, there are no stress differences of significance between the different cases for a specific number of layers. The magnitudes of von Mises stresses will increase for each added layer of CFRP for all the configurations, as a result of the increased confinement. However, small differences can be observed where the stresses from Case8 and Case5 are slightly above the other Cases with CFRP. For Case5, this can be explained by discontinuity in the wrapping (small width of each strip), resulting in stress concentrations in the edges of the wrapping. This is also valid for Case8 where stress concentration will occur on edges of the wrapping due to the relatively small width of the sheet. However, as concluded with the results form Figure 4.6, the confinement pressure from the FRP will for Case5 and Case8, not be as beneficial as from the other cases, Case3, Case6 and Case7. The reference values for Case1 and Case2B will lay slightly above the stresses when the first layer of FRP is added. This is not an expected result but as mentioned under Figure 4.5, it can be related to the unsymmetric placement of the reinforcement within the quarter column, since the modelling of the column have been performed using symmetric boundary condition.

4.5 Different base materials for the FRP

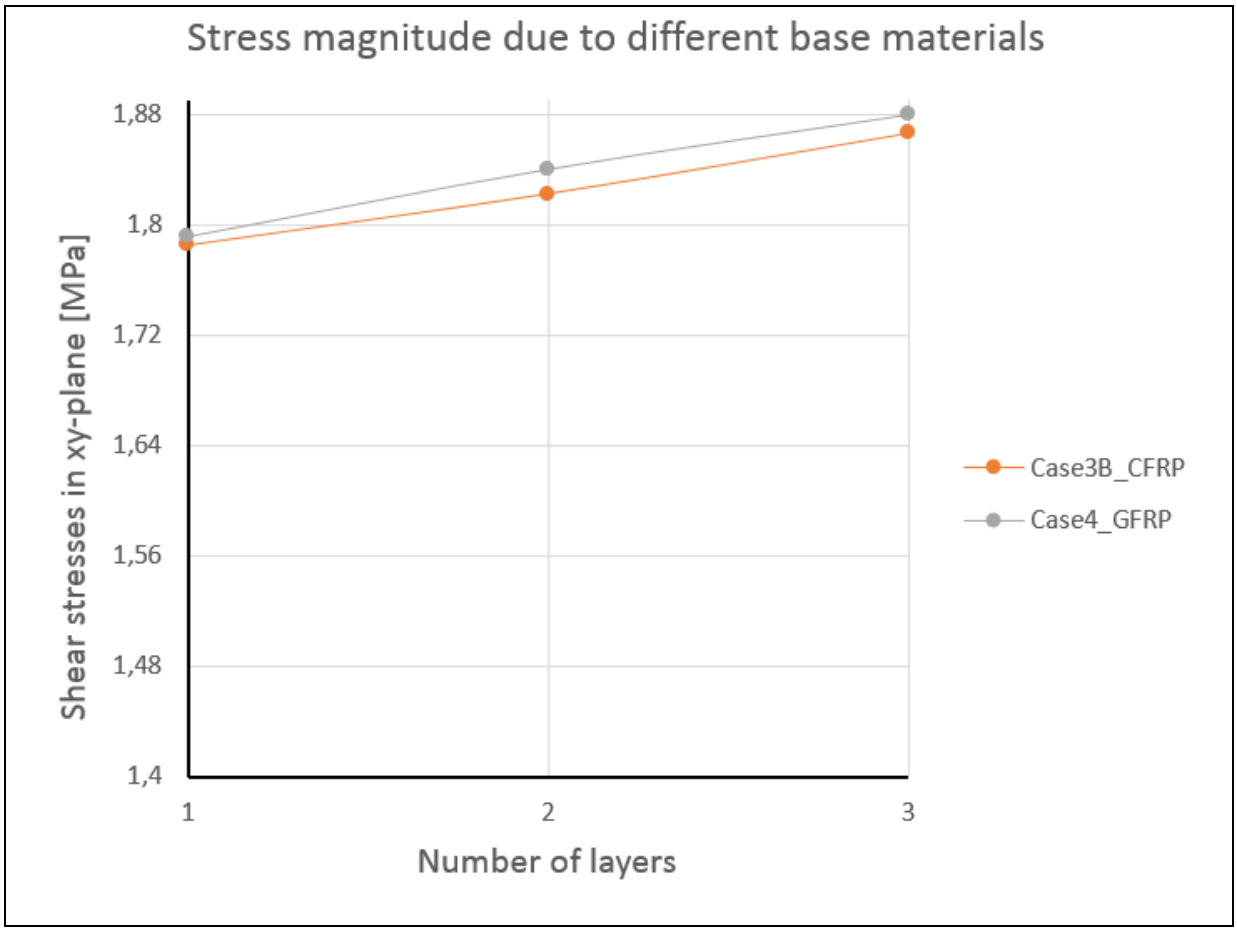

Figure 4.8. Stresses due to different base materials.

The difference between the GFRP and CFRP presented in Figure 4.8 above, are under the load regime analysed in this thesis, almost insignificant. However, when the concrete leave the linear elastic state and go over in the inelastic plastic state, larger strains will occur and the confining difference between the two base materials will increase since more of the fibres in the main fibre direction will be utilized.

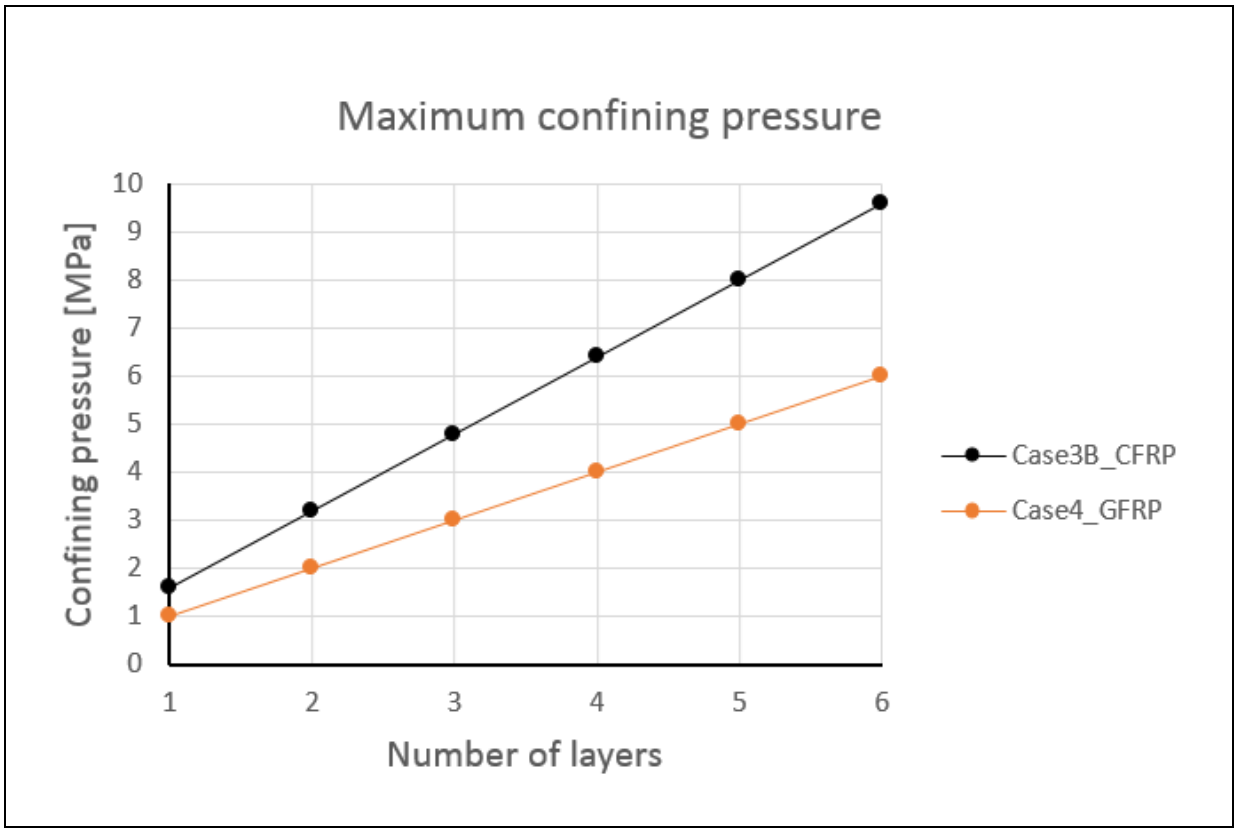

Figure 4.9. Maximum confining pressure due to different base materials.

As observed in Figure 4.9 that present different confining pressures based on theoretical hand calculations by Ghanem (2016), the confining pressure from the CFRP will be larger than from the GFRP, and the difference is increasing with the number of added layers. However, the increase in the confining pressure for both CFRP and GFRP is almost 100% from one to two layers, from two to three layers is the increase 50%, from three to four layers is the increase 25% and so on. For one layer of laminate, the maximum confining pressure from the CFRP will be approximately 60% larger than from the GFRP.

4.6 Different modelling approaches for the FRP

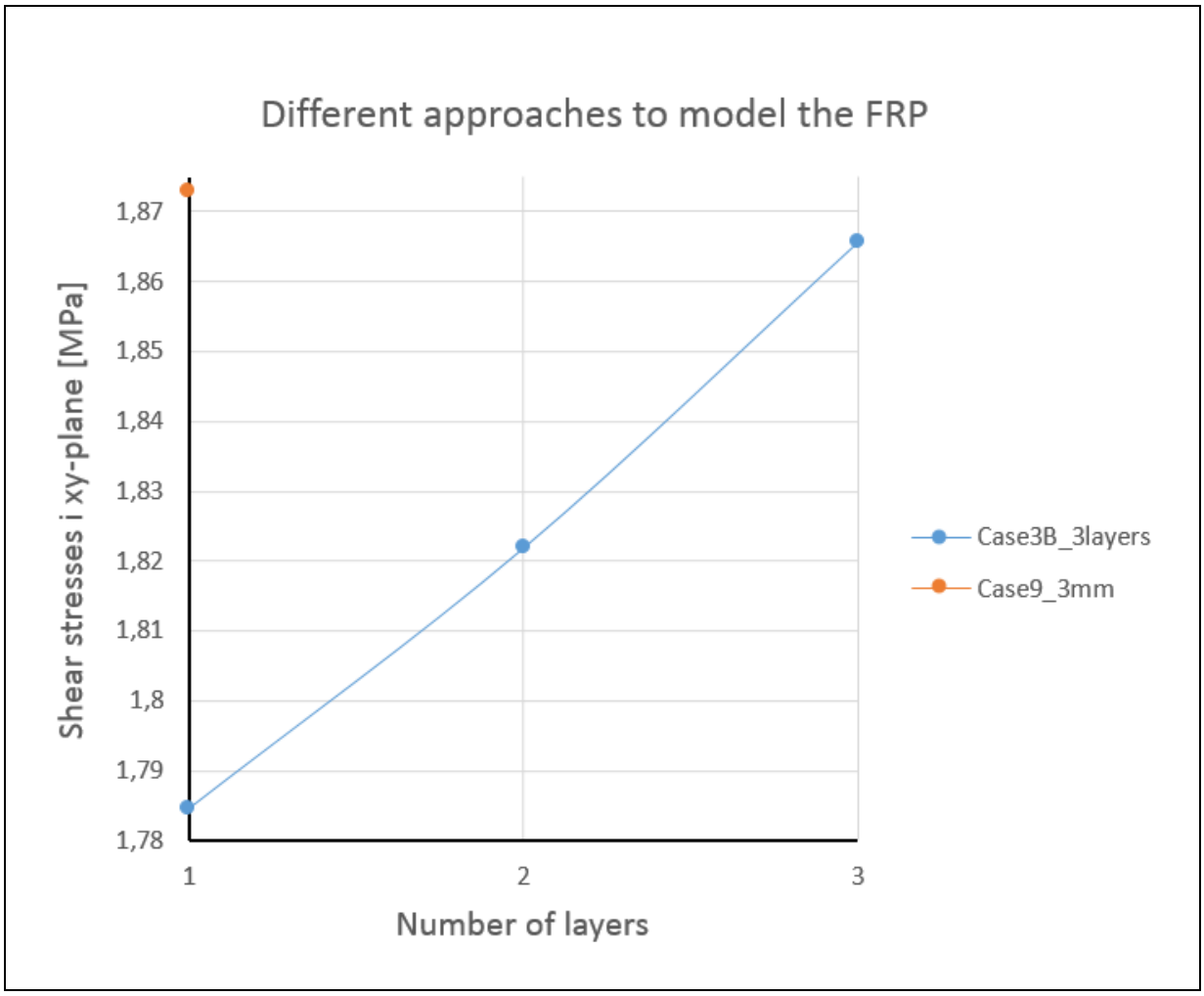

Figure 4.10. Shear stress due to different modelling approaches.

For Case9 observed in Figure 4.10, where the three laminates are modelled as one thick layer of 3mm, this will lead to increased shear stresses in the xy-plane inside the column. Based on this observation, it seems that the contact elements between each laminate layer of FRP as in Case3B, will reduce the magnitude of the shear stresses in the column when compared to Case9. Reduced shear stresses imply reduced confining pressure from the FRP on the concrete.

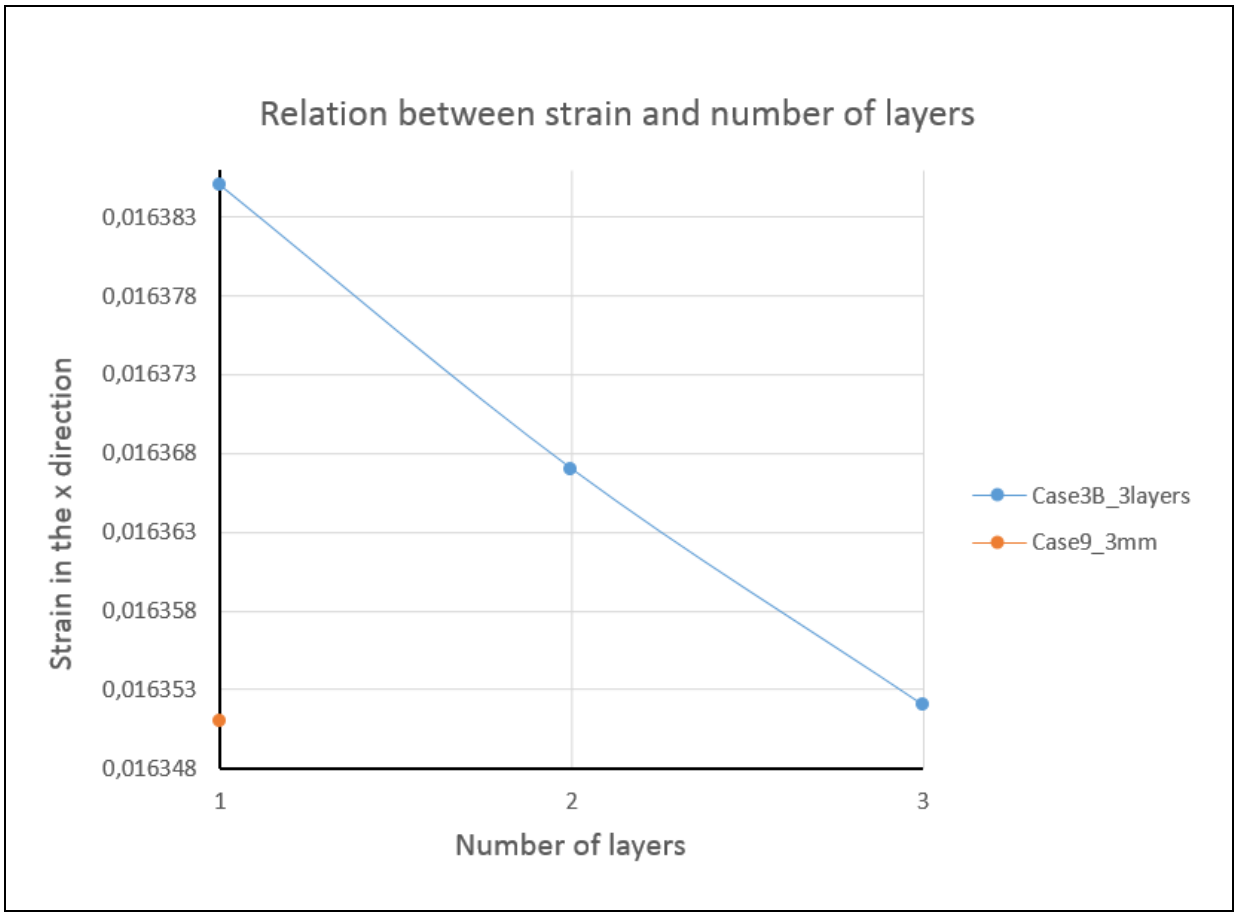

Figure 4.11. Strain due to different modelling approaches of the FRP.

In Figure 4.11 it can be observed that Case9, where contact pairs are created only between the concrete and FRP, smaller strains in the concrete in its x-direction will occur when Case9 is compared to Case3B, which has contacting elements between each laminate layer as well. This implies that the confining action from the FRP is slightly reduced when contact elements are used to connect each layer of the FRP, as in Case3B.

4.7 Stresses in hoop direction for a certain case

Table 4.2. Hoop stresses in the CFRP for Case3B.

Stresses [MPa] in the FRP for both the top and bottom part of the column				
Case	Number of layers	First layer [MPa]	Second layer [MPa]	Third later [MPa]
Case3B_ 1layer	1	Bottom: 3,86664 Top: 3,93528	Bottom: - Top: -	Bottom: - Top: -
Case3B_2layers	2	Bottom: 3,64454 Top: 3,71368	Bottom: 3,32618 Top: 3,3639	Bottom: - Top: -
Case3B_3layers	3	Bottom: 3,42693 Top: 3,49153	Bottom: 3,12511 Top: 3,15725	Bottom: 2,83404 Top: 2,8468

The CFRP wraps near the top of the column will generally experience larger stresses because larger deflections will occur in this part of the column since the load is applied to the top surface. The different hoop stresses for Case3B are presented in Table 4.2.

5 Discussion

5.1 The modelling process

In order to save both computation time and disk space, only a quarter of the column was modelled. For the SOLID65 element, the stress relaxation after cracking was chosen in order to improve the convergence. For the nonlinear material properties of the concrete the shear transfer coefficient for an open and closed crack was chosen based on research conducted by Rudeng (2008), which had great influence on the convergence ability of the model. In addition, the tensile crack factor was chosen based on trial and error of the convergence performance of the model. Both the longitudinal reinforcement and the stirrups were modelled using the smeared approach. The smeared approach for the stirrups was chosen mainly due to the benefit of saving time, while a discrete modelling of the stirrups is a relatively time consuming procedure. However, based on research conducted by (Barbosa & Ribeiro 1998), the differences between the results obtained from the discrete and the smeared modelling approaches for the reinforcement are relatively small. The smeared modelling of the longitudinal reinforcement is for this thesis considered as suitable, since the scope of this thesis is the shear behaviour of the concrete column, where the longitudinal reinforcing plays a minor role. Modelling the longitudinal reinforcement with the smeared approach is beneficial since it improves the ability of convergence for the models when these get more complex.

The smeared elements for the longitudinal reinforcement were chosen in the configuration showed in Figure 3.7 in order to get a model that could converge without any problems. Some modelling was carried out focusing the smeared elements into on large group and one smaller group. The results from these testings revealed that the smeared elements were not working properly, and that larger displacement than expected based on hand calculations occurred. It was quickly realized that the distribution of the smeared elements was the reason for these poor results. A reason for these poor results could be that if too many smeared elements were focused into a too little area, then the stiffness of these elements would be too large compared to the elements around. This would not only lead to poor results, but also to problems with the convergence of the model. The problem of convergence was also the reason why the six elements closer to the centre of the modelled quarter had a row with “empty” SOLID65 elements. If they would have been collected into a single group of elements, it would lead to problems with the convergence, especially because of the large distortion or pivot ratio of these elements. A relatively low-strength concrete was used in the modelling, because the FRP

strengthening of the column seem to produce higher results in terms of strength and strains than for high-strength concrete. Base on research conducted by Belouar et al. (2013), it is shown that the effect of FRP confinement on bearing and deformation capacities decreases with the increasing concrete strength.

The FRP composites were modelled using SOLID186 as a homogenous structural solid, since it has the features needed in order to create a realistic model of the FRP. Since the FRP layers were modelled as a separate volume in the 3D space, it was not necessary to define any section properties. The mesh that later was generated, contained one element through the thickness of the layer. In order to create a realistic interface between the concrete and the FRP and between the laminate layers of FRP, the surface-to-surface contact elements were used. Initially, it was desire to define the concrete as the target (rigid) surface because of its high stiffness and the externally bonded FRP as the contact surface (flexible), creating a rigid-flexible contact. However, this did not work out since more contact surfaces due to numerous wrapping strips, were connected to one single target surface (concrete). This happened for all the cases with externally bonded FRP, from Case3A and Case3B to Case9. If there would have been only one single contacting surface, which would have been the case with only one strip of FRP contacting one single target surface (concrete), then it would be possible to define one surface as rigid (concrete) and the other one as flexible (FRP surface). But because of the numerous strips in the different cases, the surfaces could only be assigned as flexible-flexible, even with the concrete. The symmetric contact for the contact pair was defined in order to reduce the possibility of penetration. This symmetric contact is also useful since this contact definition also enforces the constraint condition of the contact at more locations on the surface. The penetration stiffness was put to a factor of 10, which was a result of a trial and error process where different stiffness factor were tested i.e. 1, 5, 10, 15 and 20, where it was concluded that a factor of 10 gave the most realistic stresses and strains in both the FRP and the concrete. A too large penetration stiffness factor would potentially lead to ill conditioning of the model. The initial penetration was excluded in order to achieve better convergence of the model. For the contact surface offset a value of 0,5mm was used, which for model purpose was thought to act as a layer of epoxy. The augmented Lagrange was chosen for the contact algorithm since it is less sensitive to the magnitude of the contact stiffness and generally leads to better conditioning of the model as well. Since the contact detection with this algorithm take place on the integration points (Gauss points), a greater accuracy of the results will be achieved, compared to contact problems where contact detection only take place on nodal points. The behaviour of the contact

surface was put to bonded (always), which meant that two contacting surfaces would act as if they were fixed to each other, allowing no sliding between them. In order to create a realistic model for the unidirectional FRP fabric, it was essential to use the FRP's orthotropic material properties. As an alternative, the FRP can also be modelled using an isotropic model, since the fibre direction is the dominating direction, and especially the thickness is so small in comparison to the other dimensions of the FRP sheet.

The FRP could also have been modelled as a layered solid element, where each element could contain a number of layers. In this thesis however, it was emphasized on the use of contacting elements between each layer, and to see how much they contribute to the confinement of the column. Therefore, homogenous solid elements were used with contacting elements created between each layer and between the concrete and the FRP composite. Another option was to use shell elements. Shell elements would have been less time consuming for the computer to calculate, but in order to assure proper contact between specific surfaces, solid elements were used and the total volume of the FRP layer was modelled. For the shell approach, only the base area would have been created and the cross section would have been designed explicitly using section designer.

Without some experimental verifications on the tasted cases, it is difficult to know exactly if the modelled contacts are perfectly realistic or not. However, the assumption of bonded contact between the concrete and the FRP and in-between the FRP layers is acceptable based on research conducted by other within the similar field. This is therefore implying that the same contact could be created using coupled degrees of freedom or constraint equation. A different contact definition as with the use of the mentioned approaches would most likely lead to insignificant differences in the results. The results could have been different if other parameters in the *contact wizard* would have been used instead, especially the contact stiffness factor. The definition of the contact type, could also have some impact on the results, since it would been more appropriate to used the concrete as the rigid surface and the FRP surface as the flexible one. In-between the different layers, would it most likely be acceptable to use the flexible-flexible contact surfaces anyway.

The main objective of this thesis was to capture specific stress distributions and stress magnitudes when some key parameters for the retrofitted column were changed and most of the column still was in the linear- elastic state, but close to the post-elastic state. If the post-elastic state would have been reached, large parts of the concrete would start to crack, altering the stress distribution and the stress magnitudes. A load equal to 80% of the concentric capacity

of the unretrofitted column was therefore loaded onto the column. An axial load equal to the one used in this thesis, has also been used in research conducted by Abdel-Hay (2014). For lower axial loads would less of the FRP been activated for the confinement and the stress magnitudes would have been smaller, giving a weaker base for the comparison between the changed parameters. This thesis emphasized only on a static problem, where only a static design of the RC column was conducted. During the presented analysis, no dynamic aspect of the problem was considered and therefore the seismic analysis of the column was not performed. A monotonic load was applied concentrically at the top of the column, since this type of load under normal conditions is the dominating one. In Norway, until recent years, seismic design of buildings was omitted so this part was also left outside the scope of the thesis. The eccentricity of the column for simplicity of the modelling was not taken into account.

5.2 Validation of the model

According to the hand calculations for the axial shortening of the plain column, Case1, which are shown in the Appendix A.8, the axial shortening is 1,127mm by an axial load of 80% of the theoretical axial capacity. The result from Case1 in Table 4.1, shows that the axial shortening will be 1,12093mm. The numerical model will experience 0,539% lower axial shortening than it should based on the hand calculations, meaning that the model is 0,539% stiffer than it theoretically was expected to be. A typical percentage error between the FE model and experimental results of below 10% is within an acceptable range (Usefi et al. 2016). This low difference is however, not to expect if the model is forces over in the post-elastic range due to larger loads. In the linear elastic range, the FE model show a good agreement with the hand calculations. It seems like the model is capturing the compressive stress- strain behaviour of the concentrically loaded column and that the smeared modelling of the reinforcement is an acceptable approach.

Validation of the externally bonded FRP

The validation of stresses in the hoop direction of the FRP is done by omitting the singularities that will occur in the edges of the FRP sheets. Based on Equation 2-3, the confining pressure on the concrete from one layer of externally bonded CFRP in Case3B can be calculated as shown below:

$$p = \frac{\sigma_1 t}{r} \tag{2-3}$$

$p = 0{,}0446 N/mm^2$

Where:

- t = 1mm
- r = 175mm
- $\sigma_1 = 7{,}80192 N/mm^2$, which is the total stress in the hoop direction form one layer of CFRP in Case3B (Table 4.2)

Figure 4.9 shows that one layer of CFRP in Case3B maximally can increase the confining pressure on the concrete with $1{,}5965 N/mm^2$. This shows that for Case3B with one layer of CFRP, only 2,79% of the confining capacity from the FRP is utilized by the concrete. The reason for this low value is that the model under the whole loading regime remains within the linear elastic range. This confinement pressure from the CFRP will increase significantly when the model enter the post-elastic range. No exact experiments could be found for the cases modelled in this thesis, which could be used for validation of the obtained results. However, similar modelling approaches for externally bonded FRP has been used in a number of research papers (Jayajothi et al. 2013; Jayalin et al. 2015; Sayed et al. 2014; Sen & Jagannatha Reddy 2014), making it reasonable to believe that the same approach will work for cases modelled in this thesis.

For the interpretation of stresses from ANSYS, it is important to bear in mind that some extreme stress values will occur due to stress singularities in corners and edges of the element meshes. Therefore, the interpretation of the results has been done omitting these extreme values.

5.3 Interpretation of the results from the parametric study

Effect of the stirrup ratio

Due to the stirrups in a RC column under axial compressive loading, the column turns out to be in a tri-axial compressive status. In general, an increase of the stirrup ratio will significantly improve the confinement capacity of the column, which increase the load bearing capacity and improve the ductile capacity of the column. However, when Case2A and Case2B, and Case3A and Case3B are compared in Figure 4.3, it can be concluded that there is no significant difference between the shear stresses in the xy-plane, when both the cross section area of the stirrups and the centre distance of the stirrups are changed. These results are however, obtained

when the concrete is within the linear elastic range as seen in Figure 4.1. It can be expected that reduced stirrup cross section and increased centre distance will have greater impact on the stresses inside the column when the model has reached the post-elastic phase. Beside some elements that crack around the longitudinal reinforcing, as seen in Figure 4.2, the column will remain within the linear elastic range. The assumption that most of the column still is within the linear elastic range are the von Mises stresses seen in Figure 4.7. The values are well below the yield strength of the concrete of 25N/mm^2. von Mises stress is a yield criterion that compared to the yield strength of concrete gives an indicator of how much the concrete capacity is utilized and when the failure can be expected. However, Figure 4.7 present von Mises stresses in the bottom of the column, but the largest stresses will occur in the top because of the stress accumulation around the longitudinal reinforcement, as shown by the occurring cracks in Figure 4.2.

Effect from the different configurations

As a result from the tested cases in this thesis, as seen in Figure 4.4, 4.5,4.6 and 4.7, it can be concluded that the different configurations of externally bonded FRP have almost no influence on the stresses occurring inside the column. Case5 with the strips is the only case that stands out, as seen in Figure 4.5. The reason for this is that the CFRP configuration will lead to slightly higher stresses in the xy-plane because of the discontinuity of the wrapping, which will give a stress concentration near the edges of the strips. The shear stresses in Case5 will be slightly higher, but the confinement effect on the column will not be as beneficial as from the other configurations, Case3B and Case6-Case8. The reason why the stress magnitudes in the xz and the yz-plane for the same case is different, is because the longitudinal reinforcement within the modelled quarter column is not centred, but distributed as seen in Figure 3.7.

Effect from the number of layers

Each layer of laminate that is applied to the column will increase the stresses inside the column, as seen in Figure 4.3 to Figure 4.7, as a result of the increased confinement from the FRP. For each laminate layer added to the column, the stresses in the inner layers are decreasing, 6,09% and 6,35% for two and three laminate layers in the bottom of the column, respectively. This distribution of stresses for increasing number of layers, can be seen in Table 4.2 which shows the stress transfer in the bonded interface between the different surfaces, concrete and the FRP and in between the FRP laminates. It can be seen in Figure 4.9 as well, that the confinement pressure on the column will increase with the number of layers. However, there will be a

percentage decrease in the confining effectiveness the more layers that are added. The percentage increase in the confinement effectiveness for each added layer will be greatest for the first added layer, with 100% increase in the confinement effect, 50% increase in the confinement effect from two to three layers and then 25% increase from three to four layers and so on. This shows that it is most beneficial to add up to 3-4 layers, if it is desired to get most effect from the amount of materials used. It is important to bear in mind that profound FRP retrofitting in a certain section of the column significantly affects the stress distribution and the stress magnitude of the column. Large stress concentration and potentially local failure can occur in the transition zones for the stresses between the confined and unconfined concrete. It is therefore crucial to be aware of the failure modes that will change due to the retrofitting of the column.

Effect from the different base materials – CFRP and GFRP

The difference between the GFRP and CFRP under 80% utilization of the axial capacity is as seen in Figure 4.8, almost insignificant. However, when the concrete leave the linear elastic state and go over in the inelastic plastic state, larger strains will occur and the confining difference between the two base materials will increase since more of the fibres in the main fibre direction will be utilized. The difference in the maximal confining pressure from the CFRP compared to the GFRP will just increase the more laminate layers that are added to the column. This effect is seen in Figure 4.9, which show that for one layer of laminate the confining pressure from CFRP will be approximately 60% larger than the confining pressure from the GFRP. These theoretical differences are also supported by research conducted by Jaya and Mathai (2012). However, apart from lower tensile strength and therefore poorer confinement properties for GFRP compared to CFRP, the energy absorption capacity during dynamic loading is higher for GFRP due to its good strain capacities when compared to CFRP.

Effect from different modelling approaches for three layers of CFRP

When Case9 with one thick laminate layer of 3mm and Case3B with three laminate layers of 1mm are compared in Figure 4.10, it can be observed that the shear stresses in the xy-plane inside the column will increase for Case9. These increased stresses implies that the confinement from Case9 will be greater compared to the confinement from Case3B. Case9 will lead to approximately 0,4% larger shear stresses than the modelling approach used for Case3 with three laminate layers of 1mm thickness. Based on this observations, it seems that the contacting elements between each laminate layer will lead to smaller confining pressure from the

externally bonded FRP onto the concrete. The reduced strain in the x-direction for Case9 compared to Case3B as seen in Figure 4.11 also supports this assumption. The penalty stiffness factor is one of the parameters that greatly influence the transfer of stresses between each laminate layer. However, increasing the penalty stiffness factor come with a cost, potentially causing ill conditioning of the matrices and poor results for the model. The only way to validate if the results from Case9 are more realistic than the results obtained from Case3B is by conducting physical experiments.

Failure mode

Due to the externally bonded FRP, the concrete will be in a triaxial state of stress, the FRP will be subjected to tension in the hoop direction and the failure mode of the RC column will change from brittle to ductile. The governing failure mode for the axially loaded column will in most cases be crushing of the concrete or tensile failure (rapture) of the FRP. The rapture of the FRP can occur as a result from the triaxial state of stress or in real life due to poor quality of the execution, leading to stress concentrations and premature failure. The amount of composite action the FRP is exposed to is a critical factor influencing the failure of the FRP. By full composite action, the FRP jacket will undergo both longitudinal and transversal strain, reducing the ultimate stresses and strains of the FRP and potentially leading to micro buckling and delamination. It is important to keep in mind that debonding failure can occur before the crushing of concrete and/or the tensile failure of FRP. Debonding failure may occur in the concrete near the surface, in the adhesive, in the interface between the concrete and the FRP, or in between the different FRP laminates. Due to the externally bonded FRP, the failure mode for the RC column will change from brittle to ductile. The ductile failure mode is preferred over the brittle, while it generates a predictable form of failure of the structure so that it do not collapse without prior warning. Because of the FRP's capability of providing the ductile failure mode, it is frequently used in seismic retrofit of RC structures.

5.4 Recommendation

For increase in the load carrying capacity, safety and ductility of RC columns, strengthening of columns with FRP is an excellent option. FRP has a high strength to weight ratio and if applied to RC columns it provides a very small increase in the cross section area of columns. This makes the FRP retrofitting very suitable in places where space is highly valued such as office buildings etc. The alternative retrofitting methods, as mentioned in chapter 2.8 are relatively different from retrofitting with FRP, since significantly more area after the application of the strengthening is needed. Based on the results obtained in this thesis and based on former research, CFRP is recommended to use over GFRP for strengthening purposes of RC columns under axial loading. For an axially loaded column that will experience large lateral displacements in the concrete within the height of the FRP wrapping, strips with a relatively small width must be avoided because of the potential stress concentration on edges of the strips. It is recommended to use up to 3-4 laminate layers, if it is desirable to achieve the largest confinement effectiveness with respect to the amount of materials used. The protection of the FRP against environmental effects such as UV-exposure and freeze and thaw effects is highly recommended in order to enhance the service life of the retrofitting. The protection can be enabled using a suitable coating. Especially the bonding between the concrete and the FRP and between the FRP laminates is susceptible to deterioration. The reversibility of FRP retrofitted RC members is a great benefit of this strengthening method, since FRP can be fully or partially removed if more advanced techniques will be developed in the future. The presented numerical models are easy and simple to construct and can be used as design tools for retrofitted RC columns.

6 Conclusion

The following conclusions are drawn from this master thesis:

- There is no significant difference between the shear stresses in the xy-plane, when both the cross section area of the stirrups and the centre distance of the stirrups are changed.
- The different configurations of externally bonded FRP have almost no influence on the stresses occurring inside the column. Only Case5 stands out with higher shear stresses in the xy-plane due to the relatively small width of the FRP sheets leading to stress concentrations on the edges of the strips.
- For each added layer of FRP, the confinement pressure on the column is increased. However, the confinement effectiveness is largest for the first added layers, and will decrease when more layers are added. 3-4 laminate layers of FRP is recommended if it is desirable to achieve the largest confinement effectiveness with respect to the amount of materials used.
- For the stresses in the xy-plane, the difference between the GFRP and CFRP is almost insignificant. However, when the concrete leave the linear elastic state and go over in the inelastic plastic state, larger strains in the concrete will occur increasing the differences in the confinement between the two base materials. CFRP will then give a significant larger confinement pressure on the column than the GFRP.
- Based on the shear stresses in the xy-plane and the strain of the concrete in the critical height, it seems that the adding of contact elements between each laminate layer of FRP will lead to smaller confining pressure from the externally bonded FRP on the concrete.
- The governing failure mode for the axially loaded column will in most cases be either crushing of the concrete or tensile failure (rapture) of the FRP. However, debonding failure can occur before the crushing of the concrete and/or the tensile failure of FRP.
- FRP is an excellent material to increase the load carrying capacity, safety and ductility of RC columns.
- FRP composites applied to RC columns provides very little increase in the cross section area of columns, which makes it suitable in places where space is highly values such as office buildings etc.
- Protection of FRP against environmental effects is highly recommended in order to enhance the service life of the retrofitting.

7 Recommendations for Future Work

It is of great interest to investigate the behaviour of the critical height with respect to shear after the column reach the post-elastic state, in order to support the assumptions made in this thesis, especially with respect to the influence from the stirrup ratio. This can be done either by numerical models or by experiments. Some experiments should be conducted in order to quantify the influence from the different modelling approaches of the FRP and based on these results find the most realistic modelling approach for the FRP with respect to its real life behaviour. It could have been of interest to model the interaction between the different interfaces, concrete to FRP and FRP to FRP, using other contact definition such as coupling of DOF's or constraint equations to support the assumptions made in this thesis. It is also of interest to model other retrofitting techniques such as TRM, Ferrocement and Reinforced concrete Jackets and compare the different structural behaviours of the RC column for both static and dynamic loads.

8 References

Abdel-Hay, A. S. (2014). Partial strengthening of R.C square columns using CFRP *Housing and Building National Researche Center*, 10: 279-286.

Adams, V. & Askenazi, A. (1999). *Building Better Products with Finite Element Analysis*. 2530 Camino Entrada, Santa Fe, NM 87505-4835USA: OnWordPress.

ANSYS. (2016). *ANSYS Help Viewer*: SAS IP, Inc. .

Audenaert, K., Marsavina, L. & De Schutter, G. (2009). *Influence of Cracks on the Service Life of Concrete Structures in a Marine Environment*. Key Engineering Materials, Timisoara, Romania, pp. 153-160. Stafa-Zürich, Switzerland: Trans Tech Publications ltd.

Bajer, M., Kala, J. & Barnat, J. (2007). *MODELING CHEMICAL ANCHOR PLACED IN CONCRETE USING DIFFERENT FEM SYSTEMS*. Brno University of Technology.

Bakis, C. E., Bank, L. C., Brown, V. L., Consenza, E., Davalos, J. F., Lesko, J. J., Machida, A., Rizkalla, S. H. & Triantafillou, T. C. (2002). Fiber- Reinforced Polymer Composites for Construction - State-of-the-Art Review. *Journal of Composites for Construction* 6(2): 73-87.

Bangash, M. Y. H. (1989). *Concrete and Concrete Structures: Numerical Modeling and Applications*. London, England 687 pp.

Barbosa, A. F. & Ribeiro, G. O. (1998). *ANALYSIS OF REINFORCED CONCRETE STRUCTURES USING ANSYS NONLINEAR CONCRETE MODEL*. COMPUTER MECHANICS, New Trends and Applications Barcelona, Spain pp. 1-7: Inrenational Center for Numerical Methods in Engineering.

Bath, K.-J. (2014). *Finite Element Procedures*. 2nd ed. Watertown, MA, USA: Prentice Hall, Person Education, Inc. .

Belouar, A., Laraba, A., Benzaid, R. & Chikh, N. (2013). Structural Performance of Square Concrete Columns Wrapped with CFRP Sheets. *Procedia Engineering*, 54: 232-240.

Benzaid, R. & Mesbah, H. A. (2013). *Circular and Square Concrete Columns Externally Confined by CFRP Composite: Experimental Investigation and Effective Strength Models*. InTech ed. Fiber Reinforced Polymers - The Technology Applied for Concrete Repair: InTech.

Chung, D. L. (2012). *Carbon Fiber Composites*. 1st ed. 313 Washington Street, Newton, MA, US. : Butterworth-Heinemann 1994.

Cogswell, F. N. (1992). *Thermoplastic Aromatic Polymer Composites: A Study of the Structure, Processing, and Properties of Carbon Fibre Reinforced Polyetheretherketone and Related Materials.* 313 Washington Street, Newton, MA, US. : Butterworth- Heinemann.

Dandapat, R., Deb, A. & Bhattacharyya, S. (2011). Failure modes for FRP wrapped cylindrical concrete columns. *Journal of Reinforced Plastics and Composites*, 30 (7): 561-579.

Dhakal, D. (2014). *Investigation of Chloride Induced Corrosion of Bridge Pier and Life-Cycle Repair Cost Analysis Using Fiber Reinforced Polymer Composites*. Las Vegas, USA: University of Nevada, Civil and Environmental Engineering 78 pp.

Dubey, R. & Kumar, P. (2016). Experimental study of the effectiveness of retrofitting RC cylindrical columns using self-compacting concrete jackets. *Construction and Building Materials*, 124: 104-117.

Einde, L. V. D., Zhao, L. & Seible, F. (2003). USE OF FRP COMPOSITES IN CIVIL STRUCTURAL APPLICATIONS *Construction and Building Materials*, 17 (6-7): 389-403.

Ghanem, S. Y. (2016). *CIRCULAR RC COLUMNS PARTIALLY CONFINED WITH FRP*. Doctoral Dissertation UKnowledge: University of Kentucky, Civil Engineering. 183 pp.

Hibbeler, R. C. (2008). *Mechanics of Materials*. 7th ed. Upper Saddle River, New Jersey 07458: Pearson Prentice Hall.

Hollaway, L. C. & Teng, J. G. (2008). *Strengthening and Rehabilitation of Civil Infrastructures Using Fibre-Reinforced Polymer (FRP) Composites*. 1st ed. 6000 Broken Sound Parkway, NW, Suite 300, Boca Raton, FL 33487, USA Woodhead Publishing.

Institute, C. R. S. (2017). *Reinforcing Steel*. 933 North Plum Grove Road, Schaumburg, IL: CRSI. Available at: http://www.crsi.org/index.cfm/basics/reinforcing-steel. Cited:27 April, 11:30

International Federation of Structural Concrete, *f.* (2001). Externally bonded FRP reinforcement for RC structures. . Case Postale 88, CH-1015 Lausanne, Switzerland: fédération internationale du béton (*fib*).

International Federation of Structural Concrete, *f.* (2007). FRP reinforcement in RC structures. Case Postale 88, CH-1015 Lausanne, Switzerland: fédération internationale du béton (*fib*).

Islam, N. & Hoque, M. M. (2015). Strengthening of Reinforced Concrete Columns by Steel Jacketing: A State of Review. *Asian Transactions on Engineering* 5(3).

Izzet, A. F. & Zahra, H. D. (2016). BEHAVIOR ANALYSIS OF POST-TENSIONING CONCRETE BEAMS EXPOSED TO HIGH TEMPERATURE BY USING FINITE ELEMNET METHOD (ANSYS PROGRAM). *Applied Research Journal*, 2 (4): 220-227.

Jaya, K. P. & Mathai, J. (2012). *Strengthening of RC Column using GFRP and CFRP*. 15 th. WORLD CONFERENCE ON EARTHQUAKE ENGINEERING Lisbon, Portugal, p. 10.

Jayajothi, P., Kumutha, K. & Vijai, K. (2013). FINITE ELEMENT ANALYSIS OF FRP STRENGTHENED RC BEAMS USING ANSYS. *Asian Journal of Civil Engineering* 14 (4): 631-642.

Jayalin, D., Prince Arulraj, G. & Karthikja, V. (2015). ANALYSIS OF COMPOSITE BEAM USING ANSYS. *International Journal of Research in Engineering and Technology*, 4 (9): 11-15.

Kachlakev, D., Miller, T., Yim, S. & Chansawat, K. (2001). FINITE ELEMENT MODELING OF REINFORCED CONCRETE STRUCTURES STRENGTHENED WITH FRP LAMINATES. In Group, O. D. o. T. R. (ed.). *Final Report*: Oregon Department of Transportation Research Group. 99 pp.

Kachlakev, D. I. (1998). *Finite Element Method (FEM) Modeling for Composite Strengthening/Retrofit of Bridges*. Research Project Work Plan. Oregon State University, Salem, Oregon, US: Civil, Construction and Enviromental Engineering Department.

Kachlakev, D. I. & McCurry, D., Jr., . (2000). Simulated Full Scale Testing of Reinforced Concrete Beams Strengthened with FRP Composites: Experimental Results and Design Model Verification. Salem, Oregon, US.

Karbhari, V. M. & Gao, Y. (1997). Composite jacketed concrete under uniaxial compressionverification of simple design equations. *Journal of Materials in Civil Engineering*, 9 (4): 185-193.

Karim, H., Sheikh, M. N. & Hadi, M. N. S. (2016). Axial load-axial deformation behaviour of circular concrete columns reinforced with GFRP bars and helices. *Construction and Building Materials*, 112: 1147-1157.

Kaw, A. K. (2006). *Mechanics of Composite Materials*. 2nd ed. 6000 Broken Sound Parkway NW, Suite 300 Boca Raton, FL33487-2742, USA: Taylor & Francis Group, LLC.

Khalifa, A., Gold, W. J., Nanni, A. & Aziz, M. I. A. (1998). Contribution of Externally Bonded FRP to Shear Capacity of Flexural Members. *ASCE- Journal of Composites for Construction*, 2 (4): 195-203.

Lam, L. & Teng, J. G. (2003). Design-oriented Stress-Strain Model for FRP-Confined Concrete in Rectangular Columns. *Journal of Reinforced Plastics and Composites*, 22 (13): 1149-1186.

Moshiri, N., Hosseini, A. & Mostofinejad, D. (2015). Strengthening of RC columns by longitudinal CFRP sheets: Effect of strengthening technique. *Construction and Building Materials*, 79: 318-325.

Oehlers, D. J. & Seracino, R. (2004). *Design of FRP and Steel Plated RC Structures: Retrofitting Beams and Slabs for Strength, Stiffness and Ductility* 1st ed. The Boulevard Langford Lane, Kidlington, Oxford OX5 1GB, UK: Elsevier Ltd. .

Parvin, A. & Brighton, D. (2014). FRP Composites Strengthening of Concrete Columns under Various Loading Conditions. *Polymers*, 6 (4): 1040-1056.

Pawar, V. S. & Pawar, P. M. (2016). *Nonlinear Analysis of Reinforced Concrete Column with ANSYS* International Research Journal of Engineering and Technology (IRJET), pp. 2290-2296.

Rudeng, L. (2008). Values of shear transfer coefficients of concrete element Solid65 in Ansys. *Journal of JIangsu University(Natural Science Eidt)*, 29 (2): 169-172.

Sasani, M. (2004). *SHEAR STRENGTH AND DEFORMATION CAPACITY MODELS FOR RC COLUMNS*. 13 th World Conference on Earthquake Engineering Vancouver, B.C., Canada.

Sayed, A. M., Wang, X. & Wu, Z. (2014). Finite element modeling of the shear capacity of RC beams strengthened with FRP sheets by considering different failure modes. *Construction and Building Materials*, 59: 169-179.

Sen, T. & Jagannatha Reddy, H. N. (2014). Efficacy of bio derived jute FRP composite based technique for shear strength retrofitting of reinforced concrete beams and its comparative analysis with carbon and glass FRP shear retrofitting schemes. *Sustainable Cities and Society*, 13: 105-124.

Shah, S. P., Swartz, S. E. & Ouyang, C. (1995). *Fracture Mechanics of Concrete: Applications of Fracture Mechanics to Concrete, Rock and Other Quasi-Brittle Materials*. New York: John Wiley & Sons, Inc. .

Standardization, E. C. f. (2004). *Design of concrete structures: General rules and rules for buildings*, EN 1992-1-1 +NA: 2008 rue de Stassart 36, B-1050 Brussel: CEN.

Standardization, E. C. o. (2005). *Design of structures for earthquake resistance: Assessment and Retrofitting of buildings*, EN 1998-3. rue de Stassart, 36 B-1050 Brussels: CEN.

Takenaka, K. (2012). Negative thermal expansion materials: technological key for control of thermal expansion. *Department of Crystalline Materials Science, Nagoya University*, 13: 11.

Teng, J. G. (2001). *Failure modes of FRP-strengthened RC structures*. 26th Conference on Our World in Concrete & Structures, Singapore: Cl-Premier PTE LTD.

Teng, J. G., Chen, J. F., Smith, S. T. & Lam, L. (2004). *FRP- strengthened RC structures*. Chichester, UK: John Wiley & Sons, Ltd. .

Tetta, Z. C., Koutas, L. N. & Bournas, D. A. (2015). Textile-reinforced mortar (TRM) versus fiber-reinforced polymers (FRP) in shear strengthening of concrete beams. *Composites Part B: Engineering*, 77: 338-348.

Tsonos, A.-D. G. (2010). Performance enhancement of R/C building columns and beam–column joints through shotcrete jacketing. *Engineering Structures*, 32 (3): 726-740.

Usefi, N., Nav, F. M. & Abbasnia, R. (2016). Finite element analysis if RC elements in progressive collaps scenario. *Journal of the Croatian Assosiation of Civil Engineers*, 68 (12): 1009-1022.

William, K. J. & Warnke, E. P. (1975). *"Constitutive Model for the Triaxial Behavior of Concrete". Proceedings, International Association for Bridge and Structural Engineering.*, vol. 19. BERGAMO, Italy.

Xiao, Y. & Wu, H. (2000). Compressive Behavior of Concrete Confined by Carbon Fiber Composite Jackets *Journal of Materials in Civil Engineering*, 12 (2): 139-146.

Yu, Y. (2011). *Strengthening of Steel Structures* Saarbrücken, Germany: LAP LAMBERT Academic Publishing GmbH & Co. KG. 239 pp.

Appendix A. Theoretical Hand Calculations

A.1 Preface

As mentioned in chapter 3.5.1, the hand calculations of the axial capacity, rebar and stirrup amount, control of the slenderness criterion and the minimum concrete cover are based on NS-EN 1992 - 1 - 1:2004+NA:2008, while the hand calculations of the confining pressure from the FRP are based on the dissertation from Ghanem (2016).

$N_{Ed} = f_{cd}*(A_c - A_s) + f_{yd}*A_s$ general relation for the axial capacity of a short column

$f_{cd} = \frac{\alpha_{cc} f_{ck}}{\gamma_c}$ γ_c = 1.5 from Table NA 2.1N and α_{cc} = 0.85 form N.A. 3.1.6

$f_{yd} = \frac{f_{yk}}{\gamma_s}$ γ_s = 1.15 from Table NA 2.1N

f_{cd} = 0.85*25/1.5 = 14.17N/mm^2

f_{yd} = 500/1.15 = 434,78N/mm^2

A.2 Reinforcement of the column

Longitudinal reinforcement

The design of the longitudinal reinforcement was based on the assumption of the use of 6xØ16

$A_c = \frac{\pi(350mm)^2}{4}$ = 96211,27mm^2

$A_s = \frac{\pi(16mm)^2}{4}$ = 201,06mm^2 x 6 = 1206,37mm^2

$A_{s,min}$ = not smaller than 0,01A_C and not greater than 0,08A_C NA. 9.5.2(2) and NA. 9.5.2(3)

A_S = 1206,37mm^2 that is greater than 962,11mm^2 but smaller than 7696,90mm^2 => O.K

Stirrups

The design of the stirrups is conducted according to NS-EN 1992 - 1 - 1:2004, 9.5.3

Test with ø8 for the stirrups.

According to 9.5.3(1), the cross section cannot be smaller than the largest values of 6mm and ø16/4 => 6mm

According to NA. 9.5.3(3):

$S_{cl,max}$= min {15*16mm; 350mm; 400mm} = 240mm

According to 9.5.3(4)(i), the center distance is reduced with a factor of 0,6 within 350mm from both ends of the column, giving a center distance of 144mm. For simplification is this value put to 140mm. The 350mm is the critical height with respect to shear forces, which is equal to the biggest cross section dimension of the column according to 9.5.3(4)(i).

A.3 Concrete cover

Concrete cover

The column was expected to be placed inside with an exposure class of XO.

The calculations of the concrete cover for the reinforcement was conducted according to NS-EN 1992 - 1 - 1:2004, 4.4.1

c_{nom}= c_{min}+ Δc_{dev} 4.4.1.1 (4.1)

Δc_{dev}= 10mm NA. 4.4.1.3(1)

c_{min}=max {$c_{min,b}$; $c_{min,dur}$+ $\Delta c_{dur,\gamma}$- $\Delta c_{dur,st}$- $\Delta c_{dur,add}$;10mm } (4.2)

Where:

- $c_{min,b}$= 16mm 4.4.1.2(3)
- $c_{min,dur}$= 10mm when expecting X0 and M90 according to NA.4.4N and 4.4.1.2(5)
- $\Delta c_{dur,\gamma}$= 0mm 4.4.1.2(6)
- $\Delta c_{dur,st}$= 0mm 4.4.1.2(7)
- $\Delta c_{dur,add}$ = 0mm 4.4.1.2(8)

c_{min} = max {16;10;10} = 16mm

c_{nom}= 16mm + 10mm = 26mm choosing a concrete cover of c_{nom}= 30mm.

A.4 Axial capacity

The axial capacity of a short column is calculated based on the following relation:

Equation A-1. Axial capacity of a short column.

$$N_{Ed} = f_{cd} * (A_c - A_s) + f_{yd} * A_s \quad \text{(A - 1)}$$

N_{Ed}= 14,17N/mm^2*(96211,27mm^2 - 1206,37mm^2) + 434,78N/mm^2*(1206,37mm^2) = 1870,7kN

The design check will be conducted in chapter A.5 below in order to find out if the assumption of a short column is valid.

A.5 Slenderness criterion used in the analysis

The slenderness criterion was checked in order to see if 2. order effects have to be accounted for or not. The normalized slenderness was checked up against the allowable upper limit of the slenderness. The loading of the column was expected to occur after a time of 10 days

$\lambda_n \leq \lambda_{n,lim}$ NA. 5.8.3.1

Where:

- $\lambda_{n,lim}$= 13(2-r_m)$A_\phi$with both ends of the column fixed. NA. 5.13.aN

- $r_m = \frac{M_{01}}{M_{02}}$ is the relationship between the smallest and largest 1 order moment in the ends of the column.

- A_ϕ= 1,25/(1 + 0,2ϕ_{ef}) ≤ 1 with ϕ_{ef} as the effective creep number

- λ_n= λ(n/(1 + 2k$_a$ ω))$^{1/2}$ ($\lambda_n$is the normalized slenderness factor for concrete)

- $\lambda = \frac{l_0}{i}$ 5.8.3.2

- $\phi_{ef} = \phi_{(\infty, t0)} * \frac{M_{0Eqp}}{M_{0Ed}}$ 5.8.4, (5.19)

r_m is according to NA. 5.8.3.1 set to 1 since the column is symmetric and the eccentricity causing M_{01} and M_{02} is expected to be the same in both ends of the column. The tension stresses in the column because of the eccentricity are expected to occur on the same side of the column.

$\phi_{(\infty, t0)}$= 2,25 based on the following parameters from Figure 3.1 in NS - EN 1992 1-1:2004:

- $h_0 = \frac{2A}{u}$ with A = 96211,27mm^2 and u = 2*π*(175mm)= 1099,56mm => h_0 = 175
- Outdoor conditions with a RH of 80%
- Concrete class R.
- t_0 = 5, the age of the concrete in days at the loading time.

$\frac{M_{0Eqp}}{M_{0Ed}}$ is the ratio between the 1 order bending moment (permanent load in SLS, service limit state) and the 1 order bending moment (design combination in ULS, ultimate limit state). In these calculations, this ratio is set to 1 because the 1. order bending moment is expected to be the same in both SLS and ULS.

A_ϕ= 1,25/ (1+ 0,2*2,25) = 0,862

That gives $\lambda_{n,lim}$= 13(2-r_m)A_ϕ = <u>11,206</u> with:

- A_ϕ= 0,862
- r_m= 1

The normalized slenderness factor is calculated with the formula λ_n= λ(n/(1 + 2k_a ω))$^{1/2}$ from NA. 5.8.3.1 where:

- $\lambda = \frac{l_0}{i}$ where $l_0$is the effective length of the column and i is the radius of gyration for the uncracked concrete
- n = $\frac{N_{Ed}}{f_{cd}A_c}$ and is the relative axial force.
- k_a= $(\frac{i_s}{i})^2$ where i_s, is the radius of gyration for the reinforcing and i, is the radius of gyration for the uncracked concrete section. As a simplification, k_a can be put to 1 according to NA. 5.8.3.1.
- $\omega = \frac{f_{yd}A_s}{f_{cd}A_c}$ which is the mechanical ratio of the reinforcement.

N_{Ed} is the design value of the axial force and is put to 80% of the axial capacity of the column, 0,80*1870,7kN = 1496,58kN. For A_c is the total cross section minus the cross section of the rebars being used. That gives a relative axial force as following:

$$n = \frac{1496{,}58kN}{14{,}17\frac{N}{mm^2} * 95004{,}9mm^2} \Rightarrow n = 1{,}11$$

The mechanical ratio ω is calculated as shown below.

$$\omega = \frac{434{,}78\frac{N}{mm^2} * 1206{,}37mm^2}{14{,}17\frac{N}{mm^2} * 95004{,}9mm^2} \Rightarrow \omega = 0{,}39$$

In order to calculate the slenderness factor, need the radius of gyration for the uncracked concrete to be found. The radius of gyration i is found below.

$i = \sqrt{\frac{I_c}{A_c}}$ where $I_c$is the moment of inertia for the concrete and A_c is the area of the concrete.

$I_{concrete} = I_{column} - I_{reinforcement}$ where I_{column} and $I_{reinforcing}$ is found below.

$I_{column} = \frac{\pi(350mm)^4}{64} = 7{,}366*10^8\ mm^4$ (about the centroid where no parallel axis theorem is needed)

$I_{reinforcement} = I_{reinforcement,centroid} + A_{reinforcement}*c^2$ (have to use the parallel axis theorem)

c is the perpendicular distance between the centroid x axis and the x' axis, about which the moment of inertia is calculated. For a given shape is the distance c, shown in Figure A.1.

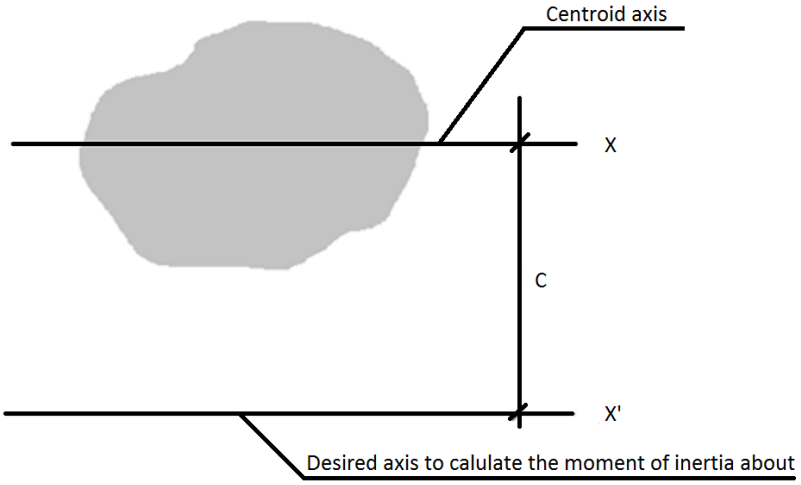

Figure A.1. The parallel axis theorem.

$I_{reinforcement}$= $\frac{\pi(350mm)^4}{64}$ + [201,06mm^2 *(175mm-30mm-8mm-16mm/2)^2]*6bars=2,007*10^{7}mm^4

$I_{concrete}$ = 7,366*10^8 mm^4 - 2,007*10^{7}mm^4 = <u>7.165*10^8 mm^4</u>

$A_{concrete}$= 96211,27mm^2 -1206,37mm^2 = 95004,9mm^2

The radius of gyration is calculated below:

i = $\sqrt{\frac{7,16510^8}{95004,9}}$ = 86,94mm

λ = $\frac{1200mm}{86,94mm}$ = 13,82mm where 1200mm is the effective length for a 2400mm tall column fixed in both ends. l_o is based on 5.8.3.2(2).

That gives λ_n= λ(n/(1 + 2k$_a$ ω))$^{1/2}$ = <u>10,77</u> with:

- λ = 13,82
- n = 1,11
- k$_a$ = 1
- ω = 0,30

$\lambda_n \leq \lambda_{n,lim}$ leading to 10,77 ≤ 11,206 => O.K

The 2. order effects do not have to be taken into account. The calculations can be executed as for a short column.

A.6 Calculation of the smeared reinforcement ratio

The quarter of the column consists of 141 120 elements in total, 588 in the cross section and 240 in the length of the column.

Smeared approach for the longitudinal reinforcement

The quarter of the column contain (201,06mm^2 + $\frac{201{,}06mm^2}{2}$)*2400mm , giving a total volume of 723 816mm^3 . With a volume of the column equal to $\frac{\pi(175mm)^2}{4}$ *2400mm = 5,773*10^{7}mm^3.

This gives a steel percentage within the quarter column of 1,254%

The cross section of the quarter column is $\frac{\pi(175mm)^2}{4}$ = 24052,82mm^2

If each stirrup section has a thickness of 10mm, equal to the element length, this section is consisting of 0,01254*24052,82mm^3 = 3016,2mm^3 of steel.

With a cross section of 24052,82mm^2, an element length of 10mm and a cross section consisting of 588 elements, do each element consist of 409,06mm^3 . This mean that $\frac{3016{,}2mm^3}{409{,}06mm^3}$ = 7,37 full elements with steel in the cross section is needed in order to have realistic reinforcement within the concrete column. For simplification are 8 elements filled with steel in the cross section.

Smeared approach for the stirrups

With a cross section of ø8:

Length of one stirrup in the quarter of the column:

L = 2*π*(175mm - 30mm - $\frac{ø8}{2}$) = 221,48mm where 30 mm is the cover of the stirrups

The cross section of the stirrup: $\frac{\pi(8mm)^2}{4}$ = 50,26mm^2 gives a stirrup volume of 11131,58mm^3

The area of the quarter column cross section and a thickness equal the element length of 10mm gives a volume for each stirrup section of 240 528,2mm^3. This leads to a steel ratio of $\frac{11131,58mm^3}{240528,2mm^3}$= 4,628%. When distributed into 588 elements, the steel ratio in each stirrup element is 0,04628/588 = 7,871*10^{-5}.

With a cross section of ø6:

$L_{stirrup}$= 2* π*(175mm - 30mm - $\frac{ø6}{2}$) = 223,05mm

$A_{stirrup}$= $\frac{\pi(6mm)^2}{4}$= 28,27mm^2

$V_{stirrup}$= 223,05*28,27 = 6305,71mm^3

The steel ratio is 2,622%

With 588 elements is that giving a steel volume ratio in each stirrup element of 4,459*10^{-5}.

A.7 Calculation of the confining pressure from each FRP layer

The hand calculations of the confining pressure are based on the dissertation from (Ghanem 2016)

The following formulas are used to calculate the confinement pressure:

$$f_{l,f,max}= \frac{\rho_f E_f \varepsilon_{fu}}{2} \quad (2\text{-}4)$$

and

$$\rho_f= \frac{4t_f w_f n_f N_f}{D l_u} \quad (2\text{-}5)$$

The confining pressure for Case3B with one laminate layer of CFRP is calculated as shown below:

- E_f= 62 000N/mm^2 – modulus of elasticity in fibre direction
- ε_{fu}= $\frac{958}{62000}$= 0,01545 – strain at failure, the material is linear elastic up to failure
- t_f= 1mm – thickness of the FRP composite
- w_f= 350mm – height of the FRP sheet
- n_f= 1 – number of FRP sheets

- N_f = 2 – number of strips along the column
- D = 350mm – diameter of the column
- l_u = 2400mm – unsupported length of the column

This gives a reinforcement ratio, ρ_f, of 3,3333*10^{-3} and a maximal lateral confining pressure of $f_{l,f,max}$ = 1,5965N/mm^2

A.8 Calculation of the axial shortening of the column

The relation used to calculate the axial shortening of the concrete column is shown below:

Equation A-2. Relation used to calculate the axial strain of the column.

$$\varepsilon = \frac{N}{E_c(A_c - A_s) + E_s A_s} \quad \text{(A-2)}$$

When the column is loaded with 80% of the axial load capacity:

$$\varepsilon = \frac{1496{,}58kN}{31\,000\frac{N}{mm^2}(96211{,}27mm^2 - 1206{,}36mm^2) + 200\,000\frac{N}{mm^2}(1206{,}36mm^2)}$$

ε = 4,697*10^4

The axial shortening when using the relationship between the strain and the height of the column is:

Equation A-3. Relation used to calculate the axial shortening of the column.

$$\Delta L = \varepsilon L_0 \quad \text{(A-3)}$$

ΔL = 0,0004697*2400mm => ΔL = 1,127mm

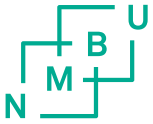

Norges miljø- og biovitenskapelig universitet
Noregs miljø- og biovitskapelege universitet
Norwegian University of Life Sciences

Postboks 5003
NO-1432 Ås
Norway